博士論文

The study of layerwise hybrid laminates for lightning strike applications

(耐雷用ハイブリッド積層板に関する研究)

MANOMAISANTIPHAP SIWAT

マノーマイサンティパープ　シワット

Department of Aeronautics and Astronautics

Graduate School of Engineering

The University of Tokyo

JAPAN

This dissertation is submitted for the degree of

Doctor of Philosophy

Dedicated to my Manomaisantiphap Family, Veerachart, Sirinuch, Siwaporn, and Yanisa for their unconditional support

Abstract

Carbon fibre reinforced plastics (CFRPs) have played an important role in the aviation industry with outstanding properties, such as high specific strength, adjustable mechanical properties, corrosion resistance, and ease of moldability. These properties have made CFRPs good substitutes for metallic materials for aircraft, for example, aluminium. Utilizing CFRPs also contributes to lower greenhouse gas emissions and higher fuel efficiency. Conventional CFRPs are made of Carbon fibres with a high strength, but insulating epoxy resin. The conductivity of CFRP with epoxy resin (CF/Epoxy) obtained only from the carbon fibres, not the resin. This results in anisotropic and non-uniform conductivity compared to metallic materials. This dielectric property has made CFRPs vulnerable to lightning strikes. Especially in thunderstorm clouds, lightning can happen frequently and cause damages to the aircraft. The lightning strikes can cause structural damages and disturb the radio system; sometimes such attacks cause lethal accidents due to critical part failure, such as fuel tanks. To prevent such incidents, aircraft manufacturers employ a lightning strike protection (LSP) system, which provides conductive paths for the lightning current to flow away from the aircraft body to prevent damage. This system requires multiple layers of materials to prevent the corrosion of metals and CFRPs. This complexity, in turn, obstructs the aim to lighten the weight of aircraft. To seek alternatives, researchers have put their efforts into finding new technologies of LSP, for example, conductive coatings, conducting nanoparticles. The method of incorporating conducting nanoparticles into epoxy resin gains interest from researchers, but it comes with the territory of agglomerations and percolation threshold. They could not yield uniform conductivity above their mixing limit.

As alternatives, conducting polymers can provide a promising solution to the current problem as well as providing intrinsic LSP. Polyaniline (PANI) has gained interests among scientists since it possesses several advantageous properties, such as ease of polymerization, low cost, availability, and tuneable conductivity. Our research group has been working on PANI-based materials and provided several options for PANI-based resin. Many of them have been tested to be effective against lightning strike. This proved that CFRP with PANI-based resin (CF/PANI) has high electrical conductivity; however, I would like to know the possibility of this material whether its strength can be improved without compromising the weight. This is because the strength of CF/PANI is much less than that of CF/Epoxy and this may be dangerous in practical application. Therefore, this thesis aims to use conventional CF/Epoxy

for their superior strength and add a number of CF/PANI layer on top to provide the structure with high resistance against lightning strikes without an increase of weight.

The product of this combination is introduced as layer-wise hybrid laminates; both laminae were fabricated layer-wisely and combine two different laminae as a hybrid laminate. These layer-wise hybrid laminates (CF/Hybrid) are expected to provide both structural strength by CF/Epoxy and electrical conductivity by CF/PANI. This thesis put efforts to verify the characterisation by using mechanical tests: four-point bending test, interlaminar shear strength test, and fracture toughness test in mode one and two.

For lightning strike preparation, the electrical conductivity in through-thickness direction was measured. There were altogether 3 cases of CF/Hybrids which were varied by CF/PANI and CF/Epoxy to obtain 8 layers of laminate: CF/Hybrid-4P4E, CF/Hybrid-2P6E, and CF/Hybrid-1P7E where the number before P represents the number of CF/PANI layers and the number before E represents the number of CF/Epoxy layers. The tests were conducted on both sides of the specimens due to different properties. The bending strength of hybrid laminates were in range of 194 MPa to 328 MPa on CF/PANI side and in range of 554 MPa to 684 MPa on CF/Epoxy side. The ILSS tests were conducted in the same manner. The ILSS were in range of 33 MPa to 53 MPa on CF/PANI side and in range of 37 MPa to 53 MPa on CF/Epoxy side. For ILSS, the results on both sides are not distinguished because the maximum shear planes were in CF/Epoxy layers. The interlaminar fracture toughness tests were conducted on both CF/PANI and CF/Epoxy sides except fracture toughness test mode I. The results show obvious differences between CF/PANI and CF/Epoxy and CF/Hybrids fall either between or higher than CF/Epoxy. This is because the interfaces were strengthened by the adhesive film. Conductivity of the specimens in this study varies from 0.49 S/cm to 0.78 S/cm.

After confirming that the CF/Hybrids have sufficient strength as well as high electrical conductivity, the CF/Hybrids were inspected using non-destructive inspection (NDI) before testing against lightning strike.

Simulated lightning strike tests were conducted with modification from the standard SAE ARP-5412B. The specimen was fixed to a picture-frame-type copper jig, which was attached to the ground of the impulse current generator. The specimen was held by the base plate and cover frame at all edges by screw-clamping. Lightning current was applied at the centre of the specimen surface, where the gap between the tip of the discharge probe and the surface of specimen is 2 mm. Additionally, several observation methods were employed to help

clarify the lightning strike phenomena: high-speed cameras, and a thermography camera. After the test, damages were evaluated and analysed.

These results have indicated that to achieve the coexistence of structural strength and electrical conductivity, at least 4 layers of CF/PANI should be incorporated on the top of CF/Epoxy. This is because the experimental results of CF/Hybrid-4P4E have proven the highest potential to withstand lightning strikes both mechanically and electrically. In terms of mechanical properties, although other specimens showed higher strength due to higher number of CF/Epoxy layers, higher number of CF/PANI layers indicates higher strength as well as effectiveness to withstand lightning strike damages. By comparing damages visually, CF/Hybrid-4P4E obviously shows less damages compared to other cases. When observing the phenomena during lightning strike, CF/Hybrid-4P4E shows the potential to conduct lightning current quickly. In high-speed cameras, the pyrolysis could, which was generated from resin burnt, expanded steadily as a sphere shape from the centre. This means the lightning moved steadily within the CF/PANI layers unlike the case of CF/Hybrid-7P1E that they could generated in a cross shape due to fast flow of lightning current. The thermography images also confirm this trend. Within the same period of time, the surface temperature of the CF/Hybrid-4P4E panel decreases considerably faster than others (less high temperature area). The other method that confirms this result is residual strength test. The residual strength of CF/Hybrid-4P4E shows residual ratio, which defines as the ratio of residual strength to its pristine strength, of 0.71 while others are more than 2.0. This meant that the CF/PANI of other cases delaminated and did not contribute to the strength, so the CF/Epoxy parts bear all the load and resulted in high strength ratios.

This thesis has introduced the concept of layerwise hybrid laminates using both CF/PANI and CF/Epoxy to achieve the coexistence of electrical conductivity as well as structural strength without compromising additional weight. This structure can cover each disadvantage and bring about possible application as LSP for aircraft. This concept has been built on simple methods and has a potential to apply with different materials or structure to accomplish synergistic results.

Acknowledgement

I could not describe in words how gratitude I feel toward my respected supervisor Associate Professor Yokozeki Tomohiro (横関先生) for accepting me into this Master and PhD program as a part of Aoki-Yokozeki Laboratory, my beloved place for 6 years. These 6 years have challenged me physically and mentally a lot. However, his kindness, understanding and supports are invaluable and put me through those bad times. I should not forget mentioning Prof. Aoki Takahira, who was the supervisor of supervisor in Thailand, Associate Professor Thanyarat Singhanart. With their relationship with this laboratory, I have this precious opportunity to pursue PhD. Prof. Aoki always set a paragon of life-long learning through his strict instruction. I am thankful for Dr Okada Takao for their advices and support for lightning strike test. Without him, I would not have such significant test results for my thesis. For simulation advices, I am grateful for Assistant Professor Higuchi Ryo, who constantly support and gives feedback. For experimental, I could not be more appreciated for Mrs. Kobayashi Yayoi for her teaching, guiding, and supporting about every experiments.

My life in Japan would not be this wonderful without Japanese Government Scholarship (Monbukagauksho, MEXT) who granted me this opportunity to experience in Japan the fullest. I would like to thank Thai language section of NHK-WORLD JAPAN RADIO for my part-time job that I can work and meet with Thai colleagues, so that I can pause my study as well as hone my language skills. The life in Aoki-Yokozeki laboratory was so fun with many generations of lab mates. One of the closest lab mates, Aoki Ryoma, has taught me many lessons about research and lives and I appreciated them all. In my PANI research group, I was surrounded by dexterous teammates who inspires me to keep improving myself: Vince, Sukantha, Kumar, Lea, Luciana, Akhsin and An.

I am always thankful to my beloved family; my parents for their supports and cares, my sisters for their fun moments, as well as other family members who always hope for good things for me.

Life in Japan was so wonderful with my dear friends Keito and Pai for always being there listening and understanding my emotional parts. Em, Muk, Pleum, Ex, Nice, Top, Tata, and many others who enjoy activities together. Japan always filled me with thrill and peace at the same time. It has been the place I love. Also, although we are apart, Nid, Penny, Poh Lee, and Koy constantly give me mental support to go through any obstacles.

Table of Contents

List of figures

List of Tables

Chapter 1   Background

1.1   Introduction

Technologies in the world have been evolving rapidly with the aim to make the planet a better place, more convenient, more liveable, and more sustainable. This evolution is a tremendous result of scientific and engineering development in every aspect. One of the revolutions of transportation nowadays is aviation. We can travel easily and comfortably thanks to the development of aircraft, models after models. To enhance the properties of aircraft, a great number of research and experiments are required. In the year 2020, an unprecedented global economic and health crisis of novel coronavirus, however, has caused a stupendous negative impact on the aviation industry. For months, several countries needed to close their borders to prevent infection spreading; therefore, almost all international flights were halted. A number of fleets must terminate their operations, and some went bankrupt.

Subsequent to this coronavirus crisis, airliners will need to operate in an efficient and safe way to quickly recover from the setback while preventing any possible infection risk. We all need to cooperate, collaborate, and combine our strengths so that we can generate the best outcome that can help accelerate the recovery. As researchers, we can test out ideas, provide possible solutions to help accelerate the process and try different approaches to support. This has emphasized the importance of research in this field even more.

This research work is an example of the trial of a different approach of possible applications for aircraft structure. The author has put the effort into adopting electrically conductive polymers to fabricate carbon fibre reinforced plastic (CFRP) panels for application in aircraft structures. This chapter introduces a number of related findings from previous studies, the motivation of the thesis, and the concept of this study.

1.1.1   Composite materials for aircraft development

In the past, aircraft composed of metal materials to ensure the strength of the materials. Despite their heavy weight, metal materials also have an advantage of intrinsically high electrical conductivity. To improve the fuel efficiency, with advance technology of composite materials, carbon fibre reinforced plastics (CFRP) has become a part of aircraft materials due to their high specific strength. In 1983, composite material had its significant use in commercial aircraft by Airbus as the rudder of A300 and A310. Later in 1985, the material was used in the vertical tail fin. Using composite material has lessened 2,000 parts of the metal fin to fewer

than 100 for composite fin as well as reduced its weight and fabrication cost. From this beginning, the manufacturers have competitively further increased the portion of composite materials in aircraft structures. Figure 1-1 shows the percentage of materials in modern aircraft. The recent Boeing 787 contains around 50% of composite materials in the structure and became the first major commercial airplane that uses composite materials for fuselage, wings and most other airframe components. Due to higher strength-to-weight ratio of carbon fibre composites, the 787 has become a lighter aircraft than ones with the conventional metal materials. With the high specific strength, and less corrosion, carbon fibre has gained attention as a material of the 21st century.

Figure 1-1 Percentage of materials in modern aircraft [1]

1.1.2 Lightning strike on composite aircraft

Common composite materials consist of two main components: fibre materials and matrix materials. In conventional CFRP for aircraft, carbon fibre is used as a fibre material and epoxy is widely used as a matrix or resin. The epoxy resin has provided favourable properties contributing to the strength of CFRP products, such as mechanical strength, chemical resistance, thermal stability. Notably, epoxy excels at adhesive compatibility with carbon fibre and the production cost is low. This has set epoxy resin an exemplar for resin material of CFRP. Unlike metal, carbon fibre does not obviously expose cracks and fatigue which is being disputed about the safety concern. Carbon fibre is less prone to corrosion than metal materials. Figure 1-2 shows the real example of aircraft made of carbon fibre composite structure.

Figure 1-2 Forward Fuselage of Boeing 787 made of carbon fibre composite structure [2]

As an airplane may face some turbulence and lightning strike during operation, the aircraft require protection for any possible damage. Compared to metal, which were used in the preceding airplanes, epoxy resin is inferior in the aspect of electromagnetic shielding effectiveness. This is because epoxy is a dielectric material and cannot resist high electrical discharge. Furthermore, epoxy does not possess fire retardancy and the replacement of components after failure is costly. Figure 1-3 shows an example of the damage from lightning strike on aircraft.

Figure 1-3 Lightning strike damage on aircraft [3]

Each airplane in the US commercial fleet is estimated on average that it is struck sparingly by lightning more than once each year. This is because aircraft often trigger lightning as they are flying through a densely charged region of a cloud. The lightning flash starts at the aircraft and flows away in other directions. Lightning can attribute to catastrophic incidents for example, the last commercial plane crash incident of TWA Flight 800 in 1967 was confirmed and it is a consequence of lightning causing fuel tank explosion. The explosion has killed all the occupants and the wreckage were retrieved from the ocean as shown in Figure 1-4. After that, the learned lessons about the effect of lightning strike on airplanes has improved protection techniques. Wayne L. Golding [4] has mentioned that the commercial airliners were quite safe to go through electrical storms due to their metal skin that conducts the current on the outside. Also fuel tanks have been designed to avert entry of electrical charges.

Figure 1-4 Reconstructed wreckage of TWA 800 [5]

P. Laroche et al. [6] has conducted an experiment of lightning strikes to aircraft based on the models that operated in the period of 1980-1986. They have raised the concern of using new technologies, such as composite material on aircraft fuselage and wings and the certification may need to be revised based on new information of electrical design of aircraft

made of carbon fibre composite material.

To identify effects of lightning on composite material, L. Chemartin et al. have studied the direct effects of lightning strike on aircraft structures [7]. They introduced the phenomenology of lightning arc attachment on aircraft by observing the shapes, the behaviors, and other specific points. From their experiment and simulations, the shapes of the shock waves originated from the lightning strike can be varied by the arc attachment setting. The behaviours of the arc attachment were the combination of several forces that formed different kinds of pressure that occurred to the panel.

Also, L. Chemartin et al. presented effects of lightning on aircraft skins in both thermal and mechanical aspects by obtaining experimental and numerical results. The direct effects are concerned with physical damages at the attachment point while the indirect effects related to the interferences due to the electromagnetic coupling with the electronic systems. They have clearly divided constraints regarding direct lightning effects into two main categories as shown in Figure 1-5:
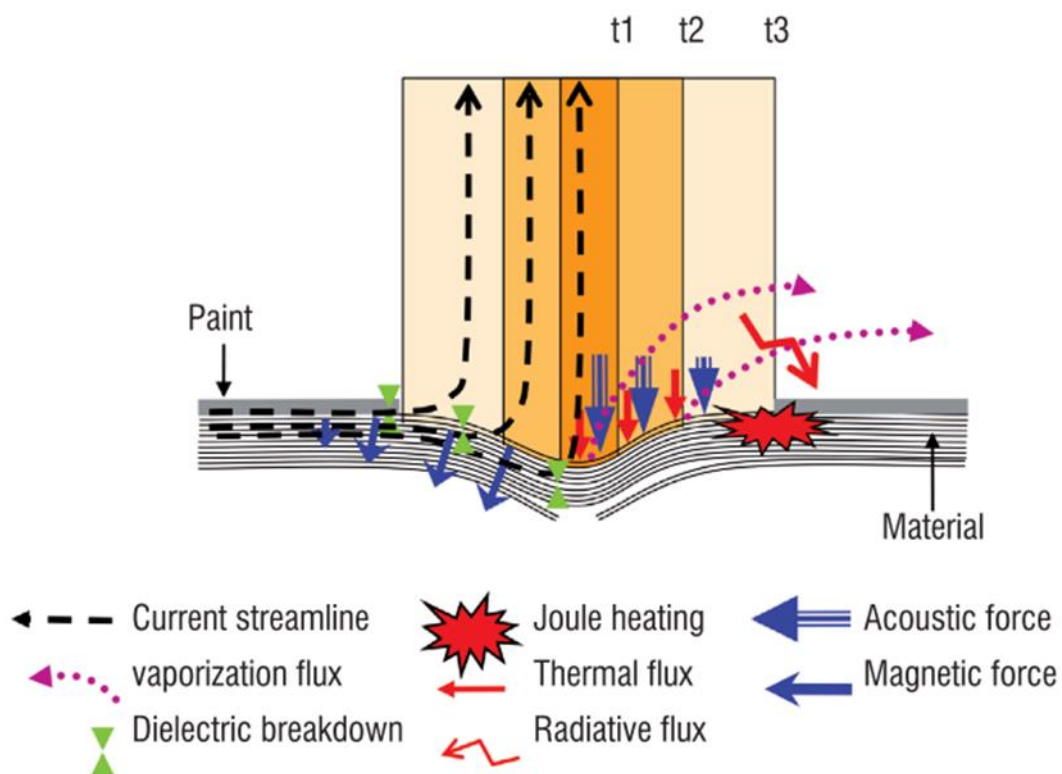
Figure 1-5 Illustration of the various direct constraints at the attachment point [7]

First, the thermal constraints lead to a rapid surge of temperature of the material, which

may result in melting or puncture. They play an important role during the continuing current stage. The main sources of energy are the direct plasma heat flux (such as conduction, and radiation flux) and the Joule heating within resistive material, especially composite materials. This is because composite materials have much lower electrical conductivity than metal structure and the laminate structure of the composite materials prevent transferring of current through the different layers of the panel.

Second, the mechanical constraints lead to breaking, delaminating and puncture. They are crucial during the current peaks. The constraints are overpressure due to explosion of the lightning channel, explosion from the fast increase in the arc temperature, and magnetic force induced by the current circulation.

From these two constraints, they have reiterated that composite structures require mechanical strength and electrical conductivity to withstand lightning strike damages.

1.1.3 Safety and Lightning strike protection

The safety of modern aircraft, which most of the components are composite materials, rely on not only mechanical strengths, but also other properties such as thermal properties, and electrical properties. Safety equipment is required to fulfil the safety measurement and prevent necessary cost for repair and maintenance. Airliners have invested a large amount of budget in research and development to invent an effective system for lightning strike protection (LSP).

A wide range of LSP solutions has been adopted for composite as their application for aviation industries has widened in the past four decades. Each aircraft model has its own unique system due to each aircraft design team addressing the issue distinctly. The common materials of choice to prevent direct effects are metal meshes and ply-integrated interwoven wires. The main function of these LSP is to provide conductivity to compensate the insulating composites. LSP must generally enable the lightning current to flow through a continuous conductive path of low resistance over the entire aircraft surface. For the lightning strike test, the LSP should be able to withstand waveforms defined by the standardized lightning current waveforms for lightning direct effect tests (ARP 5412, 2) as shown in Figure 1-6. Over the entire aircraft, lightning is most likely to attach in some zones which require extra protection.
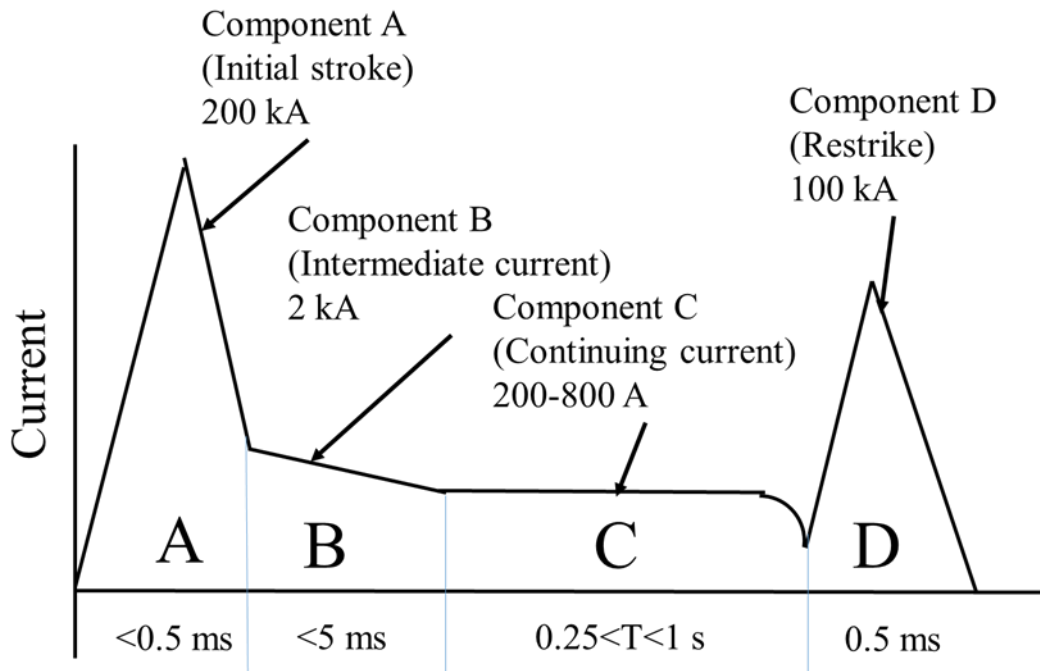
Figure 1-6 Standardized lightning current waveforms for lightning direct effect tests (Scale not to real value)

Lightning-strike zones of aircraft are defined by SAE Aerospace Recommended Practices (ARP) 5414. The airplane lightning-strike zones are separated into 3 main zones as shown in Figure 1-7:

Zone 1 indicates an area that the initial attachment of strike is likely to affect. We can usually find lightning-strike entrance and exit points in Zone 1. A lightning strike generally attaches to the airplane in Zone 1 and departs from another Zone 1 area. The external areas that are likely to be attached are radome or nose, nacelles, wing tips, and extremities of the empennage. According to U.S. Federal Aviation Administration's (FAA) Federal Aviation Regulations, those areas are required to withstand 200 kA of initial lightning attachment and first return strokes.

Zone 2 indicates an area that a swept, or moving, attachment is likely to occur. Unlike Zone 1, lightning rarely enters or exits in Zone 2. However, a lightning flow may be thrusted from a beginning entry and exit point by the motion of the airplane.

Zone 3 indicates areas that may undergo conducted currents during flowing without the direct attachment of a lightning strike. Surfaces in Zone 3 are unlikely to be any attachment of the lightning channel. Zone 3 also includes those portions of the aircraft that are underneath or

between other zones and conduct a considerable amount of electrical current attachment points. According to Boeing, a Zone 3 examination should be performed even if damage is not found during the Zone 1 and Zone 2 examinations [8].
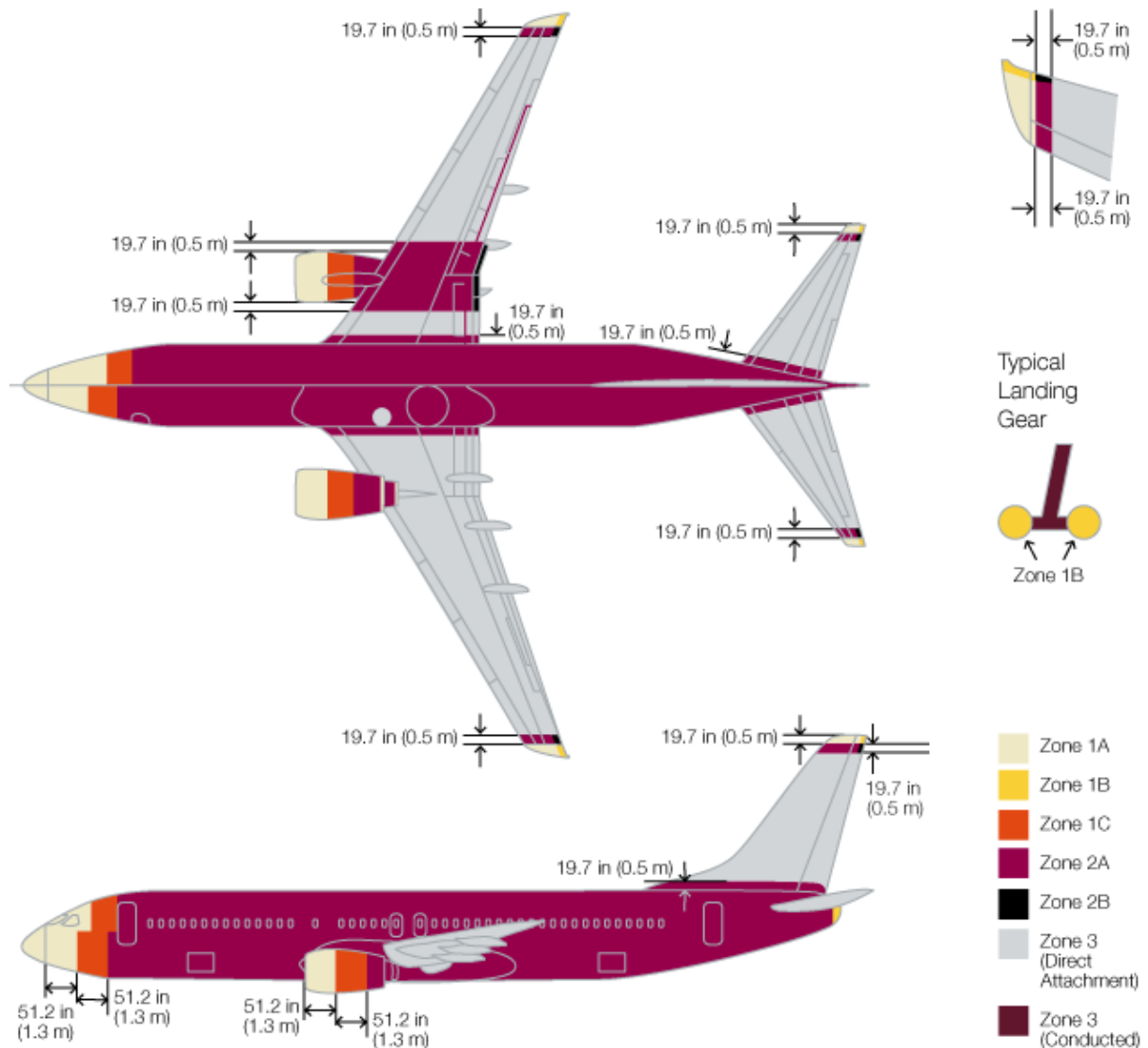
Figure 1-7 Areas of airplane prone to lightning strike by zones [8]

In conclusion, Zone 1, 2, or 3 identifies any entrance and exit points of lightning attachment. Doing so enables the operators to examine the immediate areas around the zones thoroughly and to repair if required.

In order to utilize the zoning protection and minimize the damage from lightning strike, aircraft need conductive paths to a metallic ground plane. The manufacturers typically use metal in the external skin of composite aircraft—which made of a delicate, lightweight mesh

or foil inserted in a surfacing film, or wire inserted within the outer laminate ply—to form contact with metal bonding bands or other structures that link through the outer conductive surface to a metallic ground plane, for example an engine or metal channel in the fuselage.

The primary materials of the metal LSP products are aluminium and copper. Aluminium was the first option for LSP due to its light weight. However, contacting with carbon fibre laminates brings the risk of galvanic corrosion, which occurs due to electrolyte transfer through electrical connection between two different materials. To prevent this, an isolation ply of fiberglass is applied, but, in turn, adds weight to the structure and makes the fabrication procedure more complicated as shown in Figure 1-8. Moreover, if moisture penetrates the composite layer, aluminium corrosion may occur. On the other hand, copper does not have galvanic corrosion risk, but weighs at least double as much as aluminium.

1.1.4 Metal mesh

The most frequently selected LSP solutions are metal mesh and expanded foil made of copper and aluminium. They possess high conductivity and high heat of vaporization which are required properties to withstand massive lightning strike according to the standard. The market available trademarked products are:

- MicroGrid from Dexmet Corp.

- Astrostrike aluminium mesh from Astroseal Products Mfg. Corp.

- Strikegrid from Alcore Inc.

- Aeromesh from Niles International

These products have been manufactured using their unique processes to achieve ultra-light weight and prevent galvanic corrosion with the carbon material. For example, MicroGrid has weight ranging from 0.010 lb/ft^2 to 0.040 lb/ft^2. Strikegrid is a continuous expanded aluminium foil (CEAF) which is phosphoric acid anodized and coated to prevent galvanic issues and prevent corrosion. However, to prevent such corrosion, they require several extra layers to completely avoid direct contact between metal and carbon fibre.
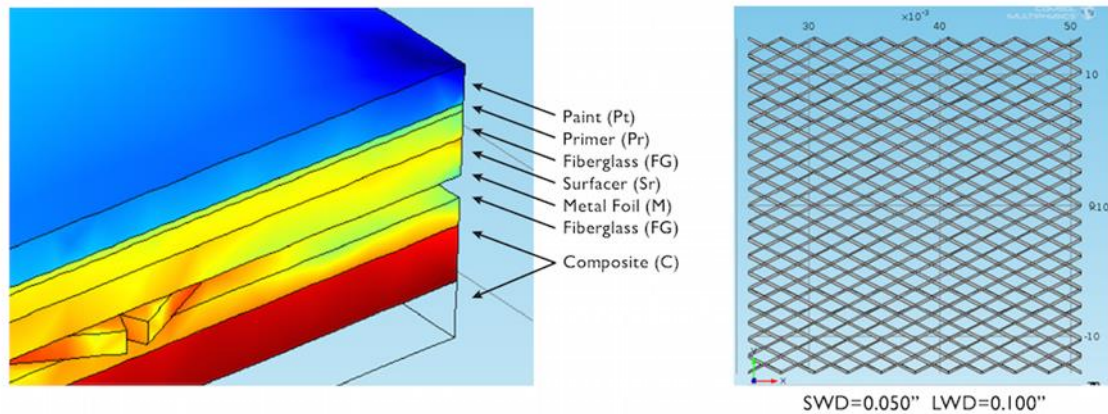
Figure 1-8 Composite structure layup for metal meshes [9]

1.1.5 Integrated LSP materials

A number of aerospace suppliers provided expanded metal mesh pre combined with adhesive films, surfacing films, or prepregs. These products aim to achieve a simple method of integration using available technologies. The trademarked products are:

- SURFACE MASTER from Cytec Engineered Materials is an epoxy-based surfacing film with embedded expanded foil.

- Redux epoxy film adhesives and Hex Ply prepreg resins from Hexcel include bronze, copper, or aluminium mesh, or expanded foils for LSP applications.

- Interwoven wire fabric (IWWF), also from HexPly, is a carbon cloth into which thin metal wires are woven.

- IWWF from Toray Composites is also similar to IWWF from HexPly.

- SkySkin from Henkel AG & Co. KGaA is a surfacing film with embedded mesh

1.1.6 Metallized fibres, fabrics and veils

This kind of LSP is made by including oriented metal-coated-carbon fibres to conductive non-woven veil or using special techniques such as nickel vapor deposition A LSP from Hollingsworth & Vose Co. is a conductive nonwoven veil made with randomly oriented nickel or copper-coated-carbon fibres. A proprietary nickel vapor deposition (NVD) is a process for coating fibres from Conductive Composites (Heber City, Utah). An example of products is metal coated carbon fibres / metal plating from Technical Fibre Products Inc. Less common other products are Peel-and-stick appliques, Metallic conformal shield mesh,

Flamespray, Integument Technologies, Lightning Diversion Systems, and Purtech. They are aiming to produce a veil which is corrosion-resistant and lightweight and is applicable for electromagnetic interference (EMI) shielding and LSP.

1.1.7   Conductive surface treatments

The other method is conductive surface treatment which are sprayable conductive paint, or a surfacing film. This type of LSP has claimed that it can conduct current with sufficient conductivity with lower weight than copper foil. The product also works well with EMI shielding property. The examples of trademarked products are:

- UltraConductive from LORD Corporation is a conductive polymeric material for LSP applications

- A conductive paint from Conductive Composites is a paint with dispersed nickel nano strand material.

One advantage of conductive surface treatment is that they can be reapplied easily. This has simplified the repair process after damage, but the effectiveness of this process should be ensured in the practical application.

1.1.8   Multifunctional materials

Apart from those add-on LSP as mentioned in the previous section, researchers and designers have investigated a new approach of making the composites multifunctional to address the parasitic weight. This promising solution aims to add electrical properties into composites intrinsically, which is adding the properties without attached or embedded additional parts. This method is believed to be less weight-intensive, and more efficiently processed options and is expected to maintain the structural function and non-structural function simultaneously. Many studies have reported methods to achieve multifunctional properties in composites.

Nanoparticles, such as graphene nanoplatelets, silver nanoparticles, and carbon nano tubes, were introduced the resin of CFRPs. These nanoparticles are required to add up to a specified amount (over the percolation threshold) to achieve and ensure high electrical conductivity. Using nanoparticles also brings another precaution that they need to be dispersed uniformly in the matrix at proper weight loadings. This is because they are likely to cling up together and become agglomerates due to their intermolecular Vander Waals forces [10].

1.2   Conducting polymers and polyaniline (PANI)

One common function of the multifunctional materials is electrical conductivity. Apart from aforementioned methods, current research on conductive matrix can be divided as shown in Figure 1-9. The previous paragraphs have shown the method of using insulating polymer resin with conductive additives, such as, nano fillers, and metal fillers. These methods have potential to increase electrical conductivity, but they come with agglomeration problems. To implement these methods, they require advanced equipment to proceed, which lead to high cost and high technical procedure. On the other hand, matrix can be substitute with conductive polymers to obtain multifunctionalities. In this case, the matrix is made by conductive polymer and/or form the cross-linking network to obtain strength. The examples of conductive polymers are polyaniline, polypyrole[11], polyacetylene [12], [13], polythiophene [14], [15], poly(3,4-ethylene dioxythiophene) [16], [17], and poly(p-phenylene vinylene) [18]–[20]. These polymers are applied in several fields.
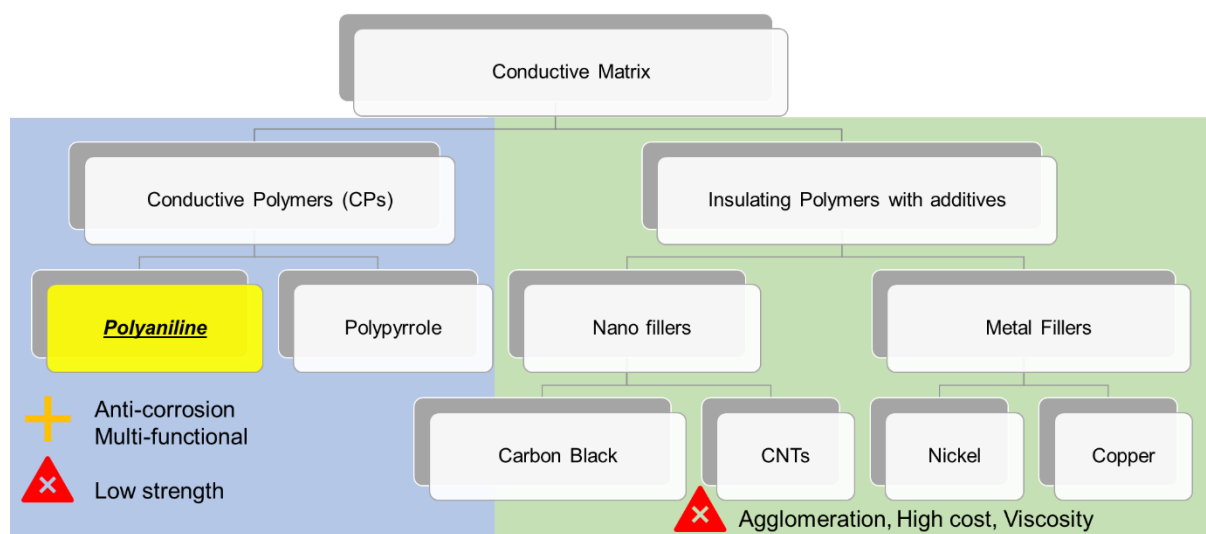
Figure 1-9 Types of conductive matrices

Polymers can be used as an option to replace several parts made of metal due to their ease of fabrication and low cost. A number of polymers are being applied in aerospace industries. For example, Polyether ether ketone (PEEK) is usually used for the interiors. Normally, we made use of polymers for their electrical insulating. However, another type of polymer which structure is alternate double bonds can be intrinsically conductive polymers (ICPs).

Among these polymers, Polyaniline (PANI) has gained much interest from the research community due to its advantages. PANI is easy to polymerize and commonly available. The compound using PANI obtains conductivity which is tuneable. One important reason to further study PANI is that PANI has already been proven the effectiveness against lightning strike. Hirano et al. [21], [22] has fabricated CFRP panels with conventional epoxy resin (CF/Epoxy) and PANI-based resin (CF/PANI). After that they conducted a simulated lightning strike test on both panels. They found that CF/Epoxy cannot withstand the lightning strike even at -40 kA current and the damage is more severe with higher current as shown in Figure 1-10. In contrast, the CF/PANI panel can withstand the lightning strike without showing any catastrophic damage up to -100 kA. This has shown the potential of PANI to be applied as LSP.
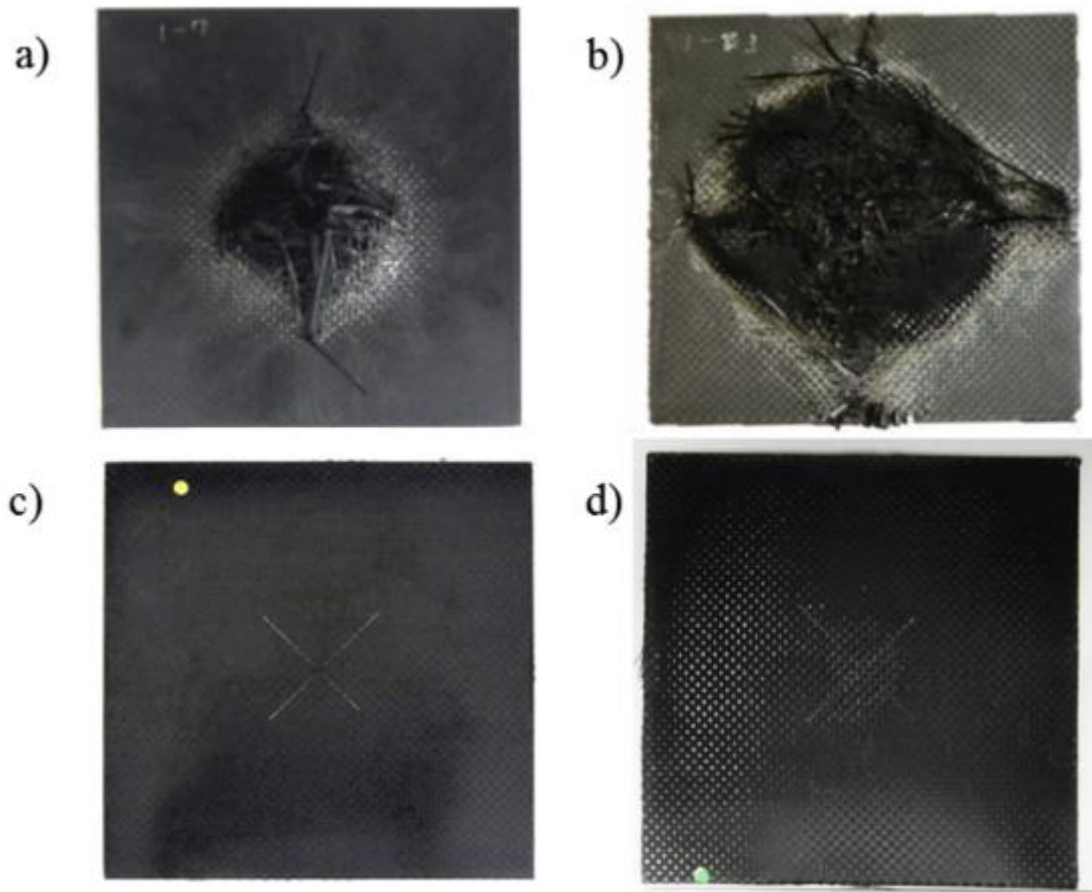
Figure 1-10 Specimen damage after simulated lightning current tests: a) CF/epoxy -40 kA, b) CF/epoxy -100 kA, c) CF/PANI -40 kA, and d) CF/PANI -100 kA. [21]

The work of Hirano has been followed by a number of studies about PANI.

Yokozeki et al. [23] have developed a one-step curing process of PANI-based electrically conductive thermoset resin to incorporate electrical properties in CFRP by substituting the conventional insulating epoxy resin. The PANI-based resin in this work consists of four components: PANI with dodecylbenzenesulfonic acid (DBSA), and p-toluenesulfonic acid (PTSA) as dopants and divinylbenzene (DVB) as a cross-linking polymer. The CFRP using PANI-based conductive polymer showed superior electrical conductivity to CF/Epoxy, as well as electromagnetic shielding effectiveness. This work has inspired many researchers to continue working with the PANI-based system.

Katunin et al. [24] adapted the recipe by using PANI doped with camphor sulfonic acid (CSA) then mixed the PANI/CSA with epoxy. They investigated the morphology of the mixture with various content proportions. At low PANI content (20-30%), the composites revealed the PANI agglomerates. As the amount of PANI increases, the conductive mixture is distributed more uniformly in epoxy resin and the measured resistance tends to be lower. From this work, I came to know that using PANI/epoxy resin confronted the issue of anisotropic properties in mechanical, electrical and thermal aspects.

Katunin et al. [25] continued the previous work by applying the resin to CFRP so that the composite panel possesses conductivity. Therefore, the panel has both mechanical reinforcement and electrical paths. They also performed lightning strike test on the panel to determine the effectiveness of the panel. The results showed that the damage of lightning strike was comparatively small compared to the samples without CF. Yet, the non-uniform distribution issue still caused undesirable deterioration of lightning strike resistance of the composites. From the works of Katunin, I can expect that using PANI in epoxy resin will face the issue of uniform distribution. This resulted in non-uniform properties of the final composites and was undesirable in practical application.

Several profound works about PANI-based resin are from Kumar and his team. They adopted a resin system similar to the one of Yokozeki et al. [23] and investigated the mechanical and electrical properties of the composites. They used PANI: DBSA in a weight ratio of 30:70 and doped (heated) in an oven for some time. Then, they mixed PANI-DBSA blend with varied amounts of DVB to optimize the properties. Using the mixing method in this work, the mixture can achieve uniform dispersion. After conducting the test, they found that as the amount of DVB increased, the bending strength of the composites increased, but in

14

turn, the electrical conductivity decreased [26]. This leads to finding the optimal DVB amount that will balance the strength and the electrical properties.

Kumar et al. also tried mixing PANI and DBSA using a roll-mill method to achieve better stability [27]. However, they achieved lower conductivity and bending strength compared to the PANI-DBSA mixture made by thermal doping. From this study, they concluded that by doping and breaking PANI agglomerates into small pieces, the PANI became more completely doped. This resulted in higher environmental stability, but lowered the conductivity and mechanical strength. Therefore, if the mixture does not suffer from stability issues, a thermal doping method is preferable.

After achieving some properties of PANI-based resin, Kumar et al. applied the resin on carbon fibres. Unlike Katunin [24], [25] who used the mixture of PANI and epoxy, they directly applied the conductive PANI-based resin as a substitution of epoxy resin and made PANI prepreg. They achieved through-thickness electrical conductivity as high as 1.35 S/cm. Then, they reapplied the heat to the finished specimen and found that the electrical conductivity decayed with the longer duration of reapplying heat or annealing. This is due to the de-doping of PANI, i.e., instead of increasing electrical conductivity as the heat applied during doping time, the conductivity decreased as the heat applied. On the other hand, the mechanical properties after reapplying heat were indifferent with the finished specimens. From this finding, they further investigated the de-doping mechanism.

Kumar et al. [28] have shown that de-doping level, so-called cationic scavenging, depends directly on the degree of doping of PANI and its dispersion state. The well mixed PANI that achieved uniform dispersion has a high degree of doping. Knowing these properties, they can control the properties of final resin. This has brought the precaution to handle the PANI-based resin properly so that we do not deteriorate desirable properties of the resin. This present study has adopted the methods in these studies to make the PANI-based resin for impregnating to carbon fibre fabrics.

Apart from the present study, our research group has several works on PANI-based resin development using different dopants and cross-linking polymers. For examples:

Santwana et al. [29] have developed a new resin system using PANI and 2-Methacryloyloxyethyl acid phosphate (P-2M) as a dopant. The resin achieved better steady state viscosity and higher mechanical properties compared to PANI-DBSA system. In this system, P-2M acts as a bifunctional material for both electrical conductivity and strength.

However, the electrical conductivity in this system can achieve only 0.5 S/cm which is lower than PANI-DBSA/DVB system. This system shows high environmental stability which may be suitable for making CFRP, but this work has not been proved to apply to CFRP.

Another work that followed the de-doping mechanism by Vipin Kumar et al. [30] has proposed a new system of PANI-based resin. They added Phenol into the PANI-DBSA/DVB system. The Phenol-DVB mixture can perform cationic polymerization in the PANI-DBSA system. Using Phenol in the system also dramatically improves electrical conductivity. This is because phenol prevented de-doping of PANI, i.e., the electrical conductivity would not decay during curing time. Yu Zhou et al. [31] has followed up this work by comparing the processability of PANI-DBSA/phenol-DVB complex using thermal doping and roll-mill process. They concluded that the roll-mill process is preferable because it broke PANI agglomerates into smaller sizes and made the PANI achieve doping better. The system is now, at the time of writing (May 2021), being tested for applicability for CFRP, LSP effectiveness and processability.

1.3   Hybridization

Hybridization is one of the ideas to combine two materials with distinct properties and synergize for better properties. Several kinds of hybridization have been studied so far. For examples, hybridization using different fibres, and fibre metal laminates (FMLs)

This kind of hybridization includes highly skilled techniques to produce the combination of fibres. However, the results of hybridization do not guarantee that the final product will be better than the separated ones. For example, in 1978, G. Marom et al. [32] examined mechanical properties of hybrid composites which consisted of two types of carbon fibres, but the test results did not show any synergy.

In 2006, Z.S. Wu et al. [33] studied models and experiments of hybrid carbon fibre-reinforced polymer (HCFRP) composites. They combined several types of carbon fibres. They found that the hybridization of several types of carbon fibres, whose strengths and young's moduli were different, can enhance mechanical properties of the final HCFRP as well as electrical resistance. Using several types of CF enabled stepwise fracture due to various strengths of CF.

In 2010, M.M. Davoodi et al. [34] proposed a hybridization of natural fibre, kenaf, with

glass fibre to enhance mechanism to enhance overall mechanical properties for car bumper beams application. The hybridized specimens showed improvement in tensile and flexural properties, not in impact properties.

In 2008, K. Sabeel Ahmed et al. [35] studied the effect of stacking sequence on properties of woven jute-glass fabric reinforced isothalic polyester composites. They drew conclusions that incorporation of glass in jute fibre composites enhanced the properties of resulting hybrid composites and the layering sequence also affected the flexural and interlaminar shear strength.

Enrique J. Garcia et al. [36] tested a hybrid composite laminate. They used the advanced technique of directly growing aligned carbon nanotubes (CNTs) on the surface of fibres. This enabled the electrical and mechanical performance of the laminate. They firstly hand-laid up the laminate and then in situ grew CNTs on the surface of advanced fibres. This method mainly focused on nano-engineering the laminate properties which is expected to improve interlaminar properties.

In 2010, Masaya Miura et al. [37] conducted an experiment and created a numerical model to study the interlaminar shear failure of hybrid composite laminates at cryogenic temperatures. They tested hybrid laminates made of woven glass fibre reinforced polymer composites and polyimide films under cryogenic short beam shear tests. They also conducted a progressive damage analysis to understand the initiation and growth of damage in specimens.

In 2012, A.I. Selmy et al. [38] studied the interlaminar shear behaviour of unidirectional glass fibre/ random glass fibre/ epoxy hybrid composites using short beam shear bending test. The hybrid composites under short-beam shear test showed linearity until an apparent elastic limit was reached and then decreased. The test has shown that apparent ILSS was enhanced by adding unidirectional fibre laminas in hybrid composites.

In 2014, Sunny S. Wicks et al. [39] studied multi-scale interlaminar fracture mechanisms. They have varied the type of epoxy and aligned CNT length to understand the mechanisms of Mode I fracture toughness enhancement. The result varied from decreasing the initial toughness to increase in steady-state fracture toughness. Long aligned CNTs could increase toughness in steady state through CNT pull-out as well as twisting paths around microfiber bundles/tows.

In 2015, Xiang Ma et al. [40] created a set of analytical design models to estimate the mechanical and electrical properties of hybrid carbon nanotubes/carbon-fibre/epoxy for aircraft

structure application against lightning strike. They conducted the optimization process to recognize the microstructural configuration of composites which provide the best electrical conductivity with the lowest weight structure. The results showed that 2% volume fraction dispersion of CNTS in the matrix resin could enhance the through-thickness conductivity of the composite laminate. They pointed that adding CNT could improve the conductivity without specific loss in mechanical properties under condition that uniform dispersions were achieved. However, improving the conductivity further with CNT fillers is a difficult challenge due to the dispersion issue of CNT.

Doris W.Y. Wong et al. [41] investigated the effect of a hybrid interleaf system which is made of either a non-woven aramid mat solely or a combination of the mat and epoxy-dissolvable thermoplastic phenoxy fibres. They found a synergistic toughening effect when combining phenoxy and aramid interleaves. This results in high damage tolerance in compression after impact test.

In 2018, M.R. Sanjay et al. [42] focused on finding candidates for better hybrid natural/glass fibre reinforced composites for engineering applications. They studied hybridization effects of E-glass with jute/kenaf woven fabric composites with epoxy resin by conducting impact and interlaminar strength tests as well as altering laminate stacking sequences. The results showed that hybridization with glass fabrics enhanced jute/kenaf fabrics composites. This is because the majority of the load was absorbed by E-glass according to SEM analysis and the good interfacial adhesion in the composites. (Is it better than CF/Epoxy)

In 2019, B. Mahmoud et al. [43] performed an experiment and numerical model of behaviour of thin carbon/epoxy hybrid laminates using unidirectional and woven fibres. They conducted the test of low and medium impact loading on the composites to observe the behaviour. They found that using different architectures of the same materials, i.e., unidirectional and woven fibres, is an alternative to mixing different materials for improving impact response of composite laminates. In this work, the impact resistance of the laminates was improved by inserting unidirectional plies between woven fabric layers. The woven layers protected the unidirectional plies by preventing traces of large interlaminar cracks.

Most of the studies about hybridization focus on hybridizing fibres in the bundles to improve or add features to the final products. However, there is another kind of methods that simplify technical difficulty and utilize the difference of materials properties. That is fibre metal laminates.

1.3.1 Fibre metal laminates (FMLs)

Fibre metal laminates comprise of a layer of metal and several layers of fibre reinforced plastics, fused together by adhesive or resin. This combination can achieve desirable properties in engineering application. Several researchers are testing these ideas in publications as follows.

E.C. Botelho et al. [44] have improved adhesion bonding between glass fibre-epoxy composite laminate and aluminium foil. They treated aluminium foil by two methods: sulfuric chromic acid etching (SCAE) and chromic acid anodization (CAA). They evaluated the properties of the treated surfaces and compared them with other types of fibre composite/metal laminates. The specimens treated with CAA have better properties.

A. Fink et al. [45] tested the industrial manufacturability of CFRP-titanium hybrid laminates. The locally hybridized titanium and CFRP to increase the load capability of bolted joints to achieve strength reinforcement. However, this method was not simple and needed to be traded off with additional cost for manufacturing.

HeeChul Kim et al. [46] studied the effects of interfacial adhesion strength on the characteristics of an aluminium/CFRP hybrid short square hollow section (SHS) beam using three-point bending test. The energy absorption capability of the hybrid SHS beam improved with the increase of interfacial adhesion strength. They varied the methods to strengthen the interfacial adhesion either by physical or chemical changes. The ability to absorb energy of the Al/CFRP SHS beam improved with the enhanced interfacial adhesion and CFRP laminate thickness.

Periyasamy Manikandan et al. [47] conducted an experiment and a numerical study of hybrid composites with metal layer interplay under low velocity impact condition. They compartmentalized the test into two test cases: (i) impact on the ductile metal layer and (ii) impact on the brittle composite layer. They also created numerical models using ABAQUS to validate the experiments. The results pointed out that the impact on both sides were significantly different. The metal layer contributed to absorb a larger amount of energy than the composite layer.

Huiming Ning et al. [48] has investigated interlaminar properties of aluminium/CFRP laminates. They employed three methods to increase interlaminar strength: acid etching, surface treatment of aluminium sheet, and addition of nanofiller to the interface. The double cantilever beam test showed improvement on the Mode-I interlaminar fracture toughness in

which the sample with combination of acid etching on aluminium sheet and addition of vapor grown carbon fibre showed the best property improvement. This has been an idea to improve the interfacial properties.

O. Laban et al. [49] has studied the effect of surface treatment on the mode I interlaminar fracture toughness of aluminium/fiberglass fibre-metal laminates. They have compared five surface pre-treatments to enhance micromechanical interlocks of aluminium. Among those methods, alkaline etched specimens could absorb energy the most and laser + N2 plasma treated specimens exhibited the highest fracture toughness. As the micro mechanical locks have improved, the mechanical locks helped prevent crack propagation and transitioned the failure mode from adhesive to adhesive-cohesive mixed mode.

Bin Yu et al. [50] introduced two methods of interlaminar improvement for fibre metal laminates mode of titanium alloy and CFRP: anodized titanium plate and CF sheets grafted with multiwalled carbon nanotubes and sandblasted titanium plate and untreated CF sheets. The former method has significantly increased interlaminar fracture toughness. After exposure to long-term hygrothermal environment (60-day immersion in simulated seawater at room temperature), the performance of both fibre metal laminates declined, but the treated specimens still had better performance.

Yingcai Pan et al. [51] conducted an interlaminar toughness test on fibre metal laminates (FMLs) which was made of CFRP and magnesium alloys sheet. The results showed the Mode I interlaminar toughness (0.23 kJ/m2) is much lower than the Mode II interlaminar toughness (5.81 kJ/m^2) owing to the fact that the effect of mechanical interlock which prevent crack propagation is smaller in Mode I loading than in Mode II. The FMLs mainly failed by adhesive failure and interfacial failure in Mode I loading, and by epoxy cohesive failure in Mode II.

Costanzo Bellini et al. [52] has evaluated ILSS of different types of CFRP/aluminium fibre metal laminates by varying the layer thickness and the bonding types of layers. The results have shown that the layer thickness did not influence the interlaminar strength but the adhesion type did.

Muhammad Akhsin Muflikhun et al. [53] studied the delamination behaviour of CFRP/SPCC hybrid laminates using ENF test. They reported that performing the test on the different sides of specimens led to different values of fracture toughness. The specimen with SPCC on top has a longer average time to fracture compared to CFRP on top specimen. This

result agreed with previous studies that putting metal materials on top provide better performance of the test. This may be because of the superior properties of the metal materials.

Previous studies of FMLs have shown a potential application of hybrid laminates that they can provide superior properties for multi-purpose application. However, the weight of metal part is heavy and counter the aim of weight saving structure. Instead, I combine the concept of FMLs with conductive polymers by substituting the metal parts with conductive polymers as layer-wise hybrid laminates.

1.4   Motivation and Objective

As the composites materials for aircraft require both mechanical strength and electrical conductivity, this study proposes alternative solution of using hybrid layerwise laminate structure. The objective of this study is to examine the hybrid laminate structure made of CF/Epoxy and CF/PANI to obtain resistance against lightning strikes without weight penalty. This is the first trial of CFRP laminates with 2 resins: electrically conductive PANI/DBSA/DVB resin and high strength epoxy. The hybrid laminates were characterized by several tests: four-point bending, interlaminar shear stress, and fracture toughness test. Electrical conductivity is also measured to ensure that the laminates have capability to withstand lightning strike. After that, the hybrid laminate panels were tested their effectiveness by simulated lightning strike test. Several equipment was employed to clarify the mechanism of lightning strike as well as damage. This study is expected to test a concept of layer-wise hybrid laminate whether it is useful for practical application, too.

1.5   Summary

The development of composite material has been advancing to apply to a wide range of industries. Due to its high specific weight properties, CFRP has been selected as a major material of aircraft to improve performance. However, the low electrical conductivity of CFRP can lead to catastrophic failure during lightning strike. Therefore, the new aircraft require lightning strike protection to prevent such failure. This chapter has covered the nature of lightning strike, given examples of current LSP as well as undergoing research.

Chapter 2   Fabrication

2.1   Introduction

In the previous chapter, I have talked about the previous studies as well as the motivation of this study. To clarify the procedures used in the studies, I introduce the techniques I used in this chapter as a guideline.

2.2   Materials

The chemicals required to make PANI-based resin consist of 3 substances. Polyaniline (PANI) in its emeraldine base form was procured from Regulus Co. Ltd., Tokyo, Japan. Dodecylbenzene sulfonic acid (DBSA), a dopant of PANI and curing agent, was procured from Kanto Chemical Co. Inc., Tokyo, Japan. Divinyl benzene (DVB), the cross-linking polymer, is purchased from Fujikura Kasei Co. Ltd., Aichi, Japan. Carbon fabric TR30-3K is purchased from Mitsubishi Rayon Co., Ltd. Epoxy resin composed of resin XNR6815 and hardener XNH6815. These are purchased from Nagase ChemteX Co., Osaka, Japan. Adhesive film (3M-Scott-Weld AF163-2k-0.600) is obtained from 3M Company, USA. For electrical conductivity measurement, we use conductive adhesive silver paste DOTITE which was purchased from Fujikura Kasei Co. Ltd. I also used Kapton® Polyimide film (DU PONT-TORAY CO., LTD.) and PTFE Teflon sheet (Tokyo Garasu Kikai Co., Ltd.) to properly make the specimen. Defoamer BYK-054 (BYK-Chemie GmBH) were used to release air inside the mixture.

2.3   Tools and Techniques

2.3.1   Differential Scanning Calorimetry (DSC)

DSC is a thermo-analytical technique that helped estimating the amount of energy for doping reaction in this study. This estimation plays an important role in controlling the resin properties. The DSC instrument used in this study is DSC-60Plus by Shimadzu Corporation as shown in Figure 2-1. By using this machine, I can study the relation of reaction heat with time and temperature. In order to obtain the heat of reaction, I place two sample pans in the machine. The one on the left side contains nothing inside and is used as a reference. The other on the right side contains 10-20 mg of the sample. Upon running the machine, the difference of heat flux is plotted with the change of time and temperature. The plot is then used for determining the state of doping of the sample for further usage.
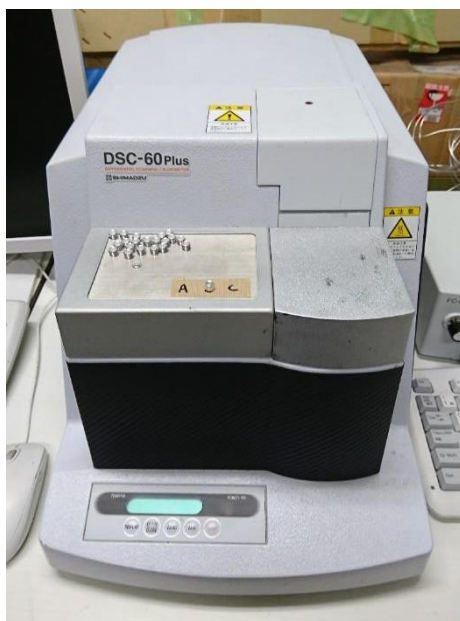
Figure 2-1 DSC instrument

The desirable range of heat from measuring DSC value of PANI-DSC mixture is 80-85 J/g. I need to adjust the doping level to match this range. Depending on the heating time and environmental factors, the doping of PANI-DSC varies greatly. Figure 2-2 and Figure 2-3 show the DSC results with heat value out of our desirable range. When the heat is lower than 80 J/g, the doping level of mixture is too high. This results in strong bond between PANI and DBSA. This made the electrical conductivity decreases. On the other hand, when the heat is over 85 J/g, PANI-DSC will highly likely cure with DSC at undesirable time. Therefore, I need to keep the heat value within the range as shown in Figure 2-4. When I found that the heat is too high, I will heat them in 60℃ for some hours more and check. Once the value fall within the range, the PANI-DBSA will be kept in a zip lock with dehumidifier to prevent changes. If the heat is lower than 80 J/g, I discard the rest of the remaining mixture.
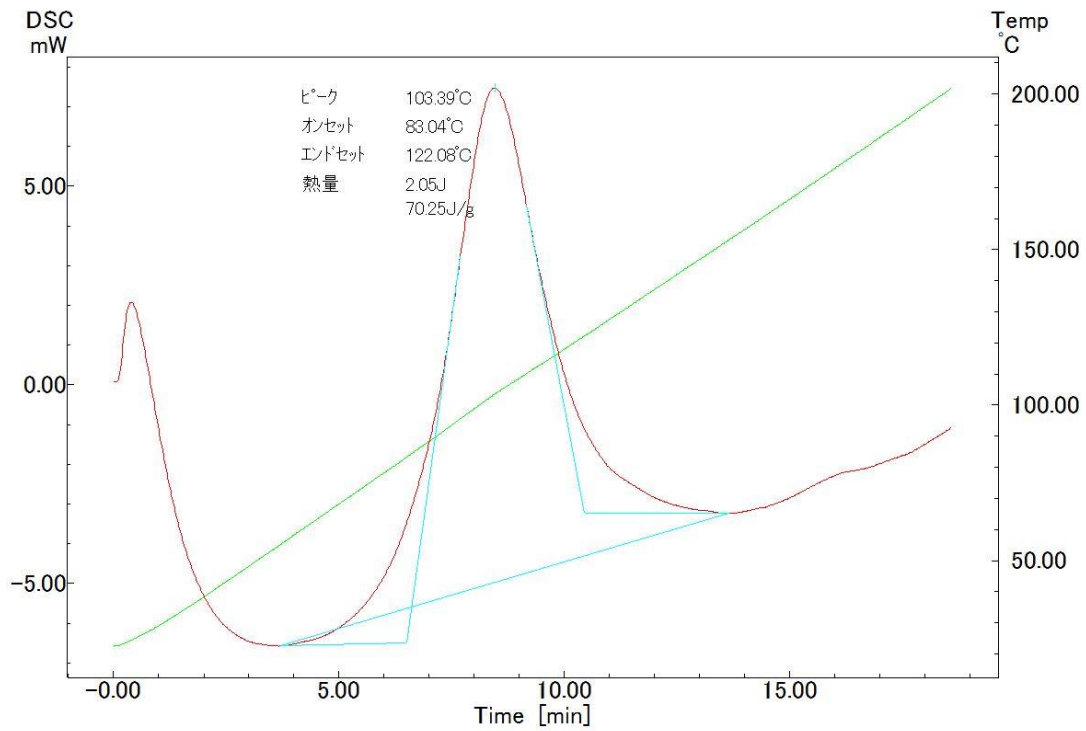
Figure 2-2 Example of DSC results that heat is lower than 80 J/g
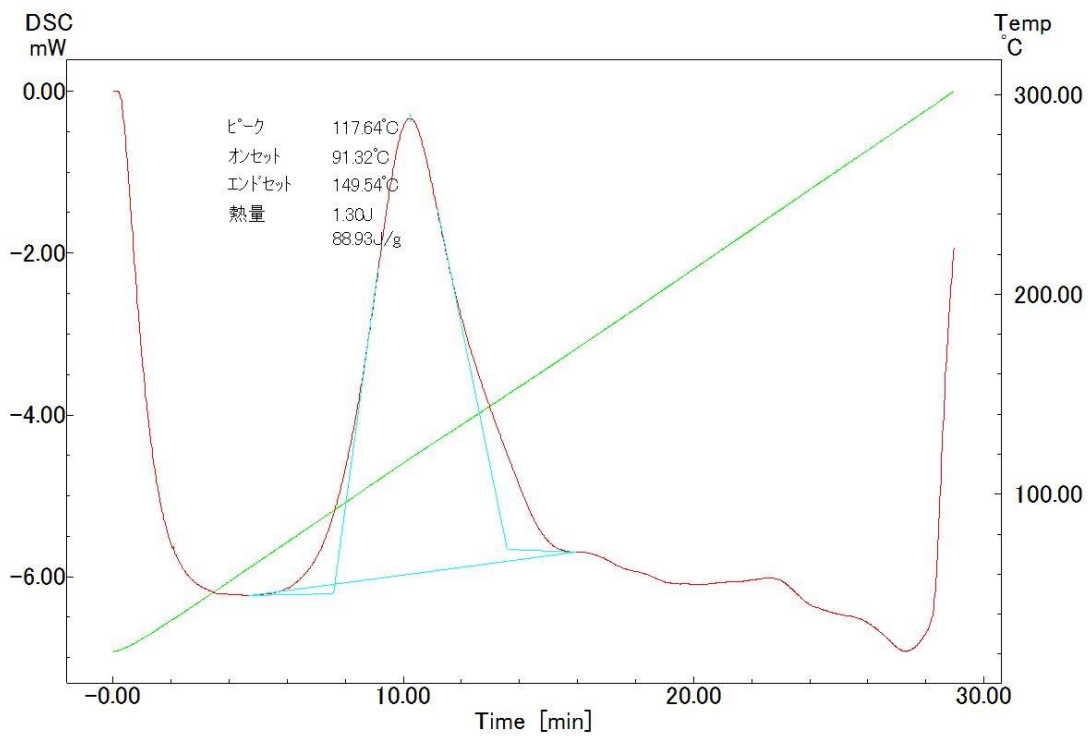
Figure 2-3 Example of DSC results that heat is higher than 85 J/g
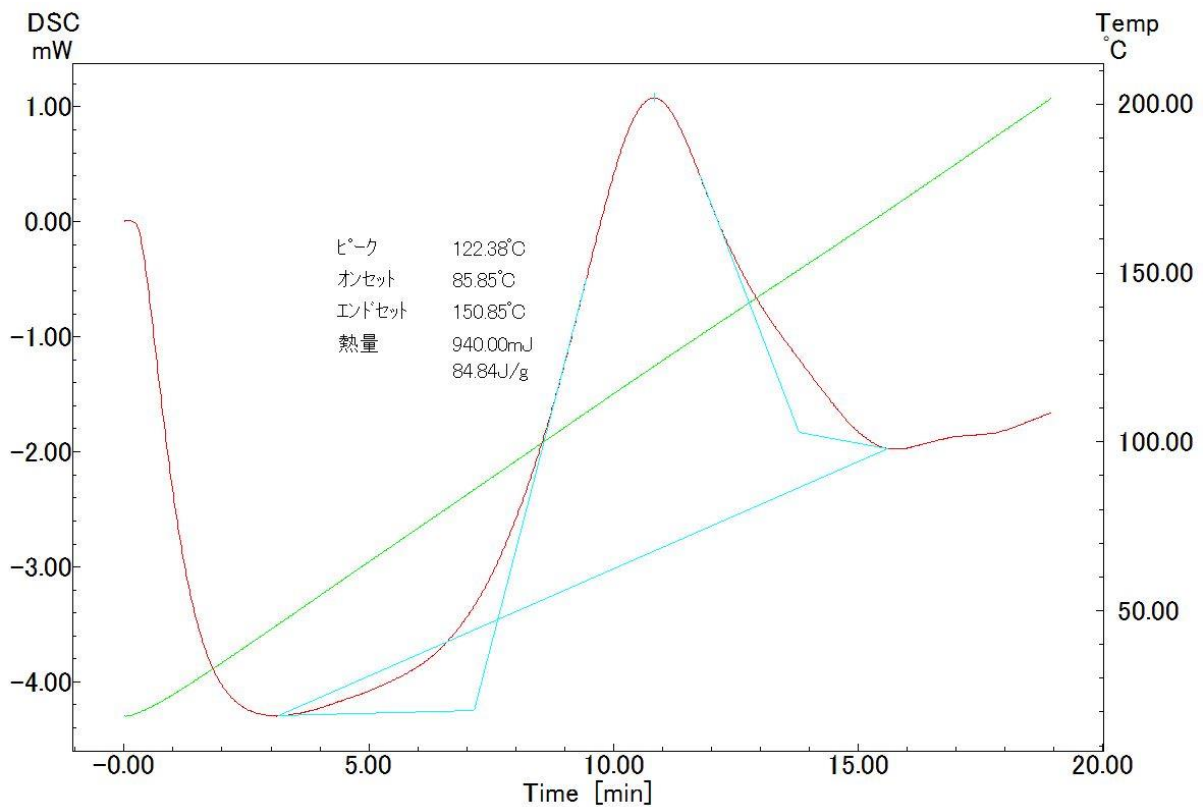
Figure 2-4 Example of DSC results that heat is in the range of 80-85 J/g

2.3.2 Electrical conductivity

Direct current (DC) electrical conductivity of specimens was measured using LCR meter (3522-50 LCR HiTESTER, Hioki E.E. Corporation, Figure 2-5) using four-probe method. The samples were cut into dimension of 25 mm ×25 mm for out-of-plane electrical conductivity and 10 mm × 25 mm for in-plane electrical conductivity. The samples were polished to scrap out the outermost surface before applying DOTITE conductive paste on both surfaces in designated direction. After that aluminium conducting tapes were attached on both surfaces. The applied samples were left for drying overnight to stabilize the paste. Then, the measuring probes were attached to the tapes and read the resistance values. The resistance values were calculated using the dimension of the sample to obtain electrical conductivity.

Figure 2-5 LCR meter

2.3.3 Ultrasonic testing (UT)

Ultrasonic testing (UT) is utilized to examine the internal damage of all specimens before and after the simulated lightning strike test. An ultrasonic flaw detector (HIS3 HF, Krautkramer GmbH) with 3.5 MHz transducer was used to conduct UT. The obtained results are C-scan, the image of the front area of specimen, and B-scan, the thickness direction of specimen. C-scan results show how vast the internal damage in the specimens and B-scan results show how deep the damage in the specimens. The tests results were shown in Chapter 4.

2.4 Fabrication procedures

The fabrication of layer-wise hybrid laminates is separated into 3 main steps: CFRP with PANI-based resin (CF/PANI), CFRP with epoxy resin (CF/Epoxy) and fusing to make layer-wise hybrid laminates (CF/Hybrid).

2.4.1 Development of PANI-based resin

The development of PANI-based resin is adopted from the works of V. Kumar [26], [27], [54]–[56]. The curing condition of PANI-based resin has been modified according to the findings by varying mainly the temperature, heating period and pressure.

In the beginning work of V. Kumar [26], they kept PANI for 2 hours at 40ºC to eliminate moisture and mixed PANI with DBSA with weight ratio of 30:70 according to the processability and molar ratio. The mixture was mixed with DVB with several ratios to investigate mechanical and electrical properties. The samples were put in the hot-press machine at 60ºC for 15 minutes and kept at 120 ºC for 2 hours under pressure of 5 MPa before processing

for measurement. From this, I adopted the process of dehumidification, slow heating as well as heating time, temperature and pressure.

In their next study, V. Kumar [27] compared the properties between making PANI-DBSA mixture by centrifugally-mixing method and roll-milling method. Despite possibility of mass production of roll-milling method, the result reported showed inferior mechanical and electrical properties to centrifugal-mixing method. Therefore, I chose the centrifugally mixing method to make PANI-DBSA mixture. Later on, I also adopted slow cool down as V. Kumar et al. [55] have tried to prevent thermal shock of the specimen.

I also used DSC analysis to control the quality of PANI-DBSA mixture by measuring DSC of the mixture before usage. The DSC value should fall between 80-85 J/g, the most appropriate condition to mix with DVB. According to V. Kumar [56], they have studied the profile of DSC of PANI-DBSA mixtures with different heating time to observe the change of properties over time. The results indicate that the properties change until the threshold and degrade thereafter. This has indicated not only the heating time, but also the important of storage of the mixture before using. DSC has become important in this process. Even though I can observe the physical appearance of PANI-DBSA mixture, I cannot know the quality of the mixture accurately. Using quantitative evaluation such as DSC helps us to decide quickly whether the mixture is ready to use, required more heating time, or should be discarded, which usually happens when the mixture was kept too long time.

Therefore, from the previous development of PANI-based resin, this study adopted several processes: dehumidifying PANI, heating time, temperature, pressure, centrifugal-mixing method, slow cooldown, and DSC analysis. These processes cover the necessary step to manufacture the PANI resin.

In my master thesis, I have involved these factors during fabrication procedure and adjust them when I found a better solution as shown in Figure 2-6, Figure 2-7, and Figure 2-8. In the beginning of the study, CF/PANI were varied the curing temperature and time to find the optimal condition that would achieve high strength and high electrical conductivity. I found that curing CF/PANI at 110 ˚C for 1 hour yield the highest mechanical properties; however, when combine with the curing time of CF/Epoxy, the electrical conductivity became very low. To tackle these problems, the total curing time needed to be adjusted. Furthermore, the interface between CF/PANI and CF/Epoxy were weak and needed improvement (Figure 2-6).
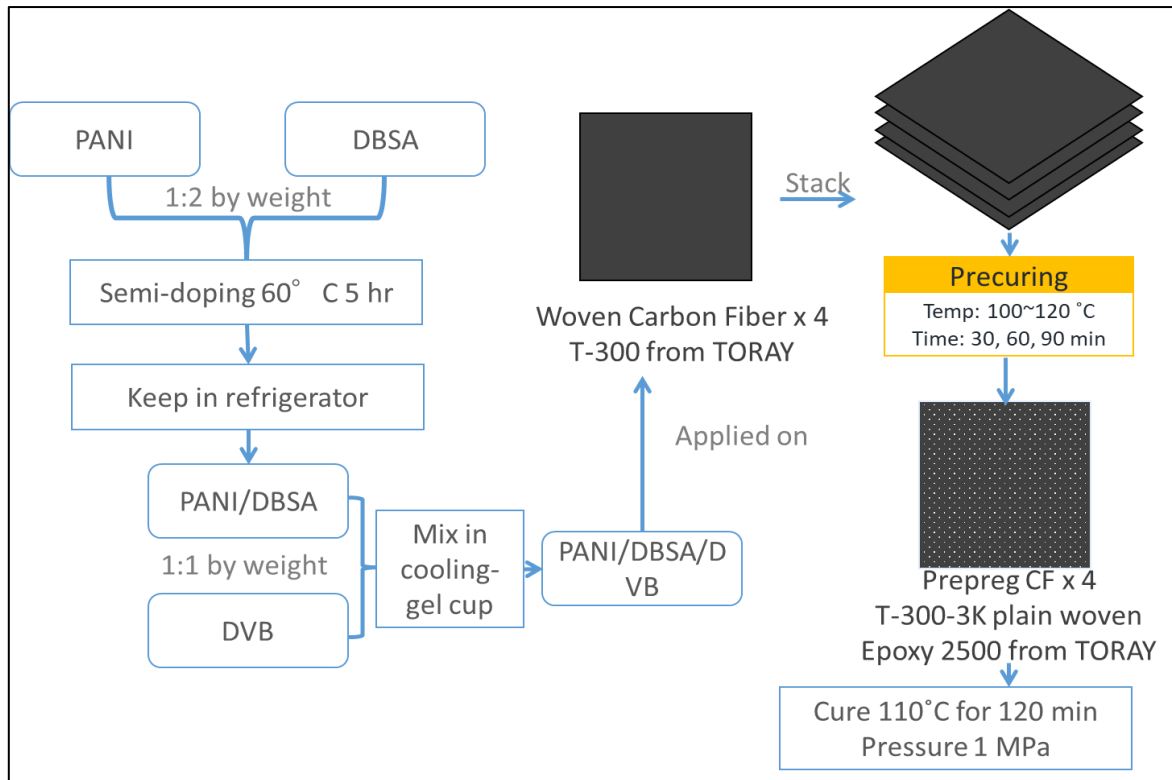
Figure 2-6 Fabrication procedure during primary study-I

From the previous lessons, the curing temperature is fixed at 110 ˚C for 1-1.5 hours. After finished curing, the surface of CF/PANI is treated with sandpaper #1000 to increase mechanical locking as well as prevent excessive coating of PANI-based resin from adhesion. Then, a layer of adhesive film was placed and co-cured with CF/Epoxy prepreg. The pressure of 1 MPa was used to ensure the uniform thickness of the specimens. With this method, the total curing time of CF/PANI was 3 hours and the electrical conductivity remained in the specimens. Also, the interfacial properties were improved by inserting adhesive film, too. This procedure was shown in Figure 2-7. During the experiment, I found that the CF/Epoxy prepreg was running out, so I tried another method to see if the fabrication procedure is suitable with other kind of CF/Epoxy made by other methods.

Figure 2-8 shows the outline of secondary curing method. Firstly, the CF/PANI were made and scrubbed its surface to prepare for attaching with adhesive film. Also, CF/Epoxy was cured separately to a certain level. After that both CF/PANI and CF/Epoxy were co-curing with adhesive film to attach together. In this study, the fabrication procedure is similar to this one. The main difference was the method to made CF/Epoxy.
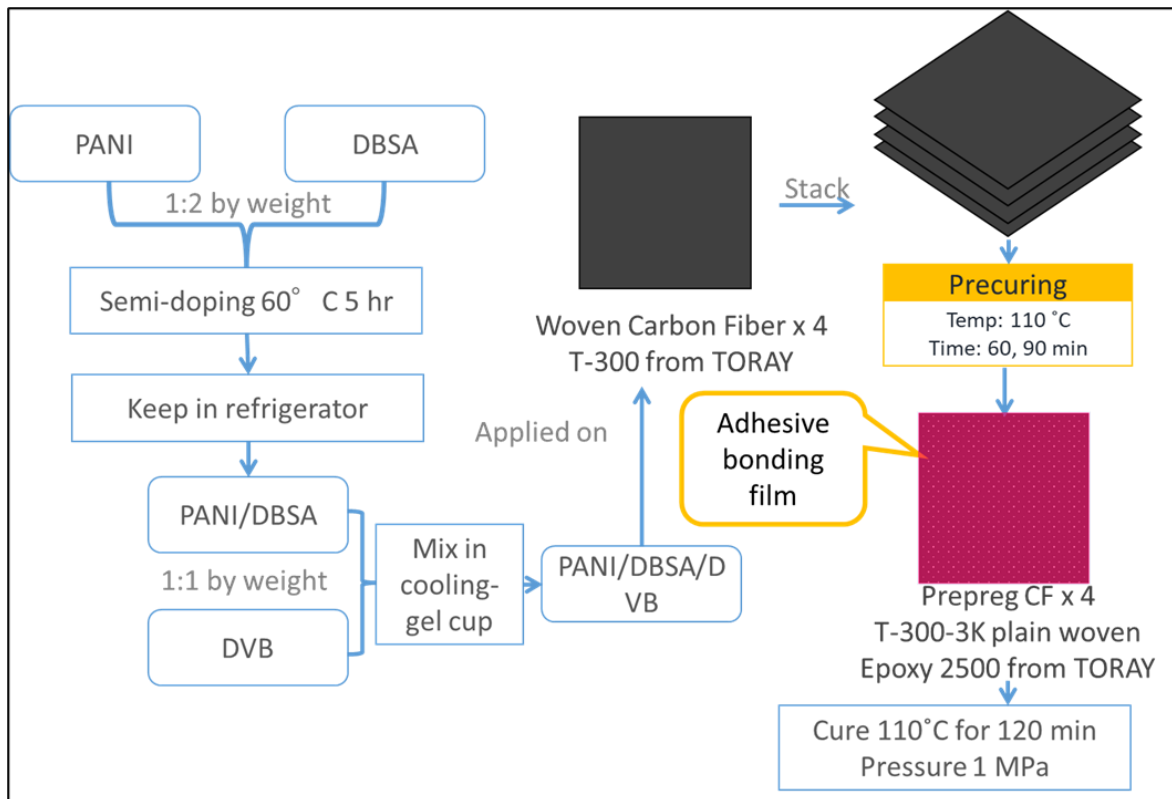
Figure 2-7 Fabrication procedure during primary study-II
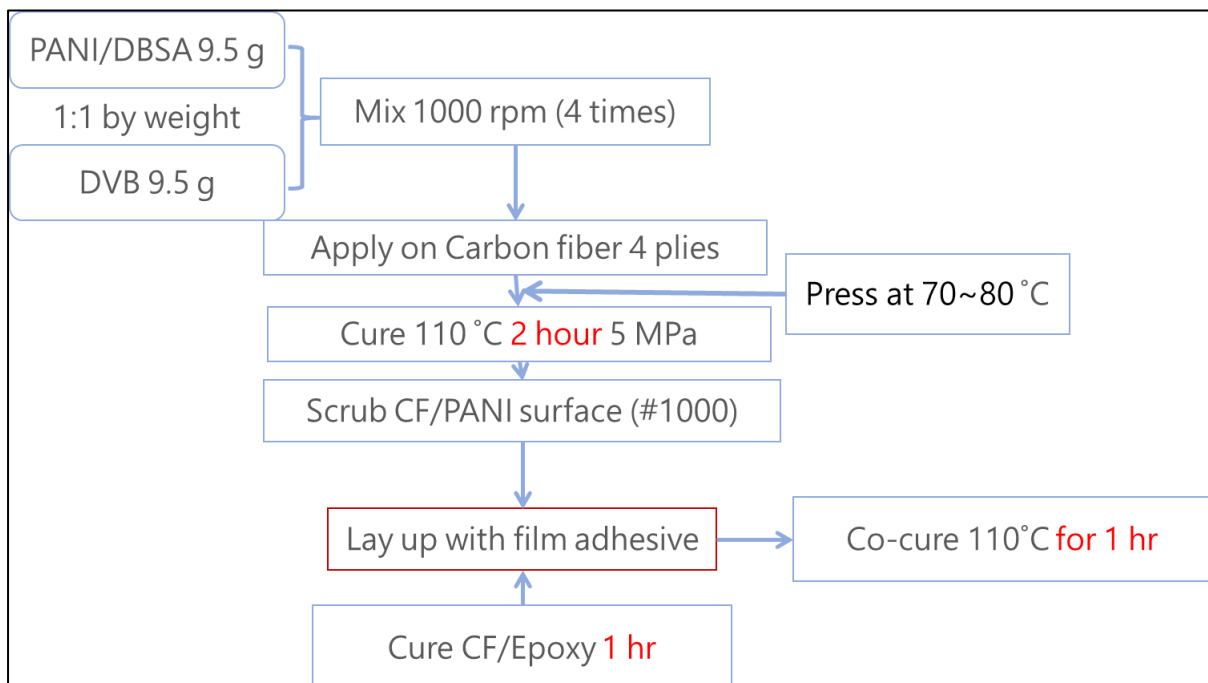
Figure 2-8 Fabrication procedure during primary study-III

2.4.2 CFRP with PANI-based resin (CF/PANI)

Polyaniline (PANI) is sensitive to moisture and this will greatly affect the properties of the resin. Prior to processing, PANI powder was kept in an oven at 60ºC for around 24 hours to eliminate moisture effect. Dried PANI was mixed with dodecylbenzene sulfonic acid (DBSA), a dopant of PANI, in the weight ratio of PANI (30 wt. %) and DBSA (70 wt. %), using centrifugal mixer at 2000 rpm for a few minutes until the mixture becomes homogeneous viscous liquid. The PANI-DBSA mixture was spread on Teflon sheet to and pressed to uniform thickness. After that, it was heated at 60 ºC for 4-6 hours to dope the mixture. In order to obtain stable mixture for the next step, DSC measurement plays an important role to determine the heat of reaction in doping reaction. Therefore, before proceeding further, the doped mixture is always measured its DSC value. The suggested range is between 80-85 J/g. If the value is higher, the mixture will not be stable and hardened easily. If the value is lower, the mixture will be stable yet difficult to mix. Usually, I can obtain such range of DSC from the specimen that was kept within one week. The longer the time I kept, the lower the DSC value became.

Upon confirming the DSC value, PANI-DBSA mixture was then mixed with divinylbenzene (DVB) in the weight ratio of PANI-DBSA (50 wt. %) and DVB (50 wt. %). As both substances were difficult to mix by using centrifugal mixer only, a cold mortar and pestle was used to break the agglomerate as well as unify both substances. The cold mortar and pestle were used in order to delay the increase in temperature during mixing and to prevent undesirable curing. Then, the mixture was transferred to a mixing cup with cooling gel and a few drops of defoamer BYK were added into it. The mixture was mixed at 1000 rpm for 4 minutes (1 minute for four times).

I impregnated carbon fibre woven fabric with the resin by applying and spreading resin into the fabric uniformly and thoroughly on both sides. The weight of the resin was controlled to be around 50% of the fabric weight. The impregnated fabrics were stacked into $[0/90]_n$, where n is the number of plies (n = 1, 2, and 4), and rolled to remove air inside. After stacking to the desired number of plies, the stack of impregnated fabrics was pressed into a hot-press machine with 5 MPa pressure. The hot-press machine was then set the temperature to 120 ºC with temperature increasing rate 10 ºC/min. After temperature reached 120 ºC, the stack was kept for 1 hour. Subsequently, the hot-press machine was turned off, but the stack was kept for another 30 minutes to cool down slowly and avoid an effect of thermal shock from abrupt temperature change.

For making pristine CF/PANI, after removing CF/PANI from the hot-press machine, the CF/PANI was further heated in the hot-press machine at 110 ºC with 5 MPa pressure to undergo the same condition as CF/hybrid.

2.4.3 CFRP with epoxy resin (CF/Epoxy)

To make CFRP, I have used 2 methods: prepreg and Vacuum assisted resin transfer moulding (VaRTM). I apt VaRTM method to make CF/Epoxy with CF fabric. Using prepreg is fast and convenient in manufacturing point of view, but when it comes to complex shape, VaRTM will be more advantage. However, in this preliminary study, I focus only one simple hybrid laminate structure.

CF/Epoxy was fabricated using Vacuum assisted resin transfer moulding (VaRTM) methods [5]. An aluminium plate was prepared by cleaning with ethanal and applying releasing agent to prevent epoxy resin stick to the plate. Several materials were placed as following order (Figure 2-9): Aluminium plate, distribution media, poreflon sheet, breather cloth, and woven carbon fibre fabrics $[0/90]_n$ (n = 4, 6, and 8). The edges of the breather clothes were sealed with clay-like sealants. In the extra area of the distribution media, a piece of cotton was put to prevent resin flowing into the outlet vacuum tube. Next, the carbon fibre fabrics were covered by breather cloth and distribution media. The whole working area was covered by a large vacuum bag. In order to generate vacuum pressure inside, the vacuum bag was cut open at the position of cotton, connected with an outlet vacuum pump and sealed with the sealants to prevent air leakage. The vacuum pump was turned on to check leakage. Any leakage should be sealed to prevent undesirable resin flow. At the centre of the carbon fibre fabrics, the vacuum bag was cut open to connect a tube for transferring resin and sealed with the sealants. This tube should be kept closing (No flow of resin) and placed at a high position while the vacuum condition inside the vacuum bag was being checked.
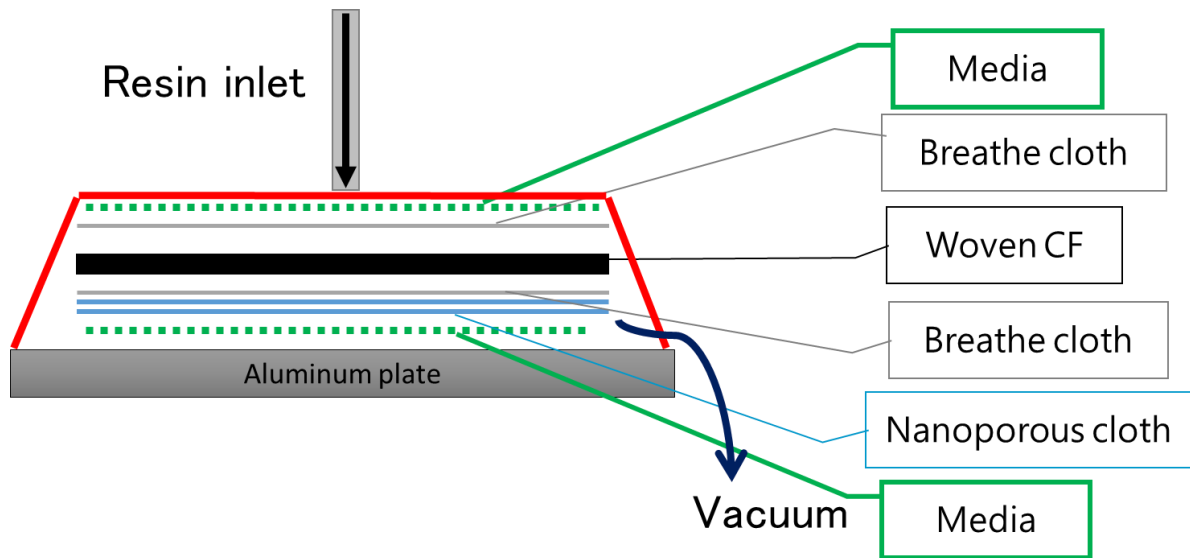
Figure 2-9 Configuration of VaRTM method

Epoxy resin was prepared by first weighting a mixing cup and recorded the weight of the empty cup. Later, the weight was used to calculated the transferred resin amount into the panel. Epoxy XNR6815 and hardener XNH6815 were mixed in the weight ratio of 100:27. The mixed resin was vacuumed 10 minutes or more to eliminate bubbles inside. After that, the resin cup was moved to the working area and dipped with the tube for transferring resin. The tube was opened to let the resin flow and impregnate the carbon fibre fabrics. After the resin impregnated the fabrics thoroughly, the tube was closed again. The resin was left to harden for at least 6 hours. The hardening time depends on the environmental temperature. When resin became hard, the CF/Epoxy was removed from the mould and used for the next processes. The CF/Epoxy may be heated in an oven at 60 ℃ to ensure that the resin is completely hardened.

2.4.4 Bonding procedure

In order to assemble CF/PANI and CF/Epoxy, I can either co-cure the uncured CF/PANI with CF/Epoxy prepreg (primary bonding) or co-cure the CF/PANI and CF/Epoxy using an adhesive film (secondary bonding). In the previous study, I have tried both methods while developing an appropriate method to fabricate CF/Hybrid.

I found that secondary bonding by incorporating adhesive film during curing results in better mechanical properties. I have compared the specimen adhered together by the resin of CF/Epoxy prepreg with the specimen adhered together by adhesive film. Due to insufficiency

of materials, I changed the fibre fabric from Toray T300 to Rayon TR30. As I do not have Rayon TR30 prepreg, I changed the fabrication method to VaRTM and use secondary to adhere both layers.

2.4.5   Layer-wise hybrid laminates (CF/Hybrid)

After preparing CF/PANI and CF/Epoxy from as aforementioned, layer-wise hybrid laminates can be fabricated by using adhesive film. The adhesive film (3M Scott-Weld AF163-2k0.600) of the same size as the CF/Epoxy and CF/PANI panels was placed between both panels. This stacking was covered with Teflon sheet on both sides to prevent the adhesive stick to the hot-press machine. This sandwich structure was cured in the hot press machine at 110 ºC for 2 hours with 5 MPa pressure. After 2 hours, the hot-press was turned off and the CF/Hybrid panel was left to slowly cool down for 30 minutes. The CF/Hybrid was then processed to prepare for other testing.

Note that CF/Hybrid consists of insulating layers of adhesive film and CF/Epoxy; therefore, measurement out-of-plane electrical conductivity will give different result with measuring only electrically conductive CF/PANI sub laminates. In order to obtain the electrical conductivity of CF/PANI from the same condition, some part of CF/PANI was cut out, covered with Teflon sheet, and placed together with the CF/Hybrid during curing period.

2.5   Summary

In this chapter, the fabrication procedures of CF/Hybrid have been introduced. The characterization and optimization are essential to evaluate the suitability of this structure for further application. The techniques of mechanical characterization are described in details. This chapter has explained the procedures to prepare the matrix, the composites, and the final laminates. The results and analysis obtained through these techniques are shown in further sections.

Chapter 3   Mechanical properties

3.1   Introduction

I have introduced how to fabricate layer-wise hybrid laminates in the previous chapter. In this chapter, I will introduce the characterization of the specimens and discuss the results obtained.

3.2   Four-point bending

Mechanical properties are significant for structural applications of materials. In this study, I characterized flexural properties and interfacial properties of the hybrid laminates. Flexural properties are measured according to JIS K7074 standard for four-point bending using a universal testing machine (Instron 5582). The test configuration is shown in Figure 3-1.The dimensions of the samples are 150 mm in length, 15 mm in width and 0.7-2.5 mm in thickness. The load cell of 5 kN is installed and the crosshead speed is fixed at 5 mm/min. The radii of loading heads and supporting heads are set at 3 mm. The span length for specimens which are thicker than 1.6 mm is 81 mm. If the thickness is less than 1.6 mm, the span length is calculated using formula ($l = 40h + 20$), where l is the span length [mm] and h is the thickness of specimen [mm]. The loading span is also calculated according to the new span length. At least two samples were measured to get an average of property. The measurement yields load and displacement data. I then use this data to obtain flexural modulus [GPa] and bending strength [MPa]. The mode of failure is also recorded for further analysis.
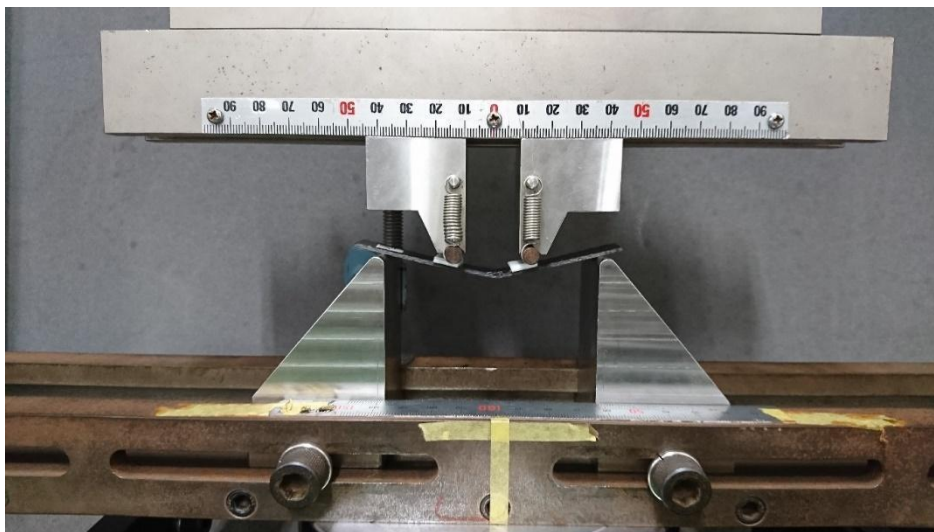
Figure 3-1 Four-point bending setup

I conducted the four-point bending test on pristine 8 sets of specimens: CF/PANI, CF/Epoxy, and 6 cases of CF/Hybrid. For each batch of CF/Hybrid specimens (i.e., CF/Hybrid-4P4E, CF/Hybrid-2P6E, and CF/Hybrid-1P7E), the specimens were separated into 2 sets to conduct the test on both sides of specimens: with CF/PANI on top and with CF/Epoxy on top. I wanted to observe if the test configuration results in different properties.

3.2.1 Results and Discussion

After conducting the test, I found that the bending strength of CF/Hybrids varies mainly with the number of CF/Epoxy layers as shown in the Figure 3-2. The pristine CF/PANI and CF/Epoxy are shown on the furthest sides for comparison. Each batch of CF/Hybrids was tested on both sides with CF/PANI on top (represented in yellow bar) and CF/Epoxy on top (represented in grey bar). I observed that the testing on the different sides of CF/Hybrid, even cut from the same panel, shows different results. In every case, the bending strength of the specimens tested with CF/PANI on top yields lower value compared to the bending strength of specimens tested with CF/Epoxy. This is because the compressive strength of CF/PANI layer is much lower than that of CF/Epoxy layer as seen in CF/PANI-8L. I can observe this from the failure of the specimens in Figure 3-3, Figure 3-5, and Figure 3-7 as well as their load-displacement curves in Figure 3-4,Figure 3-6, and Figure 3-8 respectively. All the specimens tested on CF/PANI sides failed by the compressive failure within CF/PANI sub-laminates only. This can be seen as cracks at the middle of the specimens. The crack did not propagate further into the CF/Epoxy. On the other hand, the failure of the specimens tested with CF/Epoxy on top are delamination or fibre breakage as shown in Figure 3-9, Figure 3-11, and Figure 3-13 as well as their load-displacement curves in Figure 3-10, Figure 3-11, and Figure 3-12. The delamination indicated that the interlaminar properties are lower than the strength of CF/PANI because the CF/PANI at the lower part remains intact. The fibre breakage has shown that the specimens also behave like pristine CF/Epoxy. Note that the failure defined in this experiment were initial failure of the specimens. The ultimate failure of the specimens was not shown, especially CF/Hybrid tested on CF/PANI. This is because the CF/Epoxy parts remained intact. To sum up, CF/PANI has low compressive strength, but comparatively high tensile strength.
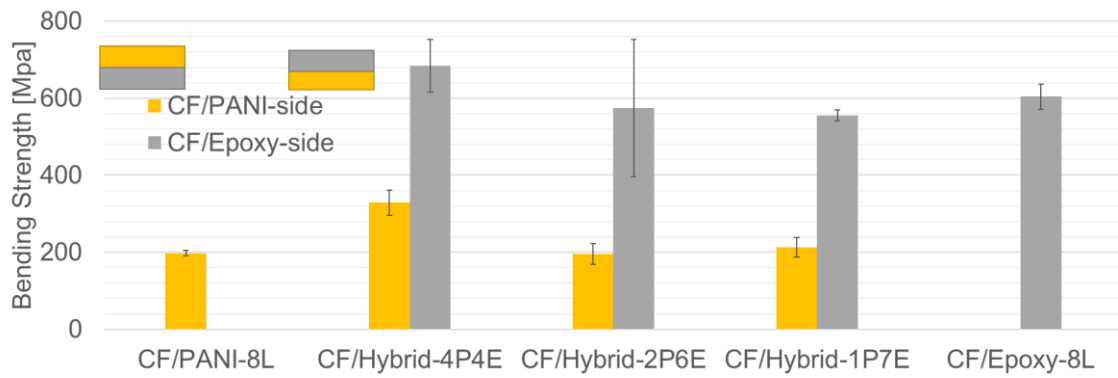
Figure 3-2 Results of four-point bending test

Table 3-1 Thickness and modes of failures in four-point bending test

	CF/PANI	CF/Hybrid-4P4E	CF/Hybrid-2P6E	CF/Hybrid-1P7E	CF/Epoxy
Thickness [mm]	1.540	2.016	2.176	2.290	2.066
Failure on CF/PANI	Compressive	Compressive	Compressive	Compressive	
Failure on CF/Epoxy		Delamination/ Fibre breakage	Delamination/ Fibre breakage	Delamination/ Fibre breakage	Fibre breakage

Figure 3-3. Cross-sectional image of CF/Hybrid-4P4E after four-point bending on CF/PANI
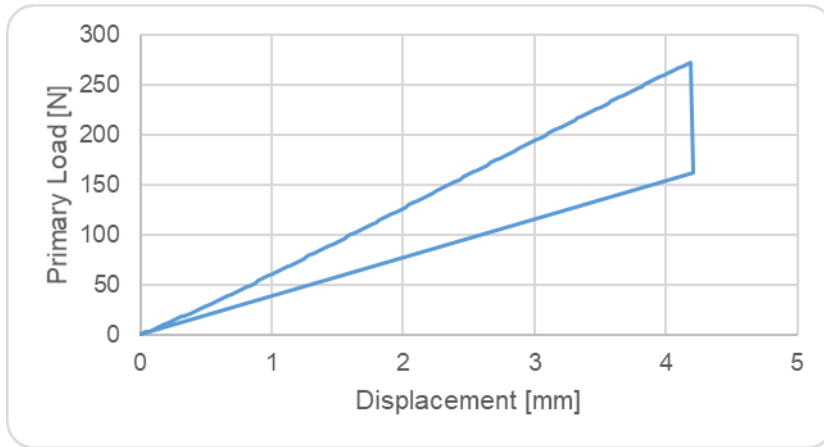
Figure 3-4 Load-displacement curve of CF/Hybrid-4P4E on CF/PANI
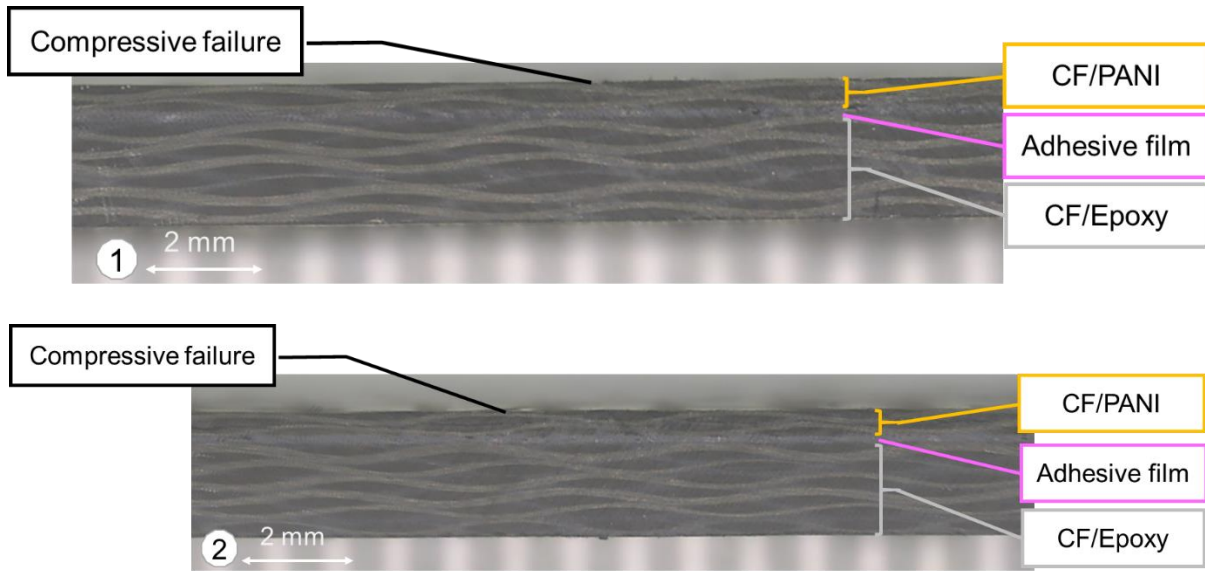
Figure 3-5. Cross-sectional image of CF/Hybrid-2P6E after four-point bending on CF/PANI
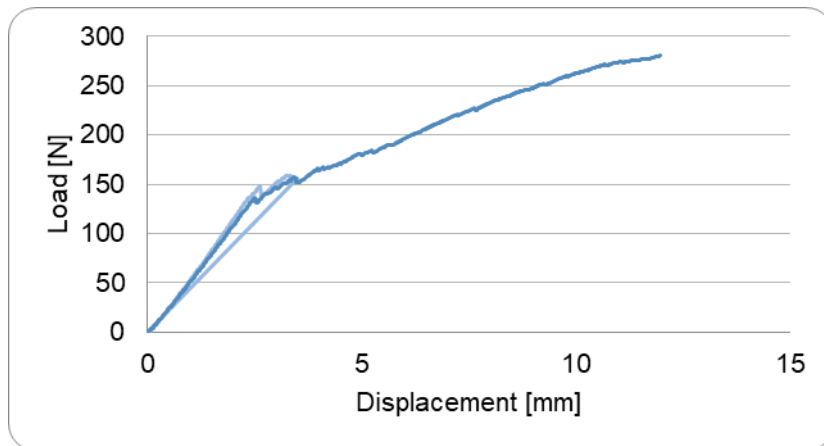
Figure 3-6 Load-displacement curve of CF/Hybrid-2P6E on CF/PANI
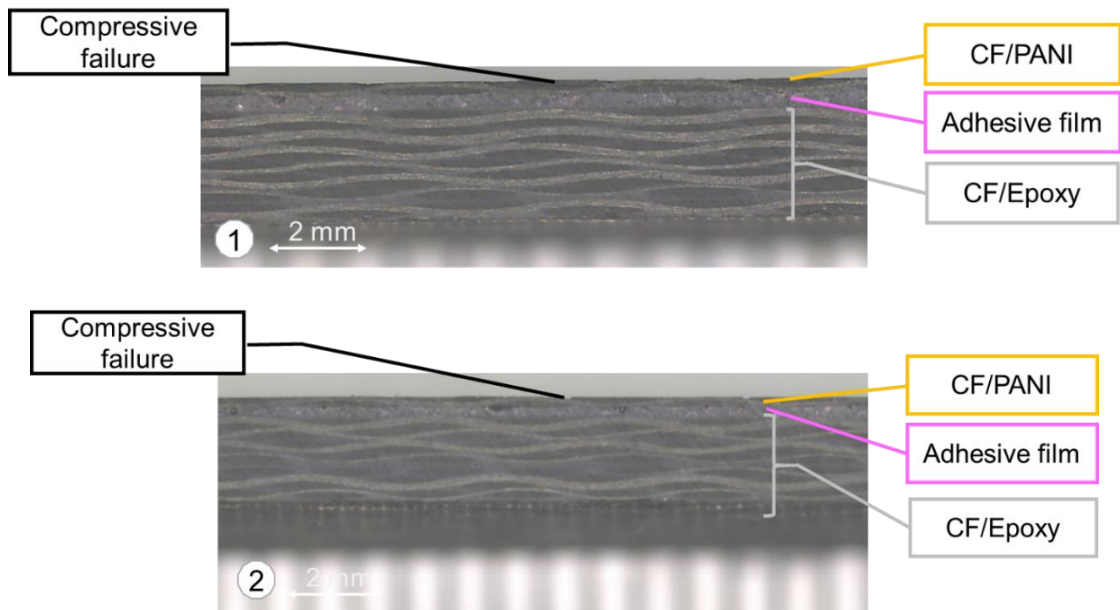
Figure 3-7. Cross-sectional image of CF/Hybrid-1P7E after four-point bending on CF/PANI
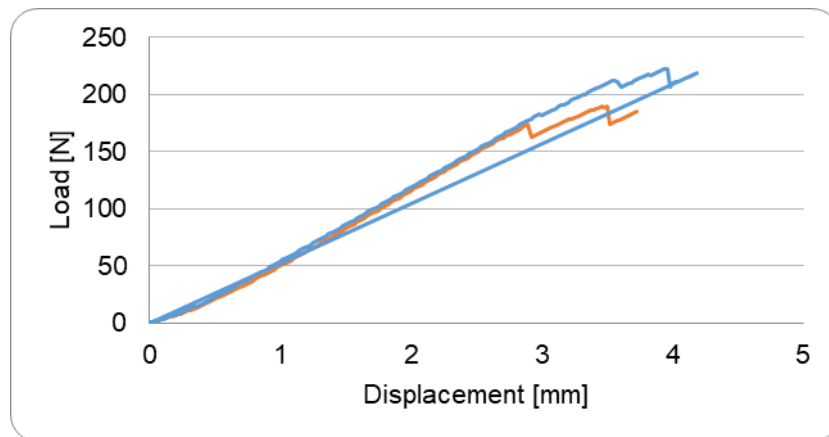
Figure 3-8 Load-displacement curve of CF/Hybrid-1P7E on CF/PANI
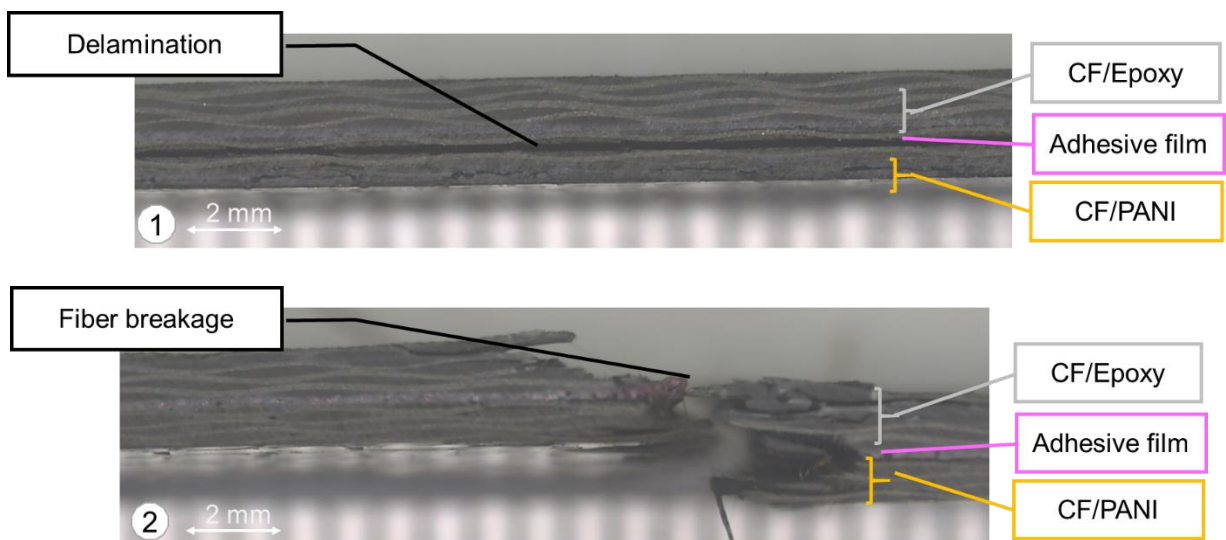
Figure 3-9 Cross-sectional image of CF/Hybrid-4P4E after four-point bending on CF/Epoxy
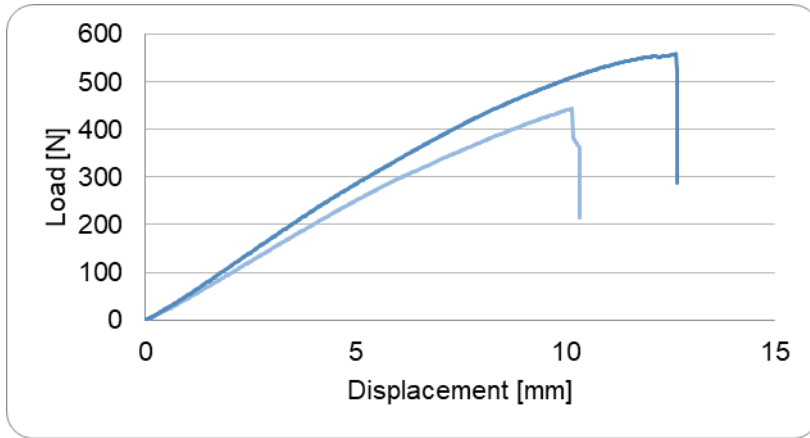
Figure 3-10 Load-displacement curve of CF/Hybrid-4P4E on CF/Epoxy
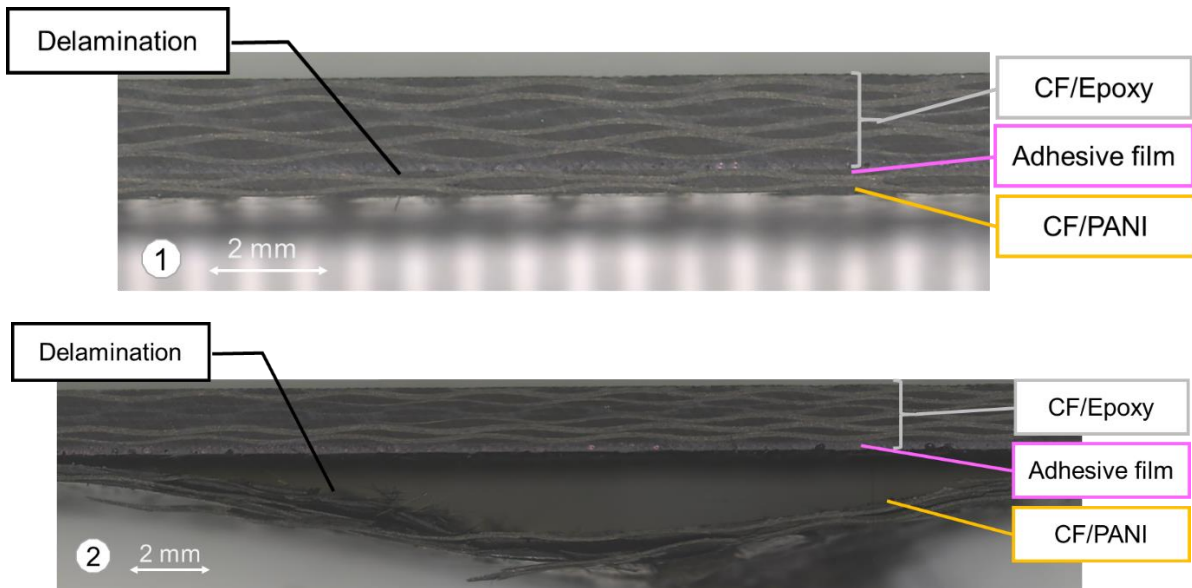
Figure 3-11 Cross-sectional image of CF/Hybrid-2P6E after four-point bending on CF/Epoxy
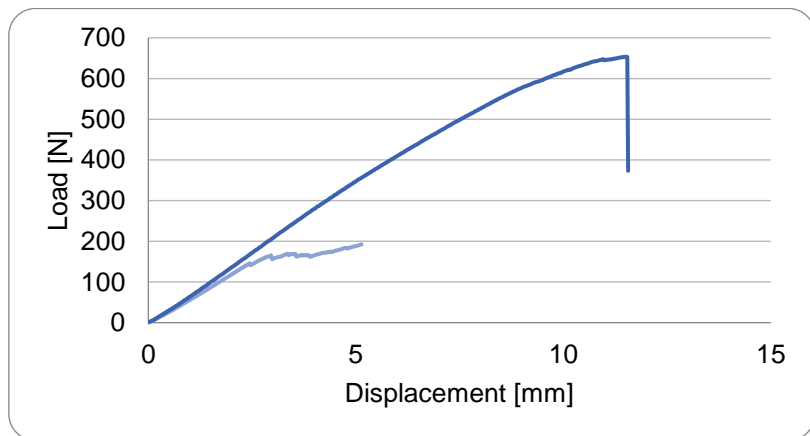
Figure 3-12 Load-displacement curve of CF/Hybrid-2P6E on CF/Epoxy
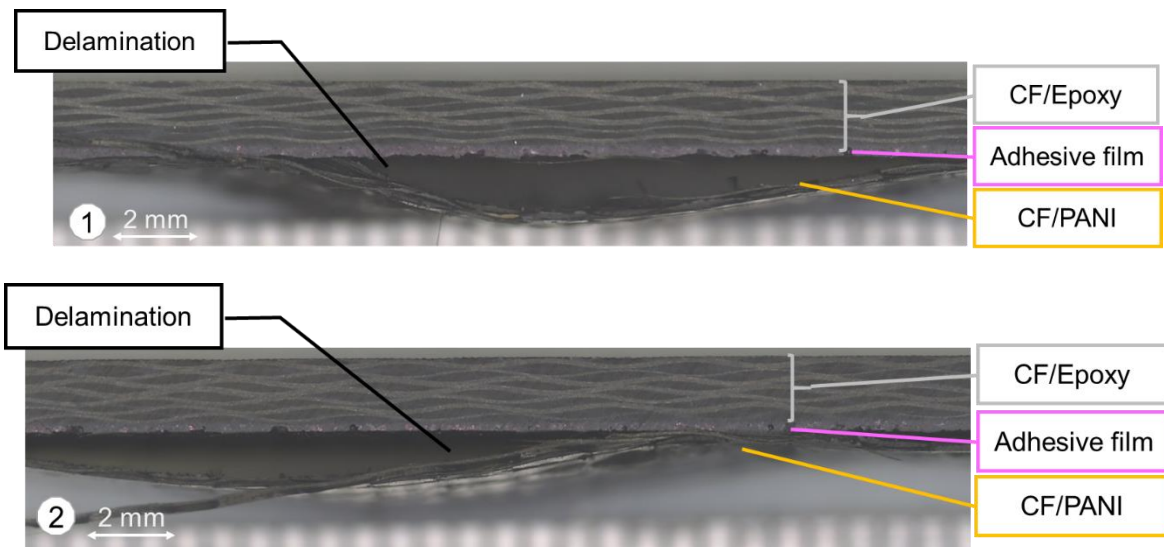
Figure 3-13 Cross-sectional image of CF/Hybrid-1P7E after four-point bending on CF/Epoxy
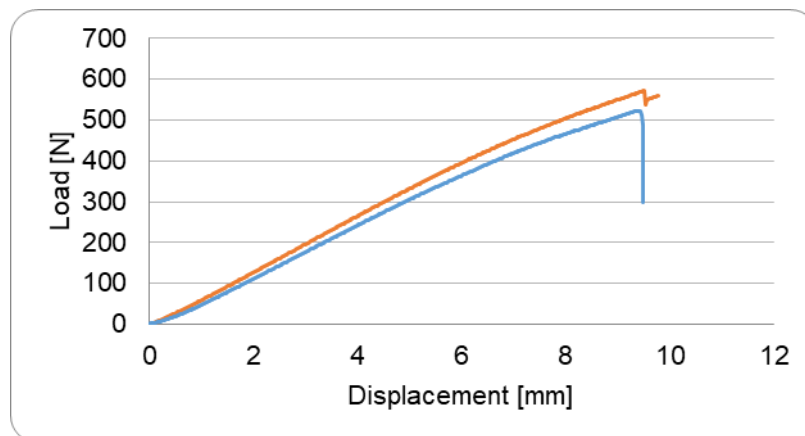
Figure 3-14 Load-displacement curve of CF/Hybrid-1P7E on CF/Epoxy

When looking at the overall improvement of CF/Hybrid, CF/hybrids tested on the CF/PANI side do not improve their properties much, but I can see that the properties do not reduce much even though I use a smaller number of CF/PANI. I can say that by incorporating CF/Epoxy, hybrid laminates can mitigate the reduction of the strength. To put this structure into practice, the configuration needs to be considered. As the calculation of bending strength included the dimension of specimens with assumption of the whole specimens are homogeneous, the bending strength may deviate from the true values that occur in specimens.

Taken neutral axis into account, bending stresses throughout the cross-section of specimens are varied. According to composite beam theory, the stresses distributed unsymmetrically with abrupt change at the interfacial connection. To observe how much

40

different, the calculation using beam theory was performed. Figure 3-15 shows the diagram of dimension used for calculation in both specimens testing on CF/PANI and CF/Epoxy. The nomenclature of the parameters is as follows.

- b: width

- h_1: thickness of material 1 (upper part)

- h_2: thickness of material 2 (lower part)

- E_1: Flexural modulus of material 1

- E_2: Flexural modulus of material 2

- h_{na}: Distance of upper edge to neutral axis

- $\sigma_{X, A}$: Stress of material X at position A

For calculation, the flexural moduli were obtained from testing the pristine specimen and the values are 63.1 GPa for CF/PANI and 43.0 GPA for CF/Epoxy. The span length (l) was kept as 81 mm. By using composite beam theory, the neutral axis can be obtained from

$$h_{na} = \frac{E_1 b h_1 \left(\frac{h_1}{2}\right) + E_2 b h_2 (h_1 + \frac{h_2}{2})}{E_1 b t_1 + E_2 b t_2} \tag{1}$$

Then, the moment of inertia at the centroid of each material are

$$I_1 = \frac{bh_1^3}{12} + bh_1 \left(h_{na} - \frac{h_1}{2}\right)^2 \tag{2}$$

$$I_2 = \frac{bh_2^3}{12} + bh_2 \left(h_1 + \frac{h_2}{2} - h_{na}\right)^2 \tag{3}$$

The moment asserting on specimen at the loading point is

$$M = \frac{1}{6} P_{max} l \tag{4}$$

The stress at the loading point is

$$\sigma_{x1} = -\frac{MyE_1}{E_1I_1 + E_2I_2} \tag{5}$$

$$\sigma_{x2} = -\frac{MyE_2}{E_1I_1 + E_2I_2} \tag{6}$$
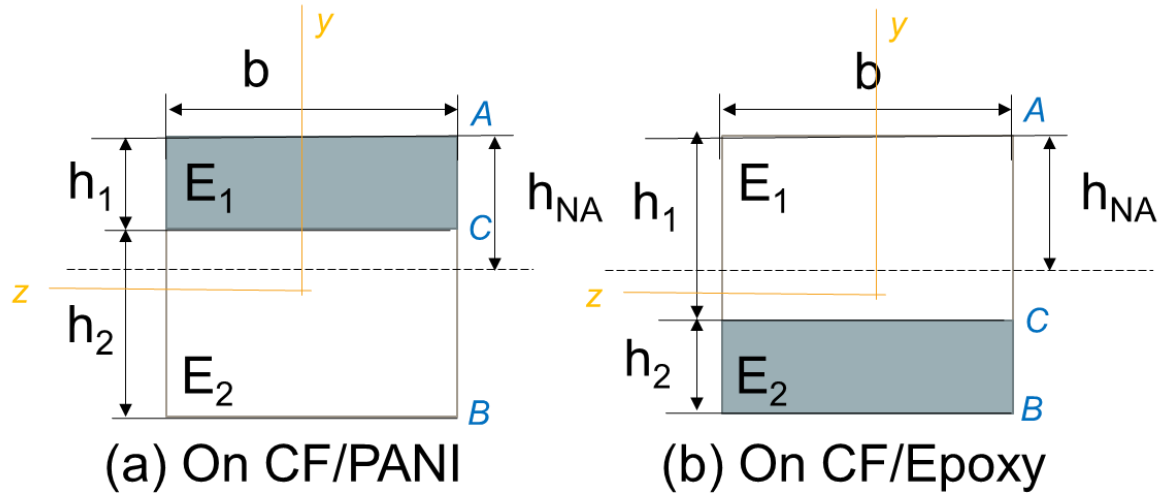
Figure 3-15 Diagram of parameters in the calculation of neutral axis of CF/Hybrid specimen testing on (a) CF/PANI side and (b) CF/Epoxy side

Table 3-2 Dimension of sublaminates and distance to neutral axis

Thickness [mm]	CF/Hybrid-4P4E	CF/Hybrid-2P6E	CF/Hybrid-1P7E
$h_{CF/PANI}$	0.780	0.387	0.206
$h_{CF/Epoxy}$	1.240	1.790	2.084
h_{na} (on CF/PANI)	0.915	1.020	1.103
h_{na} (on CF/Epoxy)	1.105	1.157	1.187

By using the aforementioned equations and dimensions, the neutral axes of each laminate can be obtained as shown in Table 3-2. With the neutral axes, the stress at point A, B, and C in Figure 3-15 can be obtained as shown in Table 3-3 for CF/Hybrid tested on CF/PANI and in Table 3-4 for CF/Hybrid tested on CF/Epoxy. From the results, it is clear that the stress values are slightly deviated from the maximum stresses calculated during the test (shown as Max test stress in the tables).

42

Table 3-3 Stresses on CF/Hybrid tested on CF/PANI

On CF/PANI	CF/Hybrid-4P4E	CF/Hybrid-2P6E	CF/Hybrid-1P7E
Max Load [N]	269	169	206
Max test stress	328	194	212
$\sigma_{PANI, A}$ [MPa]	394	228	273
$\sigma_{PANI, C}$ [MPa]	58.2	142	222
$\sigma_{Epoxy, C}$ [MPa]	39.7	96.5	151
$\sigma_{Epoxy, B}$ [MPa]	324	176	200

Table 3-4 Stresses on CF/Hybrid tested on CF/Epoxy

On CF/Epoxy	CF/Hybrid-4P4E	CF/Hybrid-2P6E	CF/Hybrid-1P7E
Max Load [N]	501	546	547
Max test stress	684	573	554
$\sigma_{Epoxy, A}$ [MPa]	604	571	532
$\sigma_{Epoxy, C}$ [MPa]	74.0	313	402
$\sigma_{PANI, C}$ [MPa]	109	459	589
$\sigma_{PANI, B}$ [MPa]	735	739	725

In this study, I keep the number of the whole laminate at 8 layers due to the requirement of the lightning strike test, in which the entire thickness of the panel should not be larger than 2-3 mm. I made a decision to vary both CF/PANI and CF/Epoxy to differentiate both conductive layers and structural layers. However, for clearer results, the number of CF/Epoxy should be fixed, so that I can compare the properties distinctively. For example, I keep the number of CF/Epoxy layers at 4 layers and vary CF/PANI from 1,2, and 4 layers, so that I can clearly state how many conductive layers are required for lightning strike protection. From the given results, I can imply that to sustain the application of CF/Hybrid when put into practice, I

should use at least 4 layers of CF/PANI. This is because they can sustain the highest bending strength value when testing on both CF/PANI and CF/Epoxy. However, this study did not consider the acoustic shock which is a unique type of loading during the lightning strike. Pursuing such characterization would be valuable for the development of aircraft structures for lightning strike protection.

3.2.2 Flexural Modulus

The flexural properties of CF/Hybrid decrease with the higher number of constituent CF/Epoxy as shown in Figure 3-16. Interestingly, the flexural moduli of CF/Hybrid on both sides yield similar values. This is because the CF/Hybrid behaviour is similar to a composite beam where both properties have an effect on the overall properties. That is the flexural modulus of each material contributes to the final properties. Although the values are similar in each case, I can see the difference in the same batch of specimens tested on the different side, i.e., CF/PANI on top and CF/Epoxy on top.
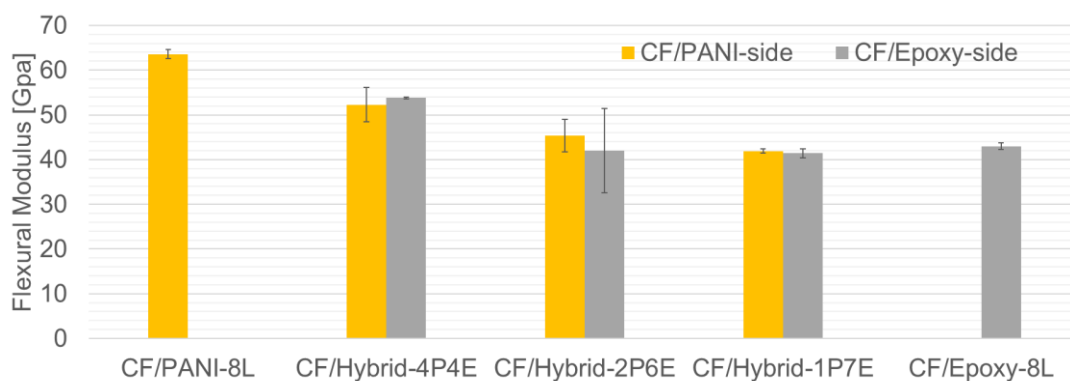
Figure 3-16 Results of flexural modulus

I have validated the properties using the calculation of composite beam theory using the flexural moduli of pristine CF/PANI and CF/Epoxy and the results are shown in Figure 3-17. The combined flexural moduli tend to decrease with a greater number of CF/Epoxy due to larger overall thickness. These results agree with the experimental results as compared in the figure. In the case of more CF/Epoxy, the experimental results show lower values than the calculated one. This is because the composite beam theory usually uses tensile modulus to calculate, but I used the bending properties to calculate: therefore, the values deviated from the actual ones.
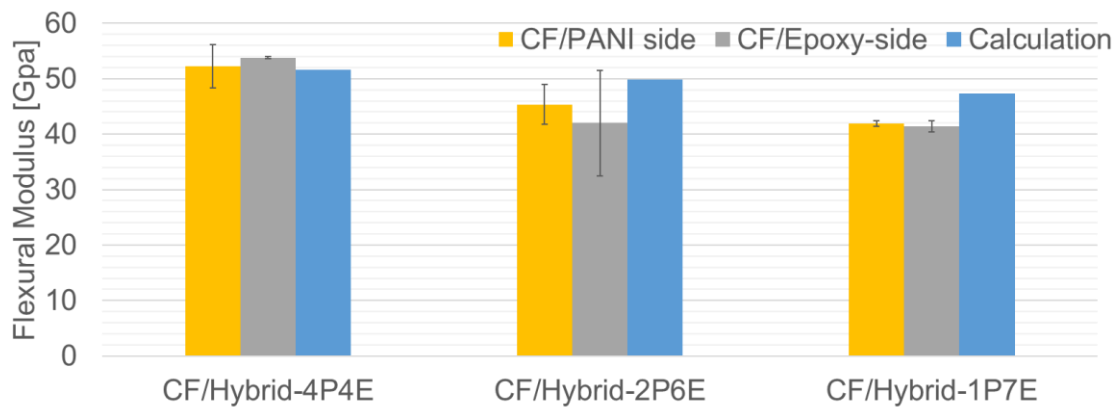
Figure 3-17 Comparison of experimental results and calculation

3.3 ILSS

Interfacial properties are determined by conducting the following three tests: interlaminar shear strength (ILSS) test, double cantilever beam (DCB) test, and end-notched flexure (ENF) test. ILSS test is conducted according to JIS K7078 standard for apparent interlaminar shear strength of carbon fibre reinforced plastics by three-point loading method. The universal testing machine (Instron 5582) was used with load cell of 5 kN and the crosshead speed was maintained at 0.5 mm/min. The radius of the loading head is 5 mm. The radii of the supporting heads are 2 mm. The dimensions of the specimens are 10 mm in width, and 1.8-4.2 mm in thickness. The length of the specimens is calculated as seven times of the thickness. The span length is also calculated as five times of the thickness. At least two samples were measured to get an average of property with less variation. The measurement yields load and displacement data. I then use the maximum load value to calculate ILSS [MPa] of the specimen. The mode of failure is also recorded for further analysis. Universal Testing machine (Shimadzu AGS-X 10kN) was used with load cell of 5 kN and crosshead speed was fixed at 1 mm/min.

3.3.1 Results and discussion

The interlaminar shear stress (ILSS) of CF/PANI improved drastically compared to pristine CF/PANI as shown in Figure 3-18. The CF/hybrids tested on the CF/PANI side shows improvement as the number of CF/Epoxy increases. CF/hybrids tested on the CF/Epoxy side do not change much among batches. Therefore, with the incorporation of CF/Epoxy in CF/hybrid, ILSS is improved. This is because the midplane of the laminates is in the CF/Epoxy part. However, in the specimens with 8 layers, the failure of specimens cannot be distinguished

clearly whether they fail by which mode (either compressive failure or delamination). Therefore, the test was repeated with 16 layers of CF/PANI, CF/Epoxy, and CF/Hybrid-8P8E as shown in Figure 3-19. With higher number of layers as well as thicknesses, the specimens clearly failed due to ILSS as the load-displacement curves Figure 3-20, Figure 3-21, and Figure 3-22. The specimens show spike drop from the peak values indicating the interlaminar shear occurred in the specimens. The results show the same values of ILSS for CF/PANI and CF/Epoxy. However, the ILSS values of CF/Hybrid-8P8E reduced with a greater number of layers.
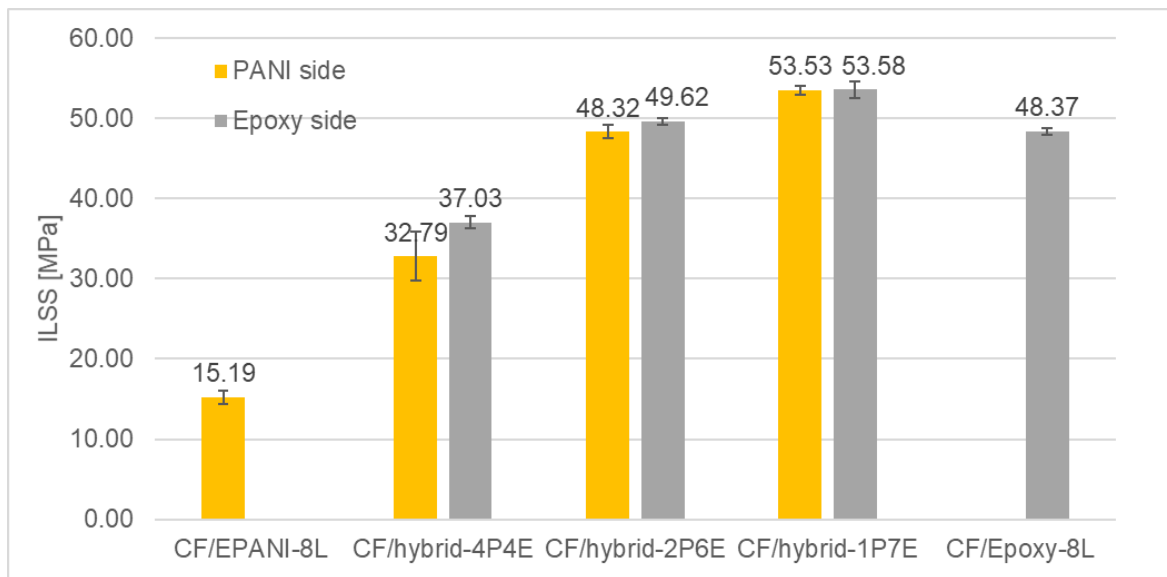
Figure 3-18 Results of ILSS-8L

Table 3-5. Thickness and mode of failure from ILSS test with 8-layer specimens

	CF/PANI	CF/Hybrid-4P4E	CF/Hybrid-2P6E	CF/Hybrid-1P7E	CF/Epoxy
Thickness [mm]	1.540	2.016	2.176	2.290	2.066
Failure on CF/PANI	Compressive	Compressive	Compressive	Compressive	
Failure on CF/Epoxy		Delamination/ Fibre breakage	Delamination/ Fibre breakage	Delamination/ Fibre breakage	Fibre breakage

Figure 3-19 Results of ILSS-16L
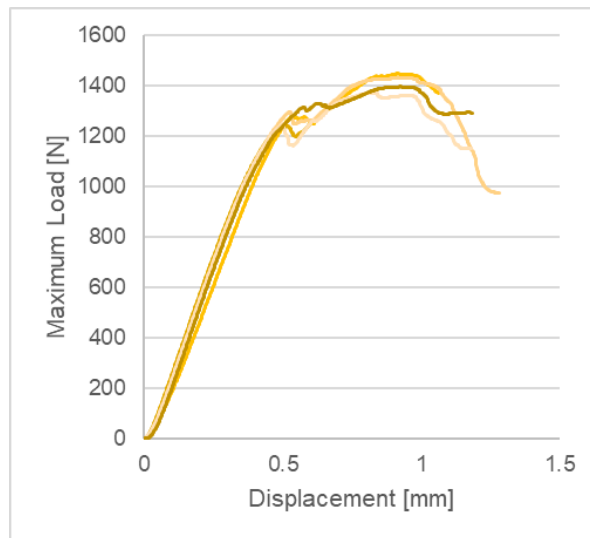
Figure 3-20 Load-displacement curves of CF/Hybrid-8P8E from ILSS test
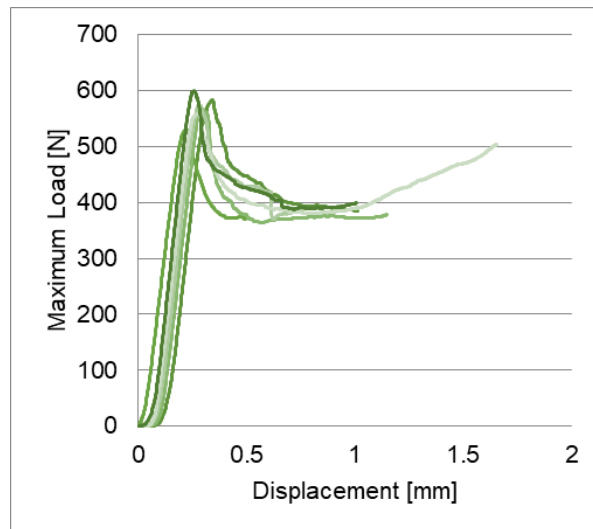
Figure 3-21 Load-displacement curves of CF/PANI-16L from ILSS test
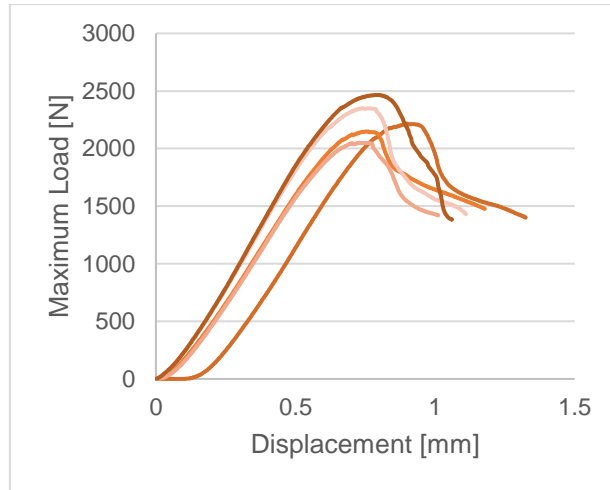
Figure 3-22 Load-displacement curves of CF/Epoxy-16L from ILSS test

Table 3-6. Thickness and mode of failure from ILSS test with 16-layer specimens

	CF/PANI	CF/Hybrid-8P8E	CF/Epoxy
Thickness [mm]	2.765	3.660	3.533
Failure on CF/PANI	Interlaminar shear	Interlaminar shear	
Failure on CF/Epoxy		Interlaminar shear	Interlaminar shear

3.4   Interlaminar Fracture Toughness

Interlaminar fracture toughness properties are important for application composite materials and are useful for model simulation. In this study, I conduct interlaminar fracture toughness to evaluate interlaminar fracture toughness between CF/PANI and CF/PANI, CF/PANI and CF/Epoxy (i.e., adhesive interlayer), and CF/Epoxy and CF/Epoxy. This is because lightning strikes and mechanical applied loads induce damages in hybrid laminates and interlaminar delamination are the most susceptible and critical for the structure.

The double cantilever beam (DCB) test and end-notched flexure (ENF) test are conducted according to JIS K7086, testing methods for interlaminar fracture toughness of carbon fibre reinforced plastics. The specimens were prepared by inserting a folded sheet of polyimide at the laminate mid-thickness with the film edge perpendicular to the fibre alignment. After curing, the test panels were trimmed the four edges and machined to obtain the desired dimensions as 25 mm in width, 140 mm or over in length and thickness around 3 mm. The cut specimens were painted with spray colour on both thickness sides in order to see crack

propagation easily.

3.4.1 Double cantilever beam (DCB)

For the DCB test, the specimens were attached with a pin loading block at the end with folded film. The specimens were attached with a scaling label for aiding reading crack propagation. The scale starts from the centre of the pin loading block (6 mm distance from the edge). I highly suggest marking the scale every 10-mm and 5-mm with two distinct colours on the scaling label so that ones can read the crack propagation conveniently. After that, the specimens were introduced a pre-crack around 2 mm to 5 mm long at the tip of the inserted film by means of opening the crack with a sharp wedge like knife. The pre-crack length on both sides should be marked on the specimens and recorded in a record sheet. Then, the pre-cracked specimen was set up on the testing machine. The testing machine should record the load to crack opening distance (COD) relationship for further calculation. During the test, the load, the COD, as well as the crack length should be recorded every time the COD increases 1 mm (from COD = 5-10 mm), 2 mm (from COD = 12-20 mm) and 4 mm (from COD = 24 mm). After recording all data, the machine should return the COD to 0 mm. G_{IC} of the specimen is then calculated according to the standard. I tested altogether 3 cases: CF/Epoxy, CF/PANI, and CF/Hybrid. 5 specimens were repeated in each case.

The load-displacement curves and crack observations are shown in Figure 3-23 and Figure 3-24. In this case the crack propagated very quickly and exceeded the length of observation.
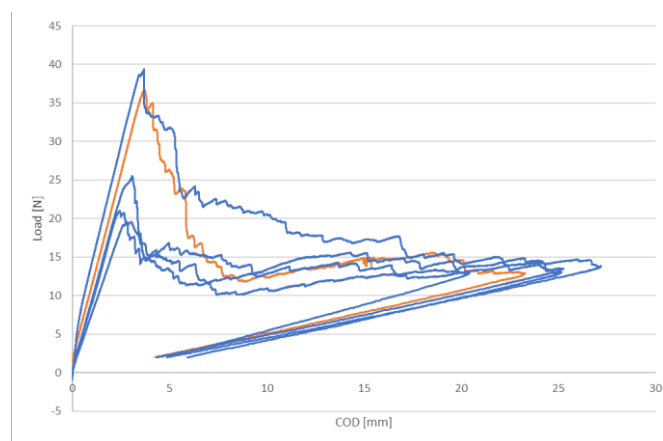
Figure 3-23 Load-displacement curves of CF/PANI in DCB test
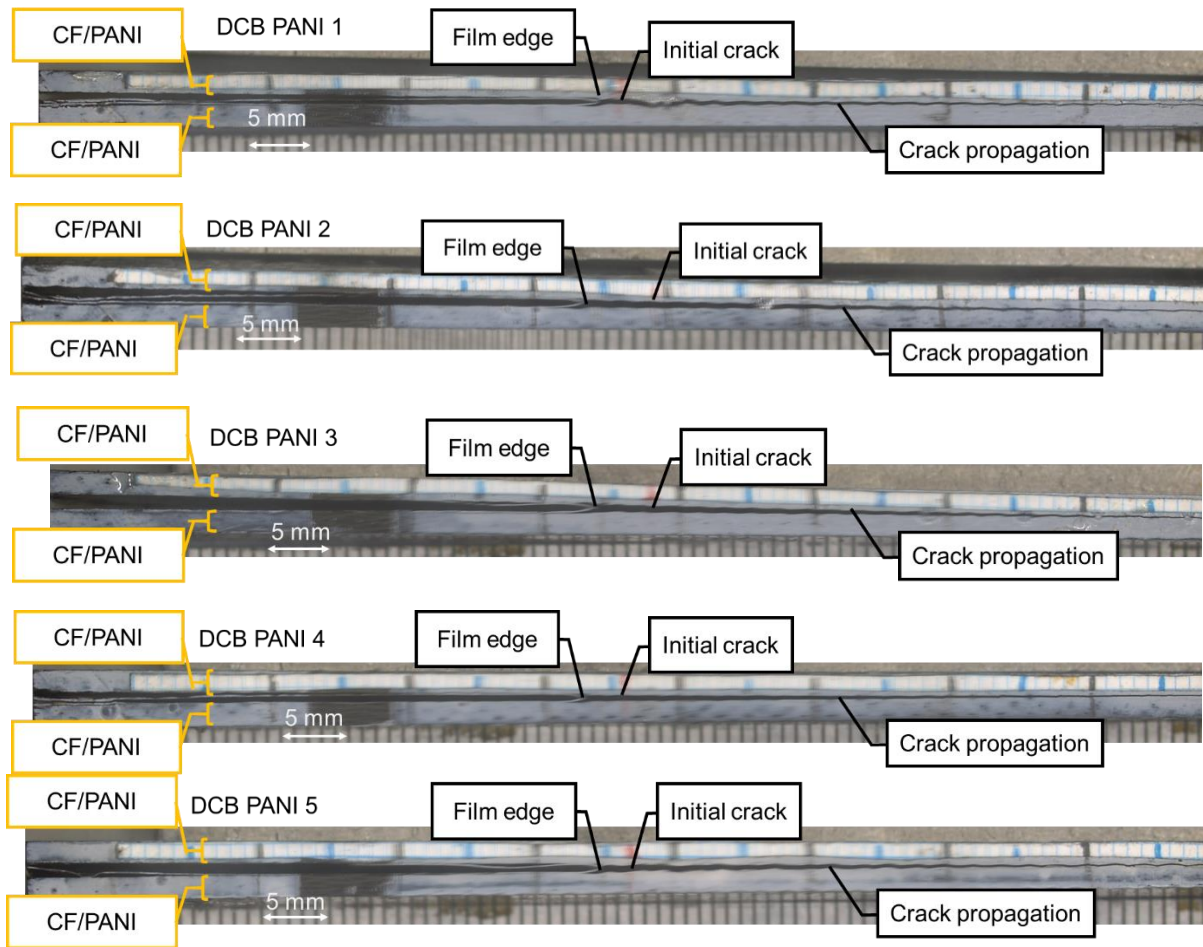
Figure 3-24 Crack observation of CF/PANI specimens in DCB test

For CF/Epoxy, the load-displacement and crack observations are shown in Figure 3-25 and Figure 3-26. As usual CF/Epoxy, the crack propagated slowly with high loading.
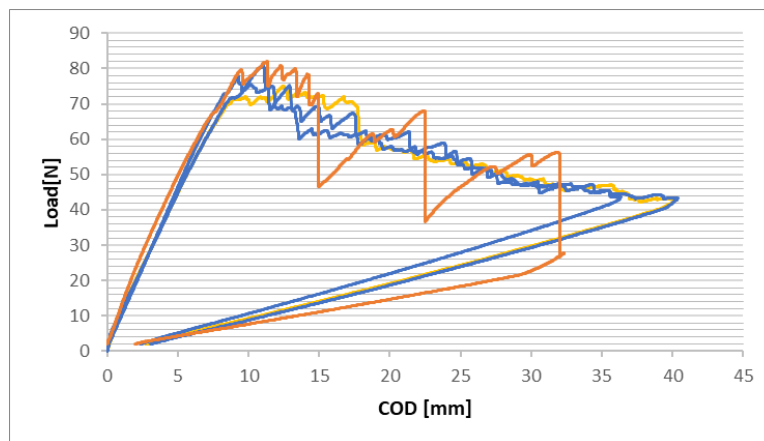
Figure 3-25 Load-displacement curves of CF/Epoxy in DCB test
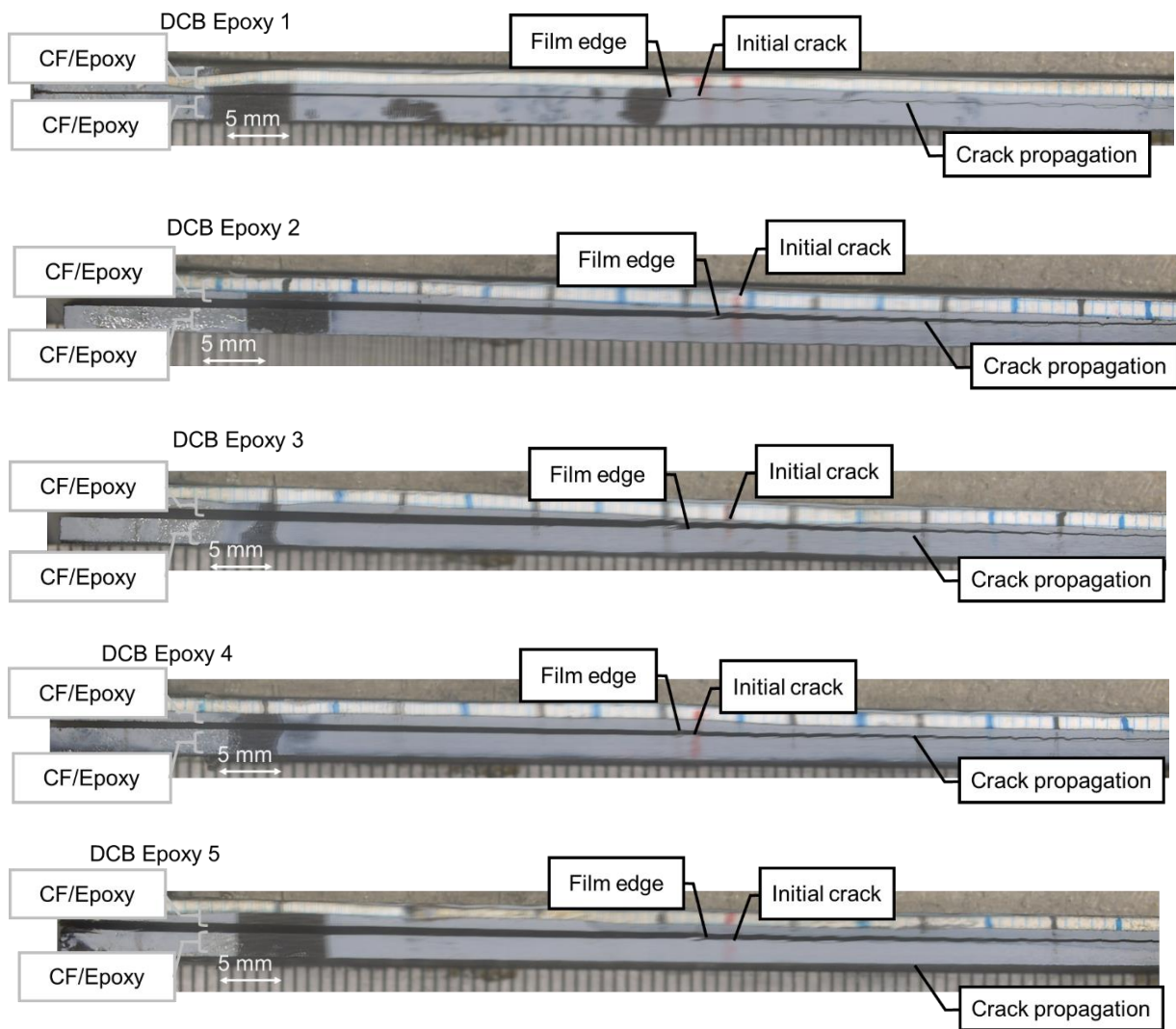
Figure 3-26 Crack observation of CF/Epoxy specimens in DCB test

For CF/Hybrid specimens, the load-displacement curves and crack observing images are shown in Figure 3-27 and Figure 3-28. However, the cracks did not propagate between both layers. Instead, the CF/PANI bend open largely. Therefore, the value obtained cannot be used as energy release rate. The reason why interlaminar cracks are kinking into CF/PANI layers is the lower interlaminar strength and fracture toughness between CF/PANI and CF/PANI, compared to those between CF/PANI and CF/epoxy (i.e., adhesive interlayer) as shown in Figure 3-28. Before interlaminar cracks propagate, damages and small cracks are generated in CF/PANI interlayers. The induced cracks in CF/PANI grow easier than the original interlaminar cracks. Therefore, cracks are propagating in CF/PANI sub-laminates.
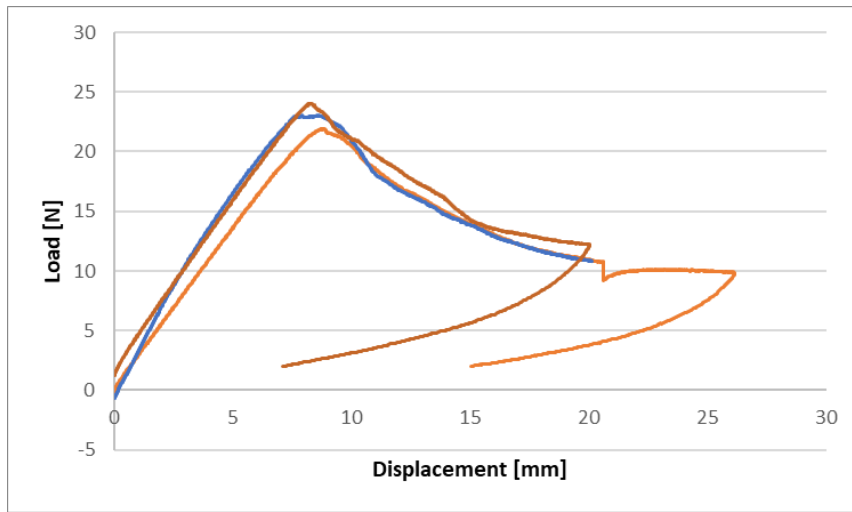
Figure 3-27 Load-displacement curves of CF/Hybrid in DCB test
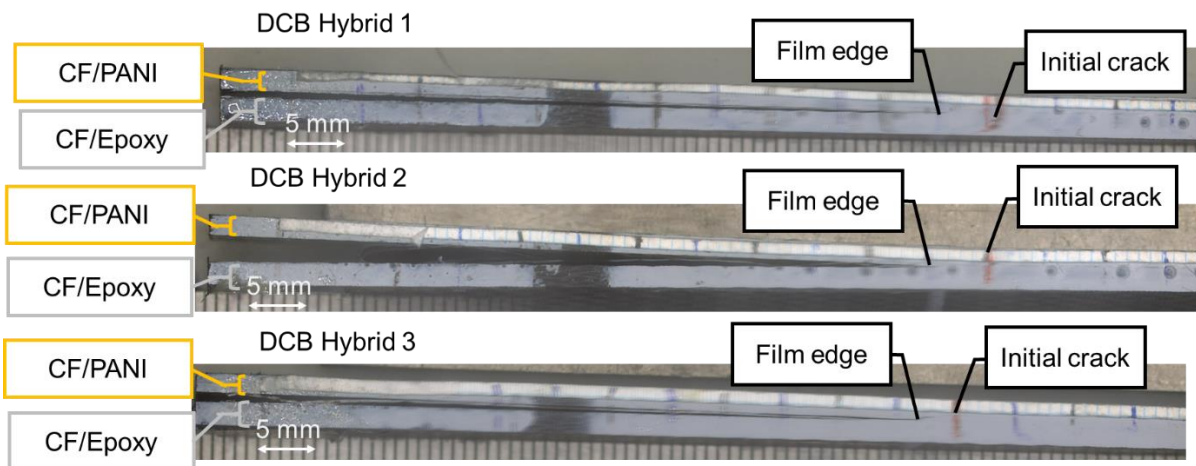
Figure 3-28 Crack observation of CF/PANI specimens in DCB test

3.4.2 End-notched Flexure test (ENF)

For ENF test, the specimens are indicated with the film edge inside specimens. Then the first supporting point is marked 25 mm from the film edge to the film end direction so that I can ensure sufficient distance between the initial crack and the supporting point. The second supporting point is marked 100 mm from the first supporting point to the other edge of the specimen. The specimens were introduced as a pre-crack around 2 mm to 5 mm long at the tip of the inserted film by means of opening the crack with a sharp wedge like knife. The pre-crack lengths on both sides are recorded. The testing machine is set up by using supporting heads

with 2 mm radii and loading heads with 5 mm radius. The distance between supporting heads (span length) is 100 mm. The specimen was set up on the testing machine. The specimens were loaded at the constant rate of 0.5 mm/min until the load drops. The G_{IIC} is then calculated according to the standard. The results are shown in Table 3-7.

Table 3-7 Results of Fracture toughness test

Properties	G_{IC} [J/m^2]	G_{IIC} [J/m^2]
CF/PANI	120.6 ± 22.2	689 ± 126
CF/Hybrid – on CF/PANI		1630 ± 318
CF/Hybrid – on CF/Epoxy	N/A	4694 ± 571
CF/Epoxy	901.9 ± 117.0	2396 ± 120.4

The load-displacement curve and crack observation are shown in Figure 3-28 and Figure 3-29 for CF/PANI. The crack propagated to a certain length with low loading compared to CF/Epoxy. With the crack propagation, the energy release rate of these specimens was obtained.
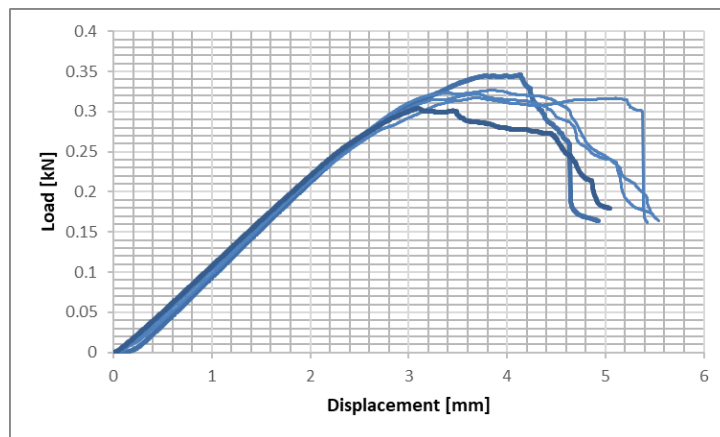
Figure 3-29 Load-displacement curves of CF/PANI in ENF test
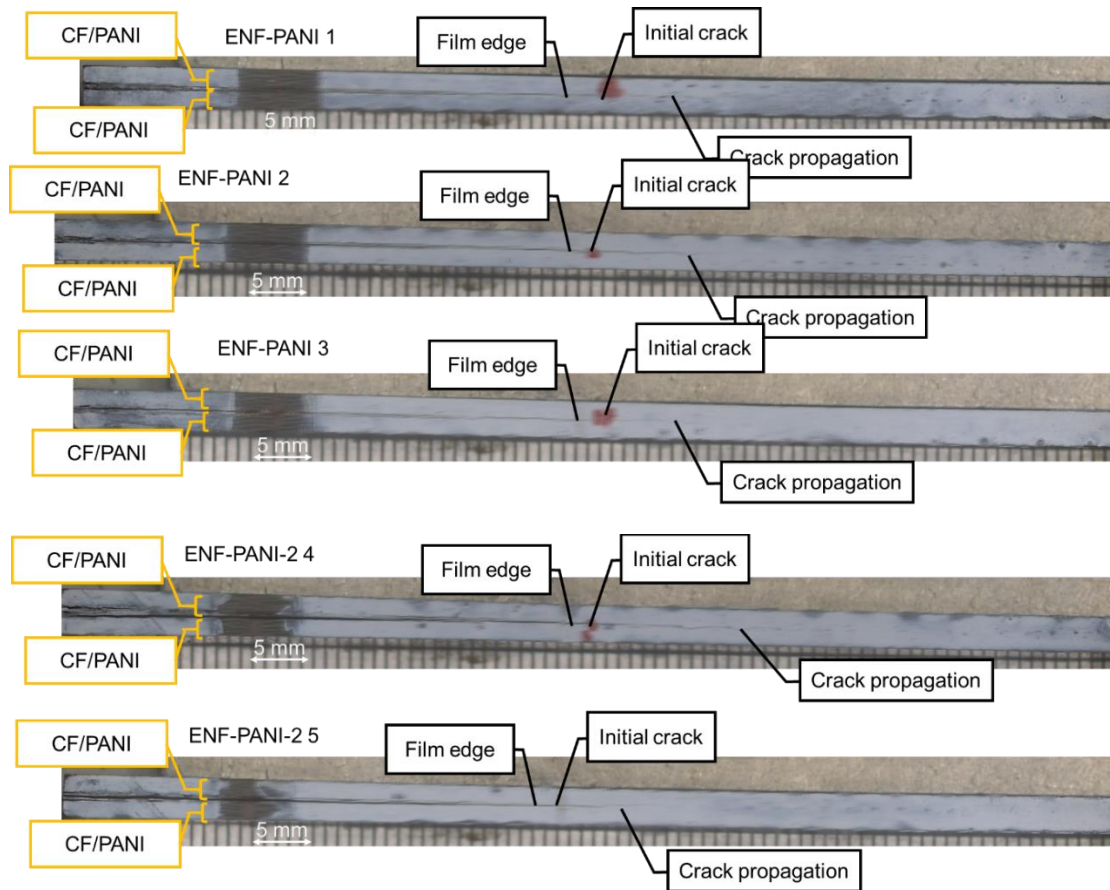
Figure 3-30 Crack observation of CF/PANI specimens in ENF test

For CF/Epoxy, the load-displacement curve and crack observation are shown in Figure 3-31 and Figure 3-32. Comparing to CF/PANI, the crack propagated longer with longer propagation which is usual for CF/Epoxy.
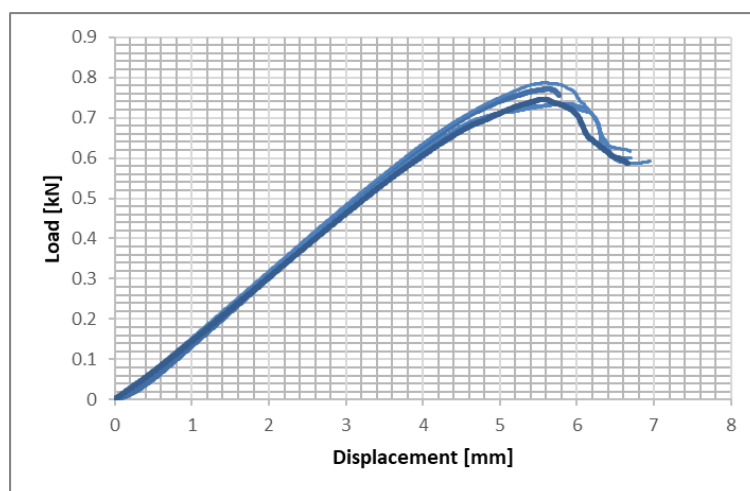
Figure 3-31 Load-displacement curves of CF/Epoxy in ENF test
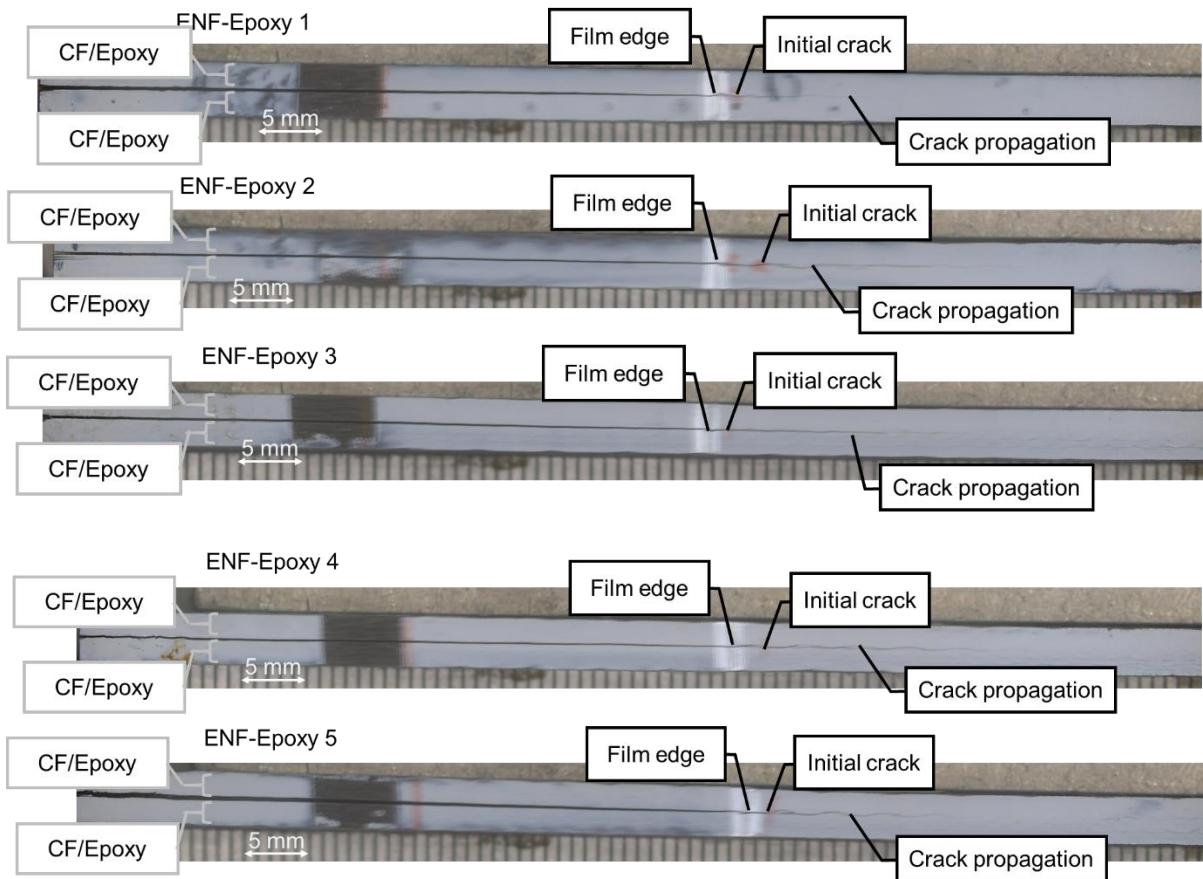
Figure 3-32 Crack observation of CF/Epoxy specimens in ENF test

For CF/Hybrid tested on CF/PANI side, the load-displacement curve and crack observation are shown in Figure 3-33 and Figure 3-34. The crack observation has shown that the main failure of this mode is compressive failure and only in some cases, cracks propagated. In every case, the specimens show compressive failure on CF/PANI side, too.
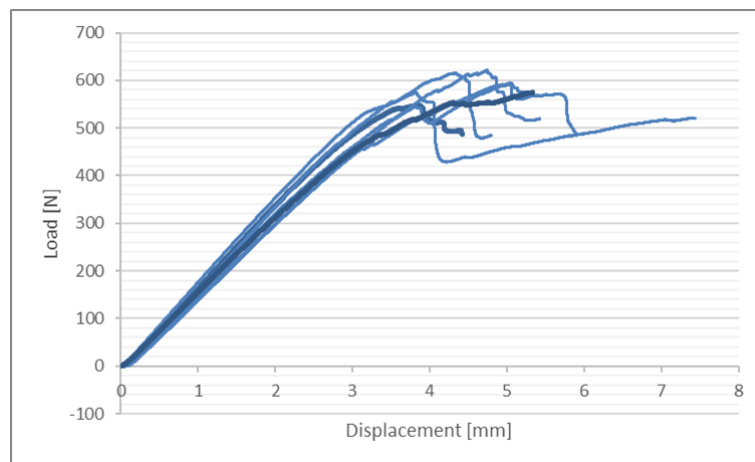
Figure 3-33 Load-displacement curves of CF/Hybrid in ENF test on PANI side
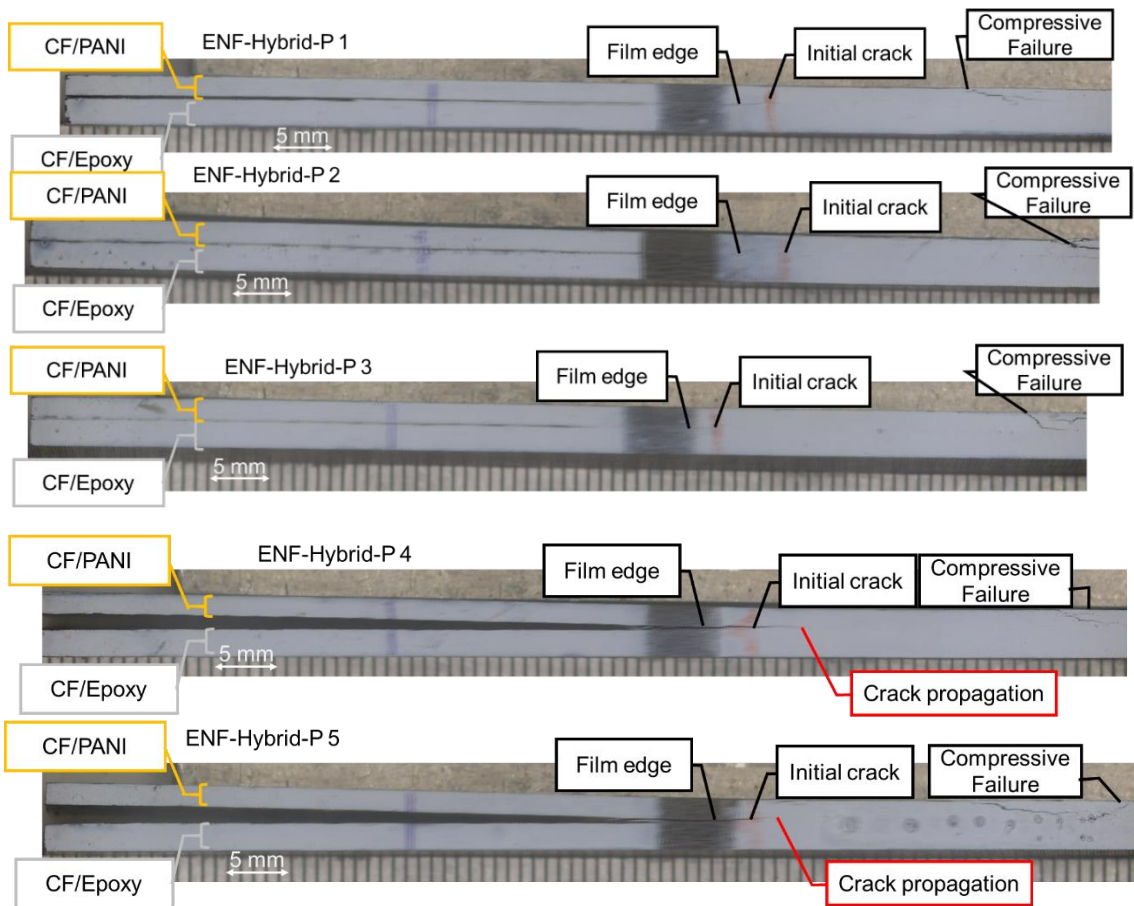
Figure 3-34 Crack observation of CF/Hybrid specimens on PANI side in ENF test

For CF/Hybrid tested on CF/Epoxy side, the load-displacement curve and crack observation are shown in Figure 3-35 and Figure 3-36. The crack observation has shown that several modes of failures: compressive failure, and crack propagation.
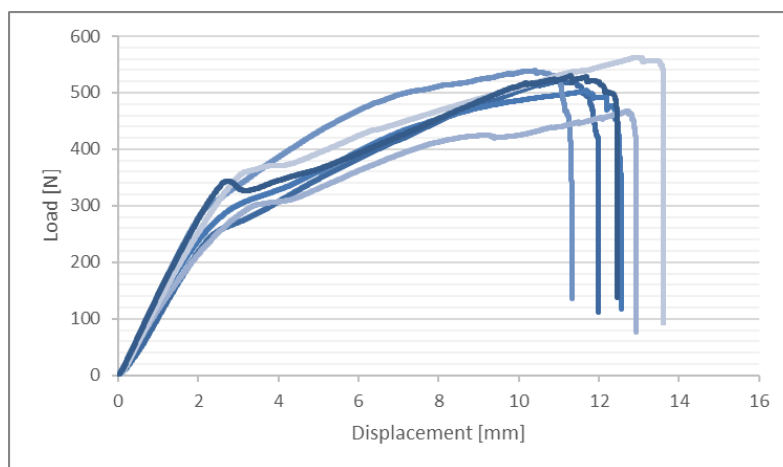
Figure 3-35 Load-displacement curves of CF/Hybrid in ENF test on Epoxy side
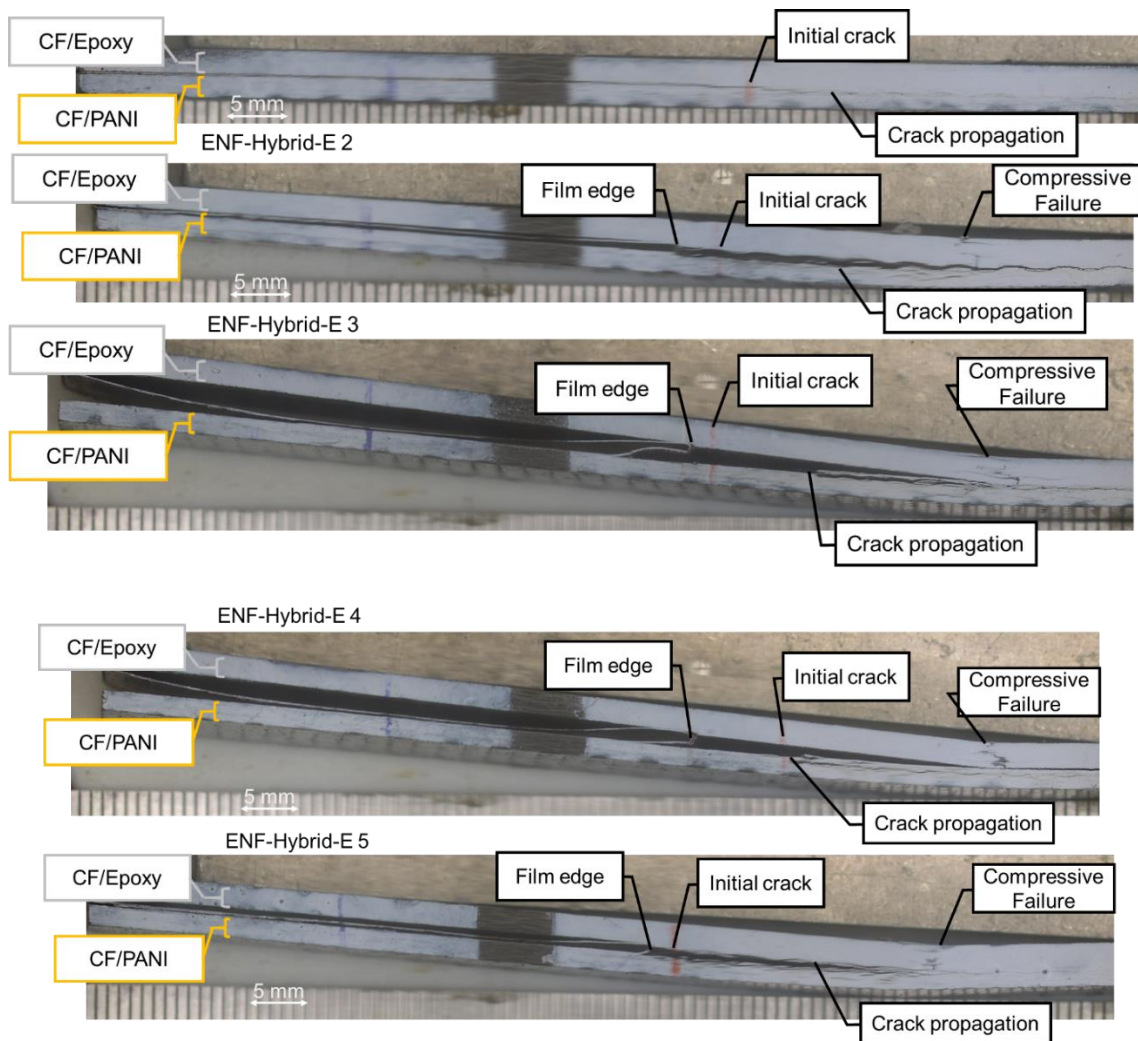
Figure 3-36 Crack observation of CF/Hybrid specimens on Epoxy side in ENF test

3.5   Summary

I have reported the results of mechanical testing of the specimens. The bending strength of the hybrid specimens did not improve significantly. ILSS have improved to a certain level due to the shift of neutral axes. Interlaminar fracture toughness has varied results depending on the materials. Although many results did become as I expected, I have learned the reality of these specimens and the needs to understand them clearly so that I can solve and anticipate properties in the next trial.

Chapter 4 Investigation of the least effective number of CF/PANI layer

4.1 Introduction

Consequent to the characterization of mechanical properties, CF/Hybrids show potential to use as a structural component. I further conduct the experiment to evaluate the effectiveness of lightning strike protection. This chapter includes electrical conductivity measurement, simulated lightning strike test, and its damage evaluation.

4.2 Electrical Conductivity

I measured the electrical conductivity of the CF/PANI sub laminates by separating the layer in advance before co-curing with adhesive film and CF/Epoxy and prepared as described in Chapter 2. Table 1-1 shows the through-thickness electrical conductivity of specimens in this study compared with previous studies.

Conductivity of the specimens in this study varies from 0.49 S/cm to 0.78 S/cm. This difference is due to the quality of the specimens after the curing process. The materials are very sensitive to heat. The study by Kumar et al. [56] has pointed out that if the specimens were heated up to a certain temperature for long periods of time, the electrical conductivity starts decreasing. This also applies to the current study. Due to the fact that the dimension of specimens being different during the fabrication, this results in different heat exposure throughout the specimens. It is interesting to explore the effect of dimensions on electrical conductivity.

The electrical conductivities of the pristine specimens CF/PANI-8L and CF/Epoxy-8L are clearly distinguishable. CF/PANI-8L has much higher electrical conductivity compared to CF/Epoxy. This is the main reason why CF/PANI specimens can withstand lightning strike damages while CF/Epoxy could not. These results also agree with previous studies. For CF/PANI-8L, the electrical conductivity is lower than the previous studies. This is due to different components of PANI-based resin. Hirano [21] used p-toluenesulfonic acid (PTSA) as an extra dopant and Kumar [[effect of through used camphor sulfonic acid (CSA). Having extra dopant which does not react with the crosslinking polymer DVB can prevent the scavenging effect as well as increasing conductivity. In this study, I did not focus on the components that contribute to electrical conductivity, so I did not adopt those methods.

Table 4-1 Out-of-plane electrical conductivity of CF/PANI

	Through-thickness electrical conductivity [S/cm]
CF/PANI [21]	0.74
CF/PANI [55]	1.35
CF/PANI-8L	0.483 ± 0.04
CF/Hybrid-4P4E	≈ 0
CF/Hybrid-2P6E	≈ 0
CF/Hybrid-1P7E	≈ 0
CF/Epoxy [21]	0.0027
CF/Epoxy	0.0018 ± 0.0001

Table 4-2 Out-of-plane electrical conductivity of CF/PANI sublaminates

	Through-thickness electrical conductivity [S/cm]
CF/PANI-4L (4P4E)	0.78 ± 0.07
CF/PANI-2L (2P6E)	0.73 ± 0.08
CF/PANI-1L (1P7E)	0.49 ± 0.12

4.3 Lightning strike test

I conducted a simulated lightning strike test with modification from the standard SAE ARP-5412B at the National Composite Centre (NCC), Nagoya University. I collaborated with Japan Aerospace Exploration Agency (JAXA), Shoden corporation, and Tokyo University of Agricultural and Technology (TUAT). I used the modified component A of the waveform according to the standard SAE ARP-5412B with the peak current at -40 kA.

4.3.1 Test setup and equipment

The setup of the testing site is shown in the Figure 4-1. The specimen holders as shown in Figure 4-2, provided by JAXA, set up inside a plastic tent. This can prevent particles generated from the explosion during lightning test to flow outside. The specimen holder was connected to an impulse current generator (developed by Otowa Electric Co., Ltd., owned by NCC). The specimen was fixed to a picture-frame-type copper jig, which was attached to the ground of the impulse current generator. The specimen was held by the base plate and cover frame at all edges by screw-clamping. The details of measuring applied impulse current can be found in the previous study of Hirano et al. [21]. The impulse current was measured with a current transducer (Model 1423 from Pearson Electronics, Inc.) and a digital oscilloscope (TD3034C, Tektronix, Inc.). The lightning current was applied at the centre of the specimen surface, where the gap between the tip of the discharge probe and the surface of specimen is 2 mm.

Additionally, several observation methods were employed to help clarifying the lightning strike phenomena. Two high speed cameras were set up: the first angle camera (Hyper vision HPV-1, Shimadzu) with 180 mm lens and frame speed of 250 kfps (4 µs) and the third angle camera (Hyper vision HPV-X2) with 105-mm lens and frame speed 200 Mfps (500 ns). A thermography camera (SC 7000, FLIR, Inc.) was also used to observe temperature variation with framing speed of 50/3 fps.

The tested samples were 3 types of CF/Hybrids with different number of CF/PANI and CF/Epoxy: CF/Hybird-4P4E, CF/Hybrid-2P6E, and CF/Hybrid-1P7E. The number in front of the letter P represents the number of CF/PANI layers and the number in front of the letter E represents the number of CF/Epoxy layers. For example, 4P4E means the specimen consists of 4 layers of CF/PANI and 4 layers of CF/Epoxy.
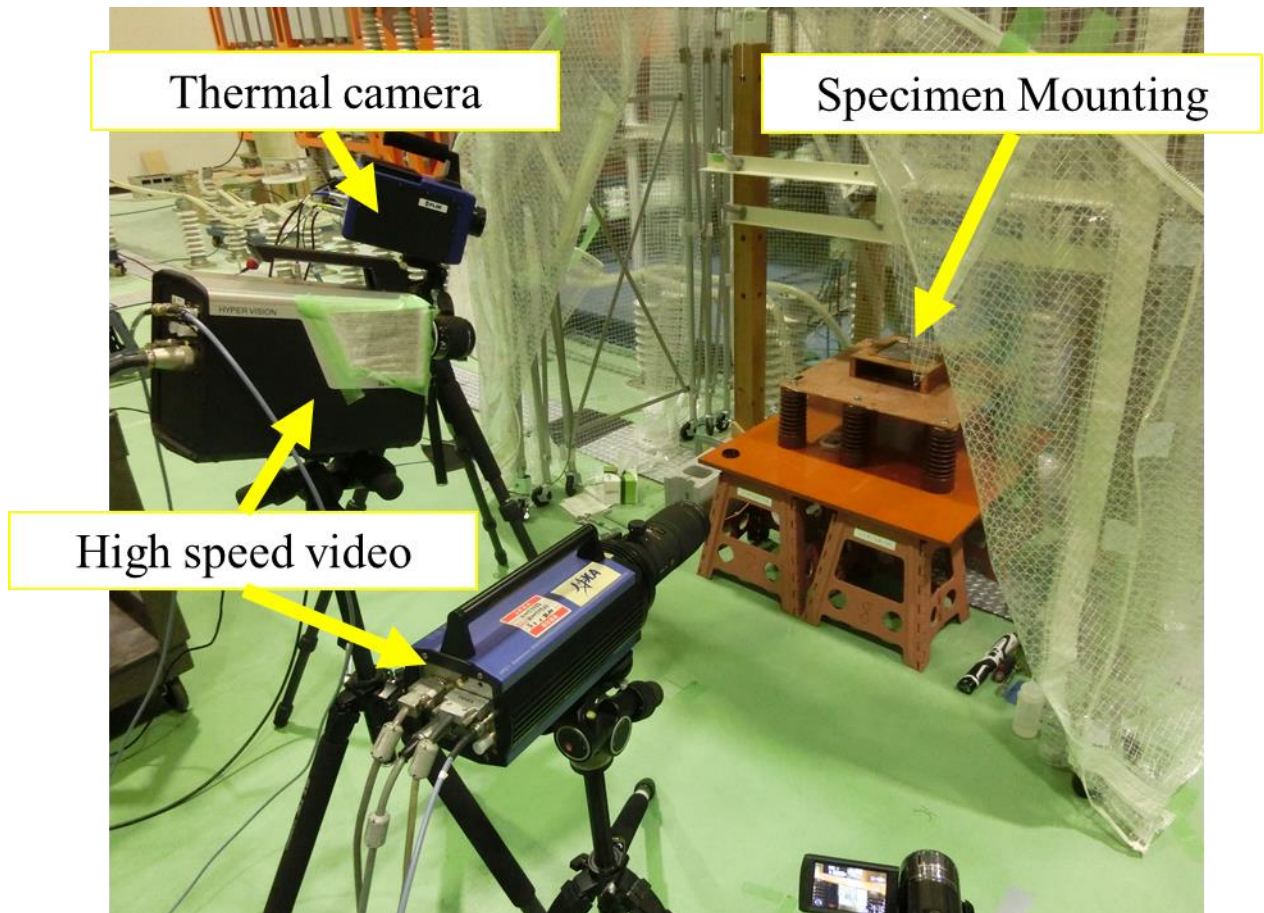
Figure 4-1 Setup of the simulated lightning strike test
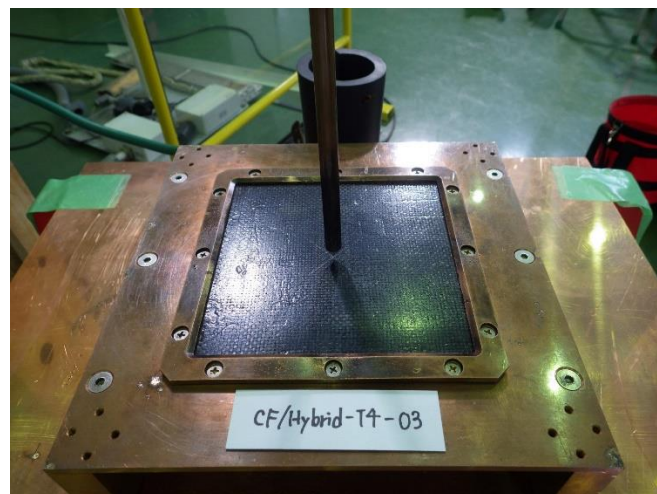
Figure 4-2 Mounting of specimen

4.3.2　Lightning Strike Condition

In this study, a current of Component A, defined in SAE ARP-5412, was modified to apply to the specimens. In this study, peak currents of -40 kA, which is one-fifth of the original Component A waveform, was applied. I can characterize current waveforms using two

parameters: the time to peak current (t_1) and the time to decay to fifty percent of its maximum amplitude (t_2).

Figure 4-3 illustrates a result of the lightning current measured by the oscilloscope. Table 4-3 shows the testing conditions of lightning currents and action integral which were calculated from integral of area under curves.
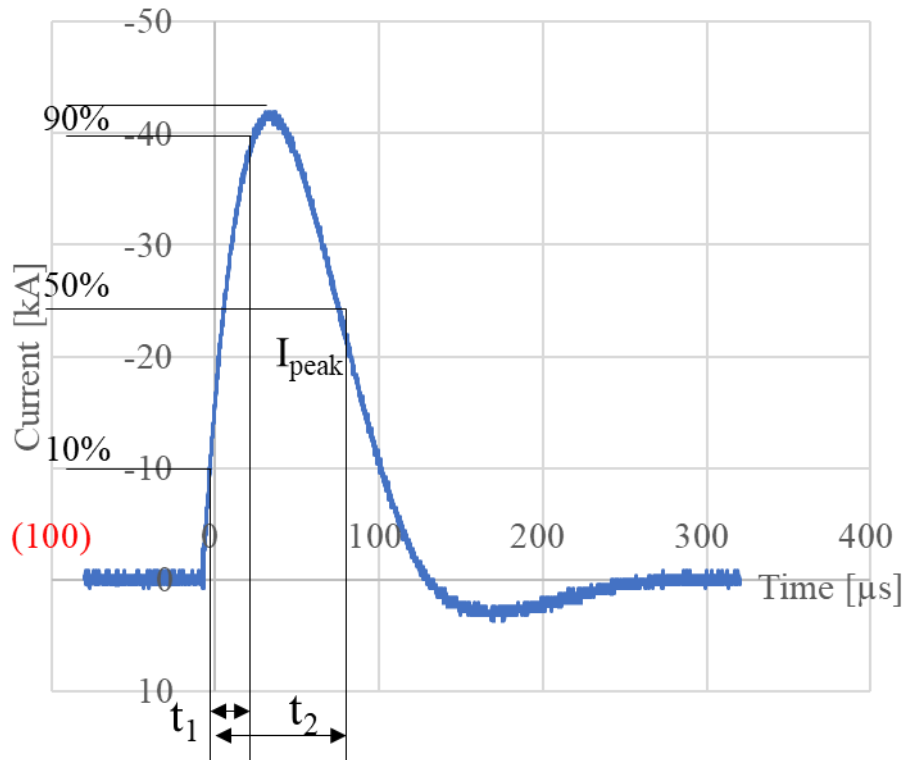
Figure 4-3 Waveform measured from oscilloscope of CF/Hybrid-4P4E

Table 4-3 Simulated lightning strike conditions

Materials	Peak Current [kA]	Waveform t_1/t_2 [μs]	Electric Charge [C]	Action Integral [A²s]
CF/Hybrid-4P4E	-40.4	26.0/86.1	-2.49	92,841
CF/Hybrid-2P6E	-39.8	25.9/87.5	-2.59	91,458
CF/Hybrid-1P7E	-38.4	26.3/90.5	-2.53	88,269

4.4   Visual inspection and Ultrasonic testing

4.4.1   CF/Hybrid-4P4E

Visual inspection is the first and simple step to perform after conducting the lightning strike test. I took photos of specimens before and after the lightning strike test. The photos of specimens before mounting to the jig were taken on both sides, but the photos of mounted specimens were taken only on CF/PANI side. Figure 4-4 shows the sample of CF/Hybrid-4P4E at the jig. Visual inspection shows that there was neither explosion nor burning of resin, unlike CF/Epoxy in the previous study as shown in Figure 1-10. The specimen did not suffer from delamination either. Figure 4-5 and Figure 4-6 compared the specimen before and after the lightning strike of -40 kA on CF/PANI and CF/Epoxy side, respectively. I can obviously see that the lightning strike damage remained only on CF/PANI where burnt traces appeared. The CF/Epoxy side remains intact. The ultrasonic testing (UT) images of this sample, shown in Figure 4-7, also confirm that after the lightning strike damages (yellow area) remained only at the centre area on CF/PANI side and confined only in the CF/PANI layers. On the other side in Figure 4-8, the CF/Epoxy does not show any damage. This specimen shows the effectiveness of electrically conductive CF/PANI layer to protect CF/Epoxy underneath. Figure 4-9 shows the diagram of position of the specimen that was cut after the lightning strike test to observe their cross-sections. The cross-section was observed with a microscope (Leica DMS1000) and shown in Figure 4-10. The cross-section images have shown that the specimen delaminated at the centre which agrees with UT images. The question is what is the least number of conductive layers required to prevent lightning strike damage.

One observation is that the insulating adhesive film plays an important role in preventing damage penetrating into the CF/Epoxy underneath as reported by Jin Hua Han et al. [57]. Although the conductive adhesive film may seem more suitable for lightning strike protection, it cannot digress lightning current away from the insulating panel underneath. One assumption is that the insulating middle layer acts as an insulating wall that completely block the lightning current penetrating. The lightning is then concentrated more within the conductive paths and damage did not occur in the layer under the insulating middle layer.

Figure 4-4 CF/Hybrid-4P4E before and after lightning strike (a) before and (b) after lightning strike
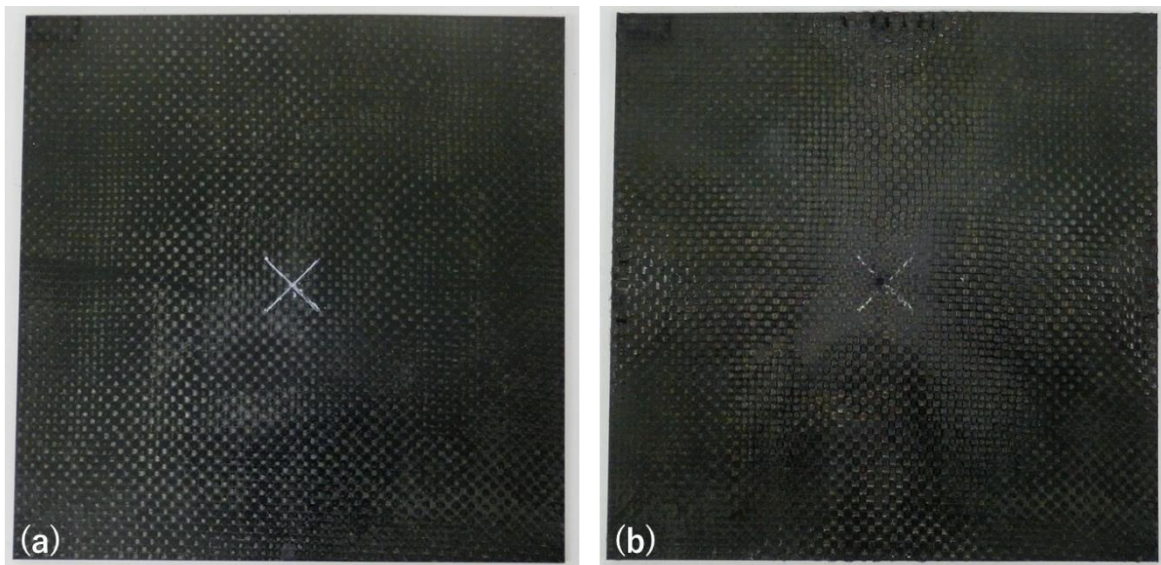
Figure 4-5 CF/Hybrid-4P4E at different angle (a) before and (b) after lightning strike
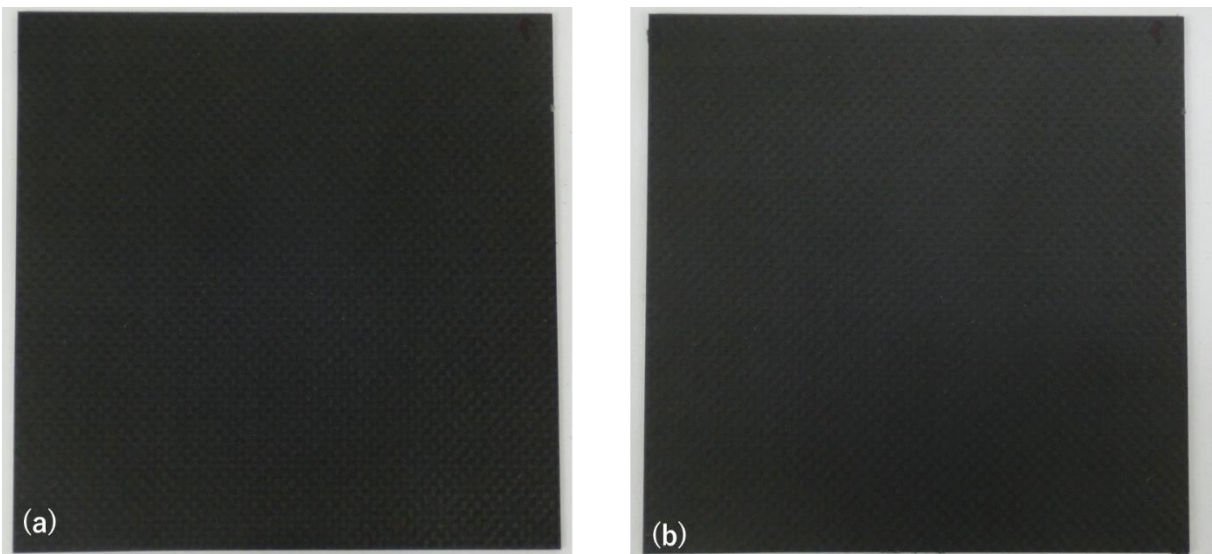
Figure 4-6 CF/Hybrid-4P4E at different angle (a) before and (b) after lightning strike
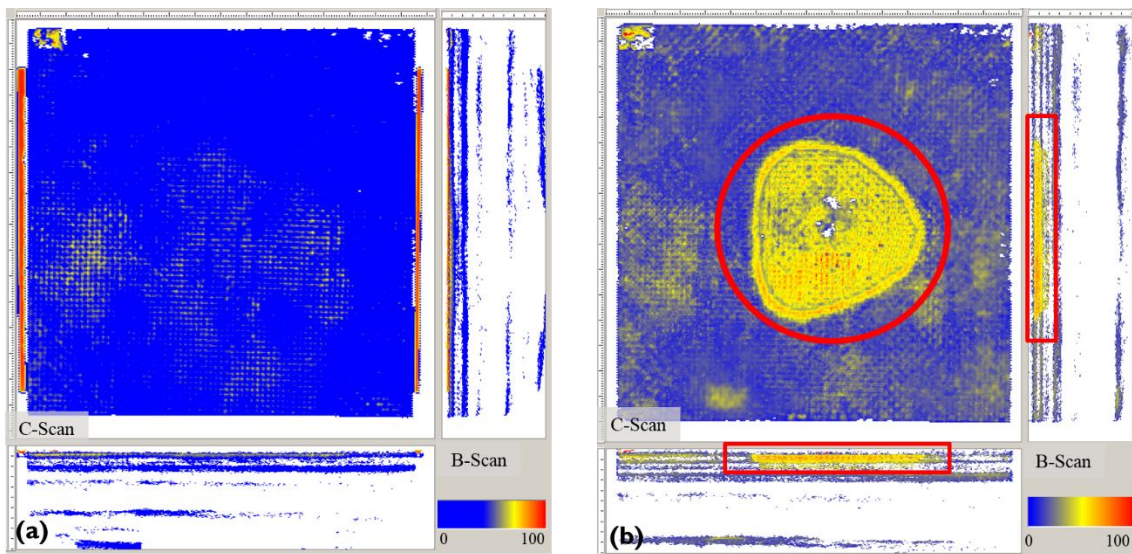
Figure 4-7 NDI images of CF/Hybrid-4P4E on CF/PANI side (a) before and (b) after lightning strike
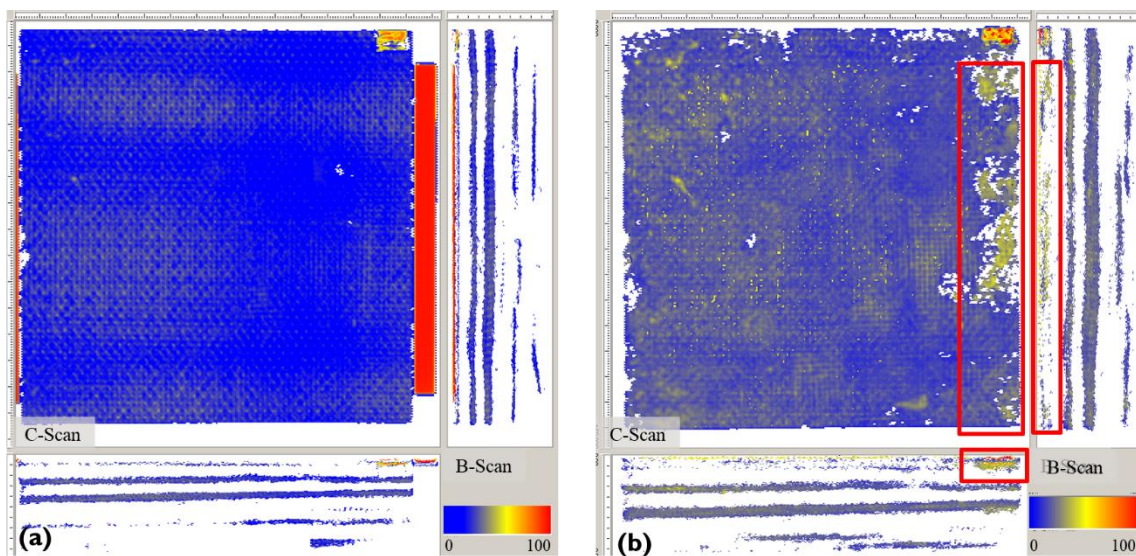
Figure 4-8 NDI images of CF/Hybrid-4P4E on CF/Epoxy side (a) before and (b) after lightning strike
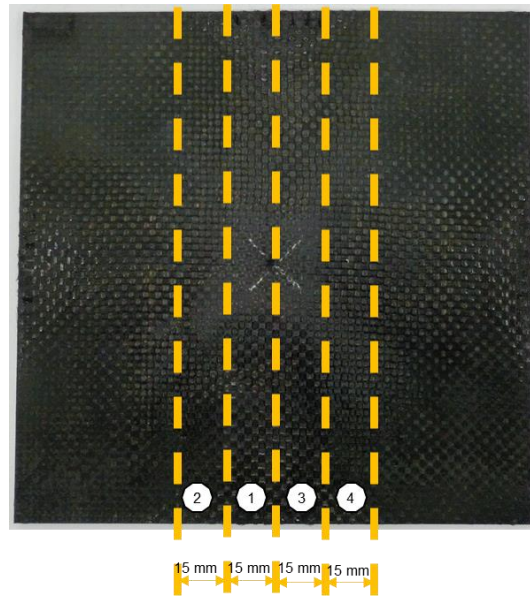
Figure 4-9 Diagram of the specimen label for cross-sectional intersection
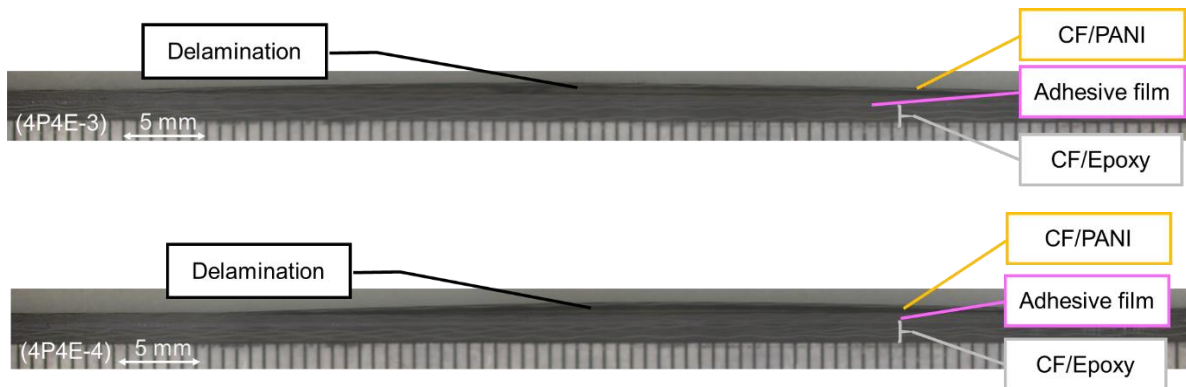
Figure 4-10 Cross-sectional images of CF/Hybrid-4P4E after lightning strike at 15 mm and 30 mm from the centre

4.4.2 CF/Hybrid-2P6E

Photos of CF/Hybrid-2P6E on the jig before and after the test are shown in Figure 4-11. The specimen does not show any severe damage on CF/PANI and CF/Epoxy layer remains intact. When I look from a different angle in Figure 4-12, I can see a little scratch at the centre of CF/PANI where the arc entered into the specimen. This specimen did not delaminate either. Figure 4-13 shows the CF/Epoxy side of the specimen that it remains intact. The NDI images in Figure 4-14 shows that the CF/PANI side after the lightning strike has a scattering large yellow area. This indicates that the lightning strike has damaged its surface in wide area on the surface. However, on the side of CF/Epoxy in Figure 4-15, it does not show any severe damage on CF/Epoxy side. Figure 4-16 shows the cross-sectional image after lightning strike. The images show some delamination at the area nearby the centre. Therefore, I can confirm that using 2 layers of CF/PANI can still confine the lightning strike damage in CF/PANI layers.
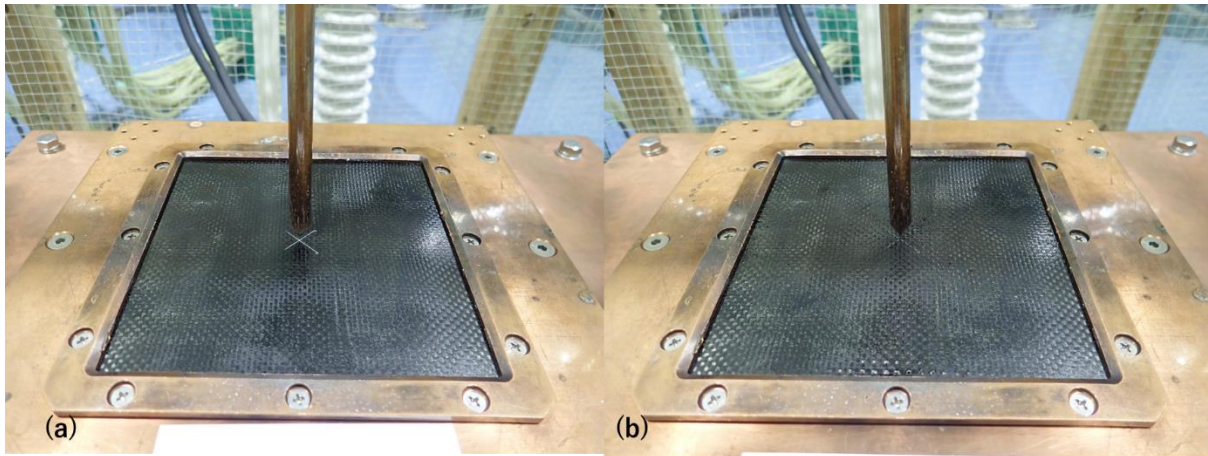
Figure 4-11 CF/Hybrid-2P6E before and after lightning strike (a) before and (b) after lightning strike
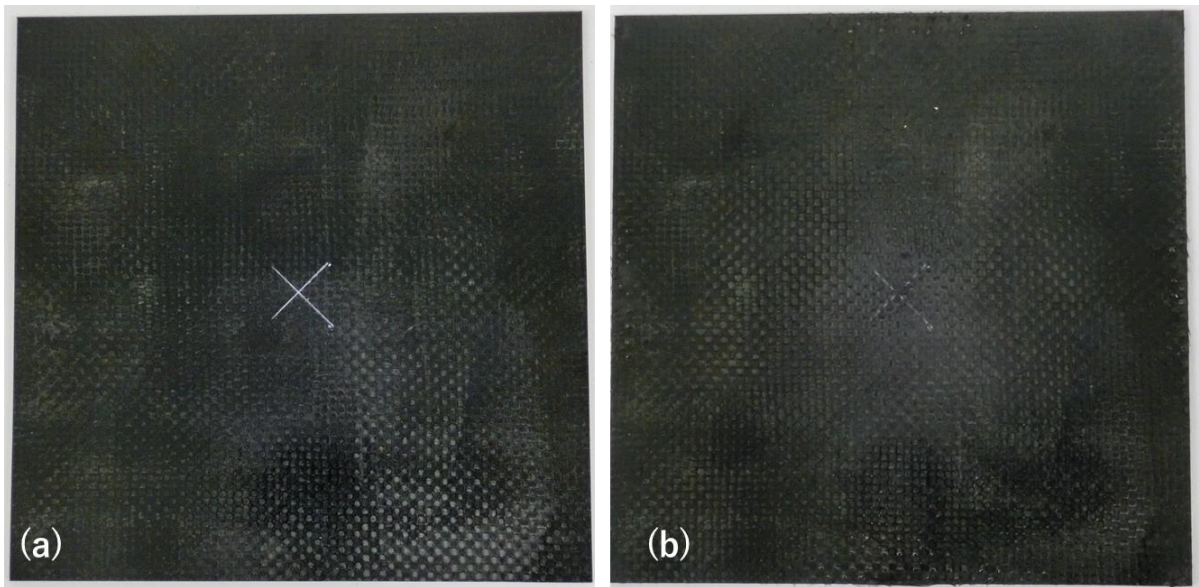
Figure 4-12 CF/Hybrid-2P6E on CF/PANI side (a) before and (b) after lightning strike
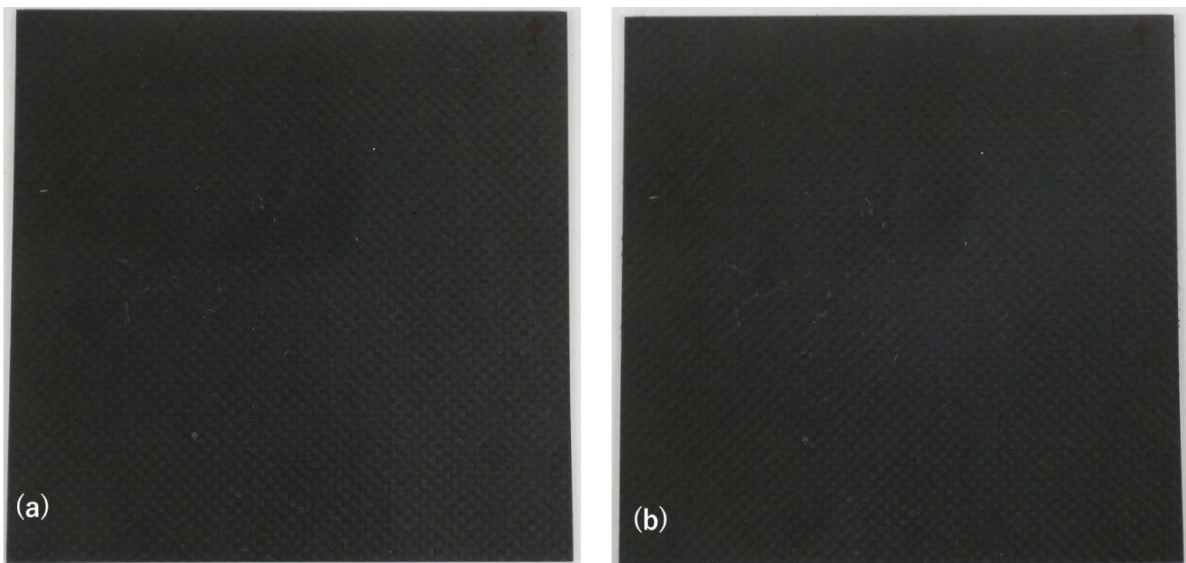
Figure 4-13 CF/Hybrid-2P6E on CF/Epoxy side (a) before and (b) after lightning strike
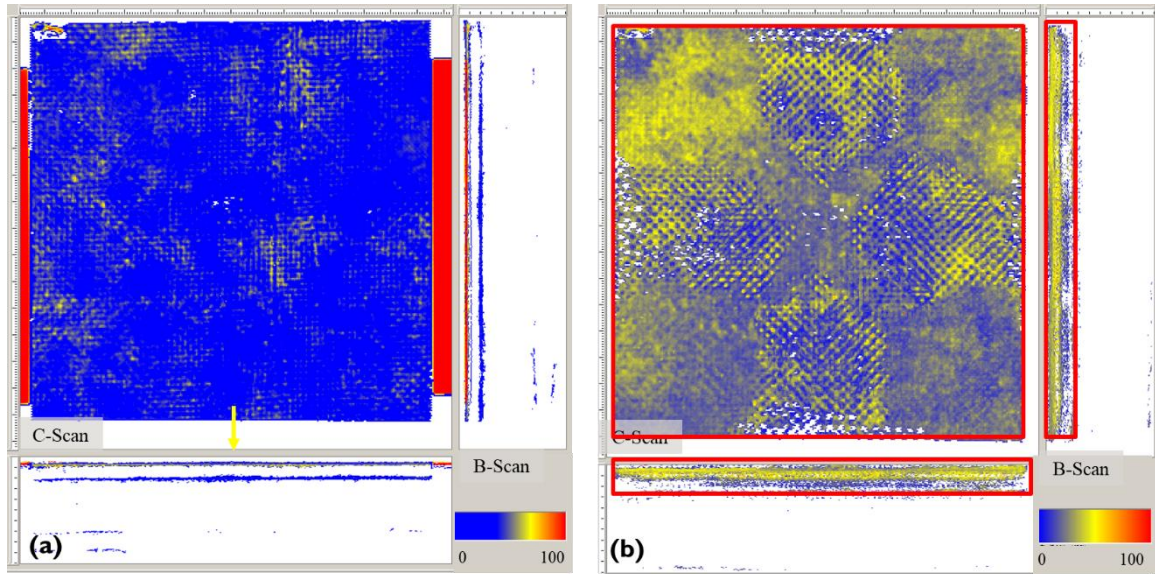
Figure 4-14 NDI images of CF/Hybrid-2P6E on CF/PANI side (a) before and (b) after lightning strike
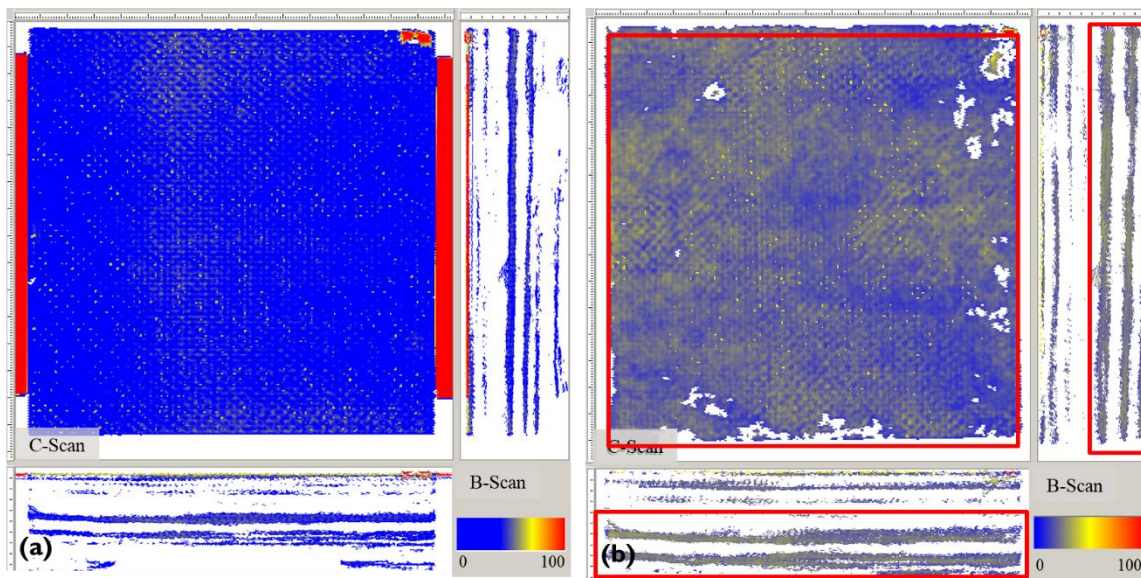
Figure 4-15 NDI images of CF/Hybrid-2P6E on CF/Epoxy side (a) before and (b) after lightning strike

Figure 4-16 Cross-sectional images of CF/Hybrid-2P6E after lightning strike at 15 mm and 30 mm from the centre

4.4.3　CF/Hybrid-1P7E

Photos of CF/Hybrid-1P7E before and after the test are shown in Figure 4-17. Unlike the previous specimens, the sample partially suffered from delamination around the centre area. Also, the trace of lightning strike is a large cross shape. Despite this delamination, the CF/Epoxy underneath remained intact. When observing from a different angle in Figure 4-18, I can see some standing fibre at the middle part of all four edges. This is due to the fact that lightning current flowed into CF/PANI and moved to the edges very quickly through the shortest path (cross shape) to the copper jig. Also, the CF/Epoxy side remains intact as shown in Figure 4-19. The damage observation using ultrasonic testing has clearly shown the cross shape on CF/PANI side in Figure 4-20. Noted that the white area in Figure 4-20 can be interpreted as unable to obtain data, which required observation from cross-sectional images. On the other side in Figure 4-21, CF/Epoxy does not clearly show internal damage after the lightning strike test. Figure 4-22 shows the cross-section around the centre area of the specimen. However, for this batch, delamination did not appear at the centre but around the edges area as shown in Figure 4-23. Even hybrid laminates contain only 1 layer of CF/PANI, the panel can avoid catastrophic damage that occurred with pristine CF/Epoxy.
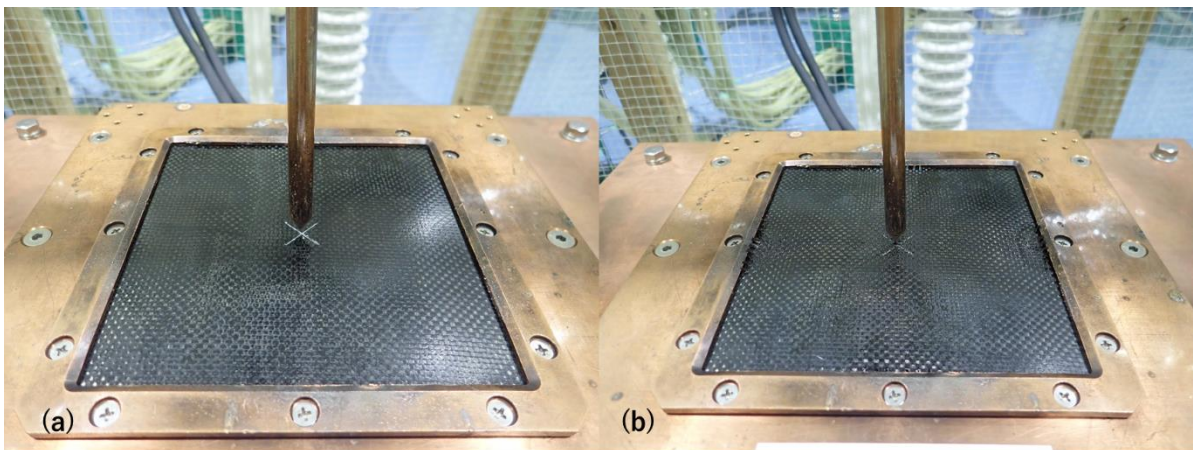
Figure 4-17 CF/Hybrid-1P7E before and after lightning strike (a) before and (b) after lightning strike
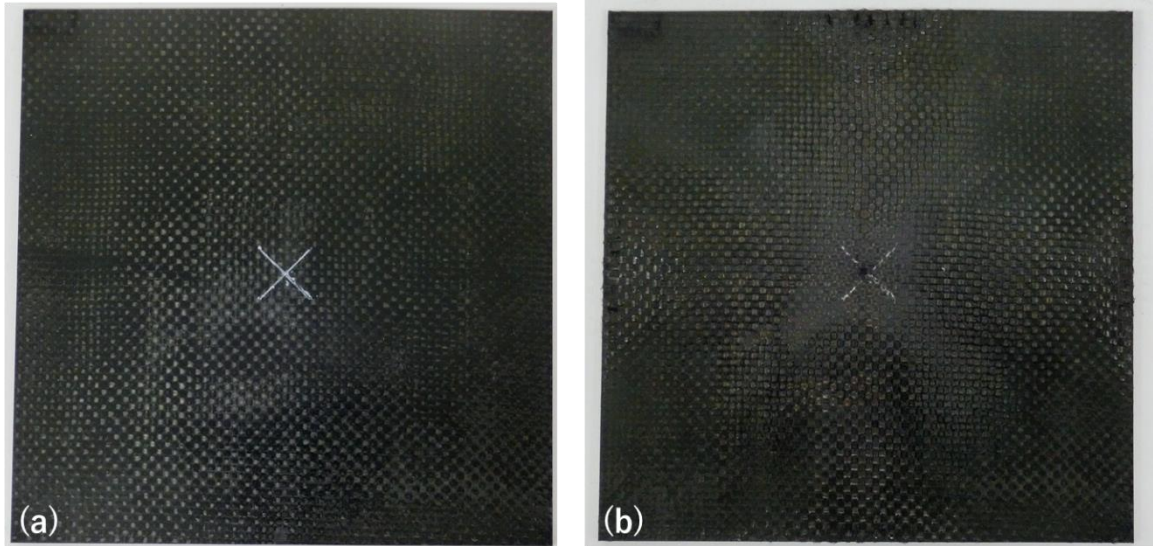
Figure 4-18 CF/Hybrid-1P7E at different angle on CF/PANI side (a) before and (b) after lightning strike
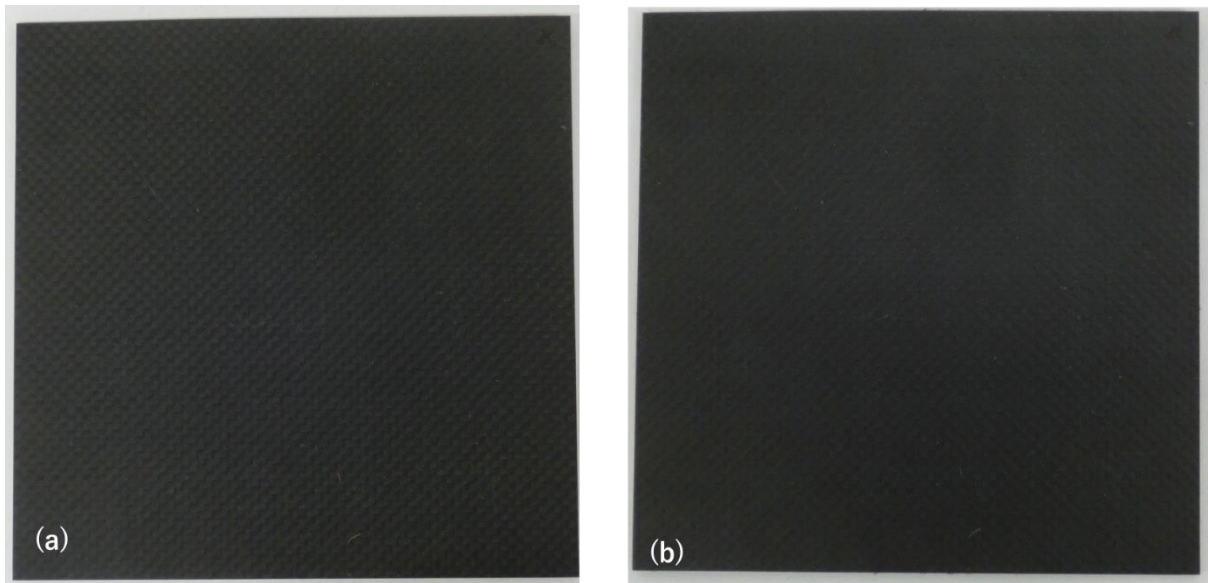
Figure 4-19 CF/Hybrid-1P7E at different angle on CF/Epoxy side (a) before and (b) after lightning strike
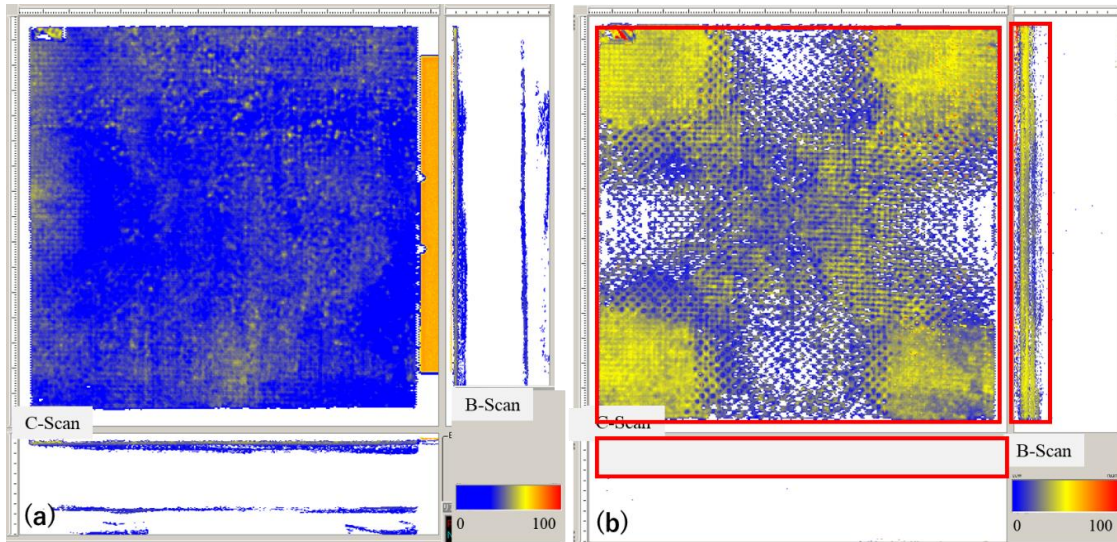
Figure 4-20 NDI images of CF/Hybrid-1P7E on CF/PANI side (a) before and (b) after lightning strike
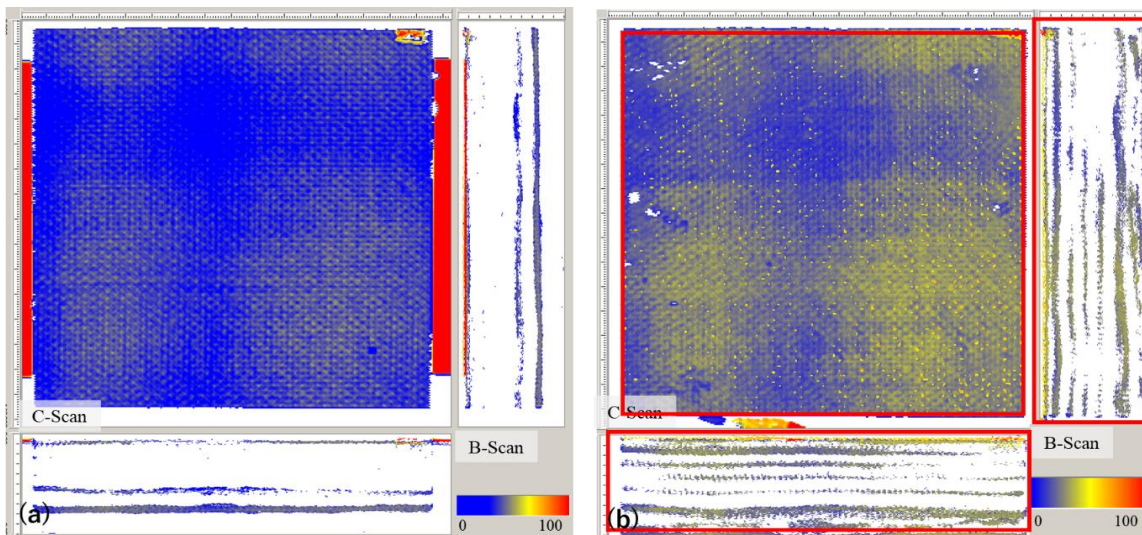
Figure 4-21 NDI images of CF/Hybrid-1P7E on CF/Epoxy side (a) before and (b) after lightning strike
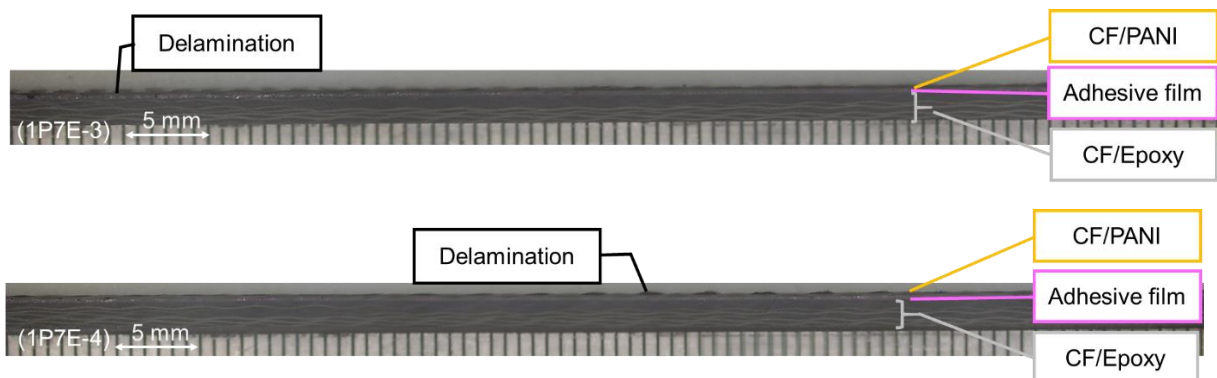
Figure 4-22 Cross-sectional images of CF/Hybrid-1P7E after lightning strike at 15 mm and 30 mm from the centre

Figure 4-23 Delamination at the edges of CF/Hybrid-1P7E of specimen number 1 and 3 (Centre parts)

The simulated lightning strike test has shown the effectiveness of CF/Hybrid structure for lightning strike protection using electrically conductive CF/PANI layer. By varying the number of CF/PANI layer, I can see that as long as CF/PANI has sufficient electrical conductivity, the CF/PANI sub-laminates could allow the lightning current to flow away from the panel without causing severe damage to the whole panel. However, when the number of CF/PANI layer becomes one layer, it could still protect the CF/Epoxy panel underneath, but it suffered from delamination. If I put this into practical application, the delaminated panels will require replacement in order to ensure the safety of the structure.

4.5   High speed images

High-speed camera has been employed to capture the phenomenon during the lightning strike. It is worth mentioning that the pattern of the lightning current flow in CF/Hybrid-1P7E is unique from the previous studies. This can be observed from high-speed images in Figure 4-24 and Figure 4-25. The images in the figure were selected to show the images at the time of the characteristic waveform; the images were indicated as t_0, t_1, t_2 and t_{last}. Typically, I can see that clouds which expanded from the lightning current flow on CF/Hybrid-4P4E and CF/Hybird-2P6E are hemispheres, similarly to the works of Kumar [54]. In contrast, the cloud on CF/Hybrid-1P7E is different from others. I can see that there is a combination of a hemisphere shape and a cross shape. The cross shape happened because the lightning current flowed through the shortest path to the copper jig. I considered that the thin layer of CF/PANI and the insulating adhesive film have allowed the lightning current to flow only in a thin layer of CF/PANI, unlike several layers of CF/PANI in other cases. This resulted in rapid flow to the copper jig and delamination in the CF/PANI layer. This phenomenon can also be observed in

the study of conducting pristine PANI-based layers with an insulating layer by Das [58]. The shapes of the cloud correlate with the thermography images and NDI images well and I will discuss further in the next sections.

The pyrolysis cloud in this study indicates the resin burnt due to high heat accumulation at the moment. This meant that the panel could not transfer the electric current from lightning strike fast enough to prevent energy accumulation and, hence, generate resistant heat that was high enough to evaporate the resin. This can be prevented by improving the electrical and thermal conductivity of the resin. However, this is out of the scope of this study.
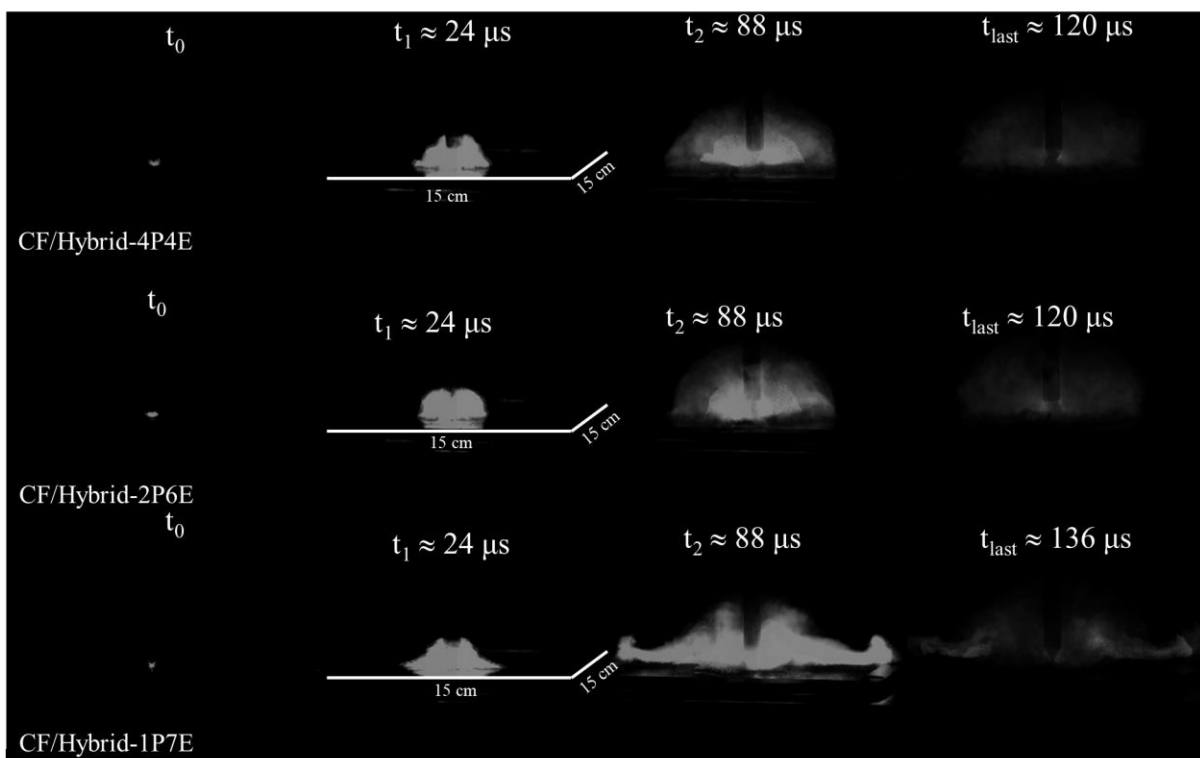
Figure 4-24 High-speed images of CF/Hybrid from front angle
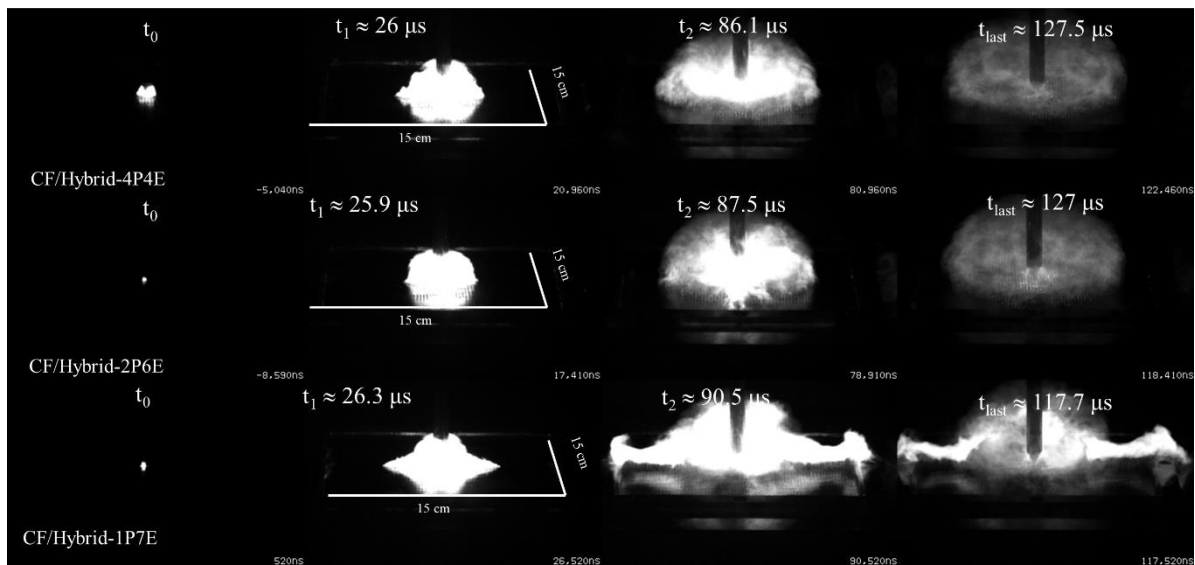
Figure 4-25 High-speed images of CF/Hybrid from different angle

4.6 Thermography images

A thermography camera has been utilized to observe the surface temperature distribution during the lightning strike. With the aid of this tool, I can obtain the surface temperature varying with time. The colours in the photos varies between 12 ˚C in blue colour to 146.12 ˚C in the pink colour. I can see different patterns in the three specimens. The shape of the lightning path changes according to the number of CF/PANI layers on top in Figure 4-26, Figure 4-27, and Figure 4-28. Each figure shows the surface temperature at the moment of lightning strike until next 0.42 seconds with 0.06-second interval (equivalent to the frame speed of the thermography camera (50/3 Hz))

Right after the burst of lightning strike, CF/Hybrid-4P4E shows the high temperature area in the shape of a circle that simultaneously expands and fades. This agrees with the pattern from the high-speed camera images that the smoke after the lightning strike is spherical.

Thermography images of CF/Hybrid-2P6E and CF/Hybrid-1P7E show a cross shape over the panel which is different from the previous results. This implies that the lightning transmitted through different paths from CF/Hybrid-4P4E. As the number of conductive CF/PANI is lessened, the amount of lightning penetrating into the depth of specimen (out-of-plane direction) decreases and the amount of lightning transmitted to the edges (in-plane direction) increases.
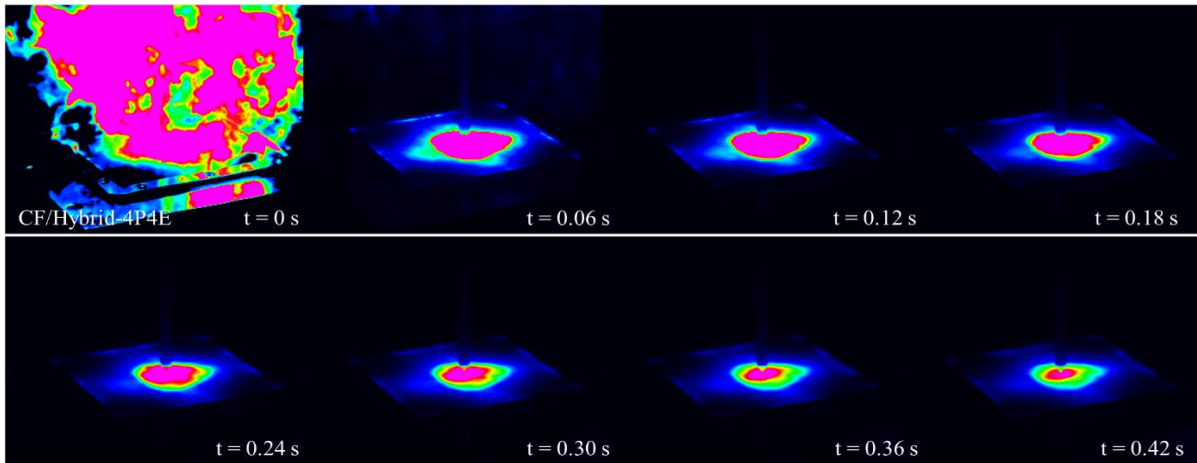
Figure 4-26 Thermography images of CF/Hybrid-4P4E
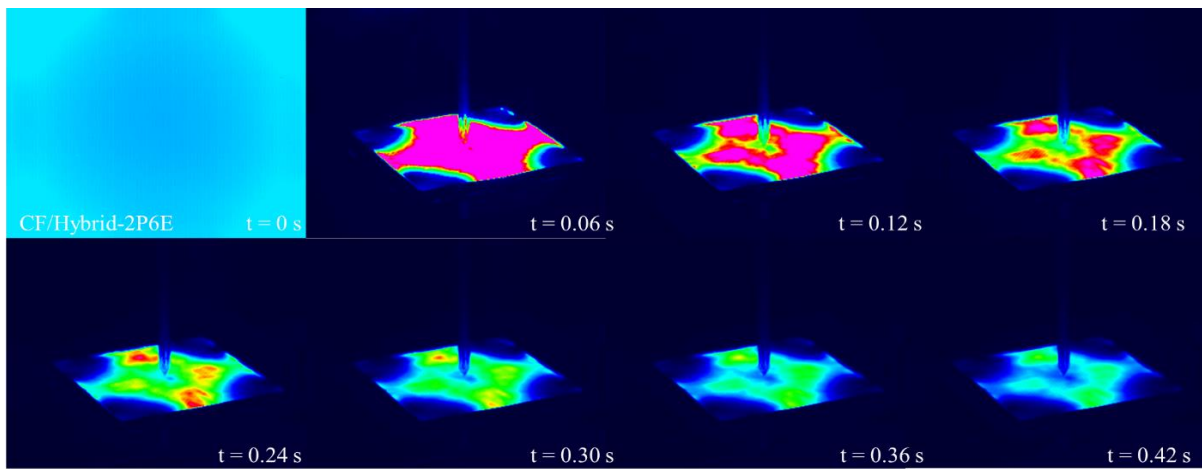
Figure 4-27 Thermography images of CF/Hybrid-2P6E
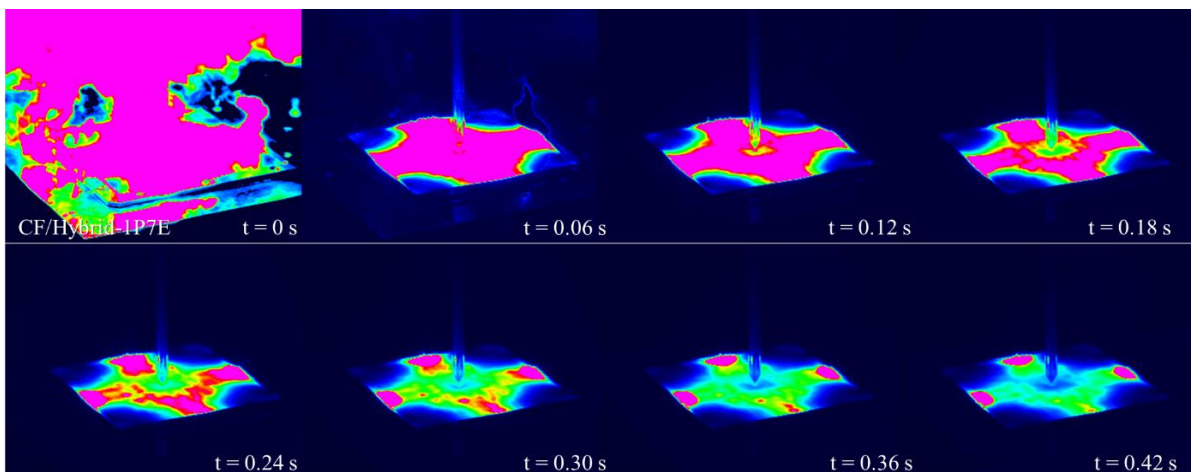
Figure 4-28 Thermography images of CF/Hybrid-1P7E
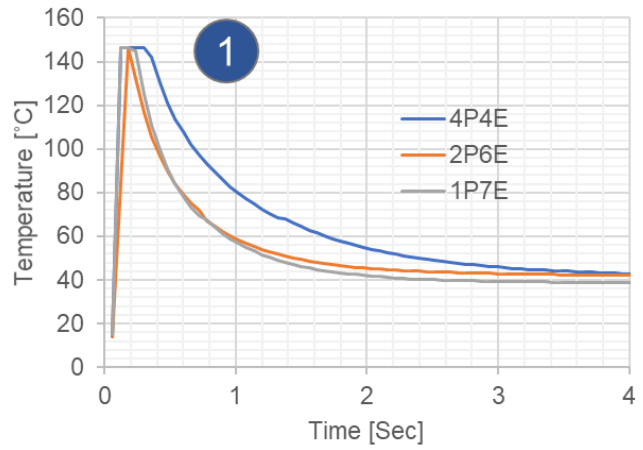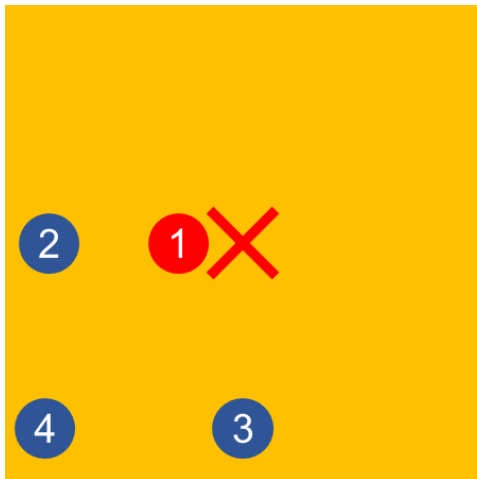
Figure 4-29 Temperature distribution over time at 5 mm from the centre
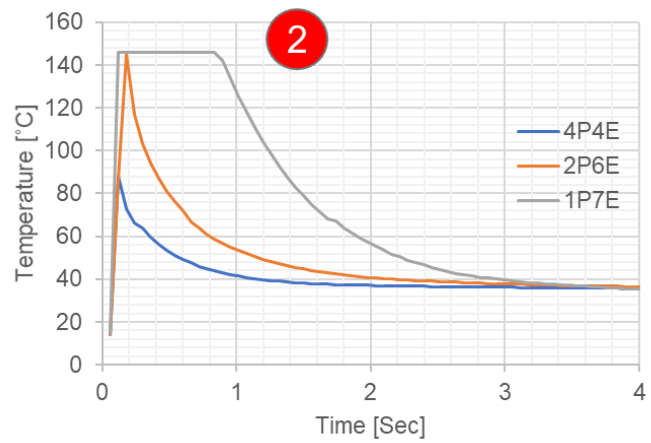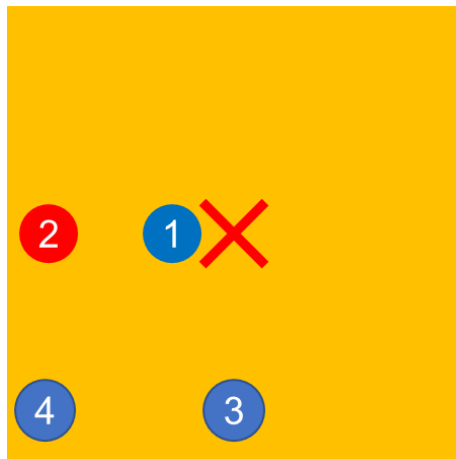
Figure 4-30 Temperature distribution over time at 70 mm from the centre
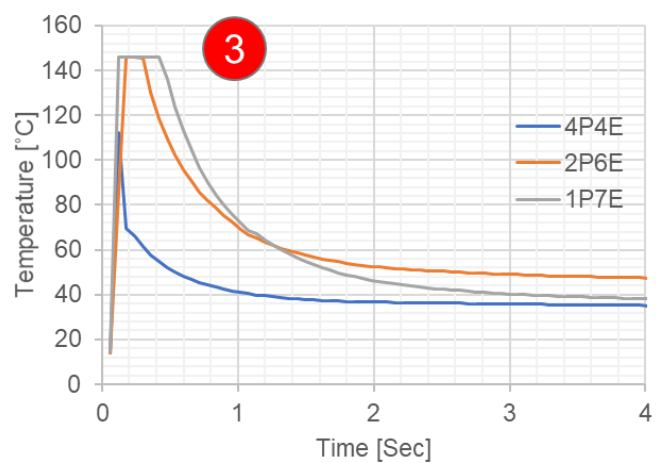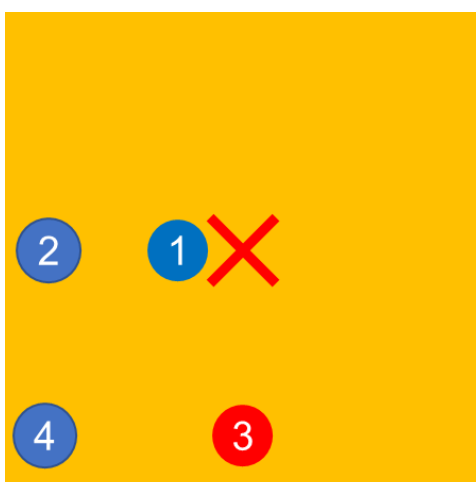
Figure 4-31 Temperature distribution over time at 70 mm from the centre
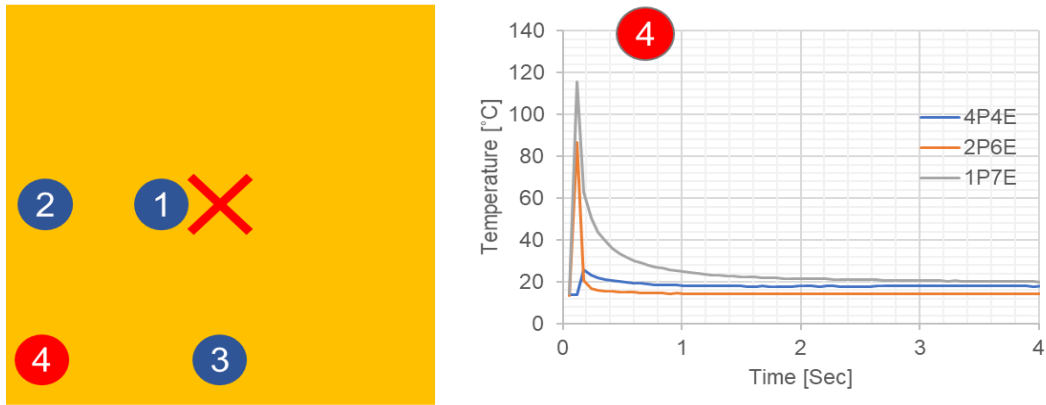
Figure 4-32 Temperature distribution over time at 80 mm from the centre

To confirm this hypothesis, I have plotted temperature changes over time at several points of the specimen surface as shown in Figure 4-29 to Figure 4-31. I observed temperature changes over the 4-second period at 5-mm from the centre, 70-mm from the centre in fibre direction (0 and 90), and 100-mm in diagonal direction. I compared the temperature change at each point among 3 specimens to see how the cooling rate differ among samples. Noted that the maximum detectable temperature is 146.12 ˚C. Any temperature higher than this will be observed as 146.12 ˚C. This results in the plateau in the temperature over time plot. If I can accurately obtain the real maximum temperature, I can further discuss the real cooling rate of the specimens. Due to the limitation of the equipment, I will focus only on the trend of temperature change.

The temperature changes over time at a 5-mm position from the centre in Figure 4-29 have shown that the specimen CF/Hybrid-4P4E have the lowest temperature dissipation. The temperature at this position took a longer time to decrease to the same level as others. While the specimens CF/Hybrid-2P6E and CF/Hybrid-1P7E did not show distinct differences. The surface temperature change at this point also implies that the lightning transferred away from the centre area quicker in CF/Hybrid-2P6E and CF/Hybrid-1P7E, but slower in CF/Hybrid-4P4E. That resulted in less Joule heating effect in the area that lightning went through, i.e., the temperature at the surface did not rise.

The thermography results indeed have several limitations: maximum measurable temperature, detection of only surface temperature, and low frame rate. Despite these limitations, the results can be interpreted by combining with other data to confirm or further explain the cause of damage. When I combine the NDI images with the thermography images, I can correlate the damage pattern as shown in Figure 4-33.
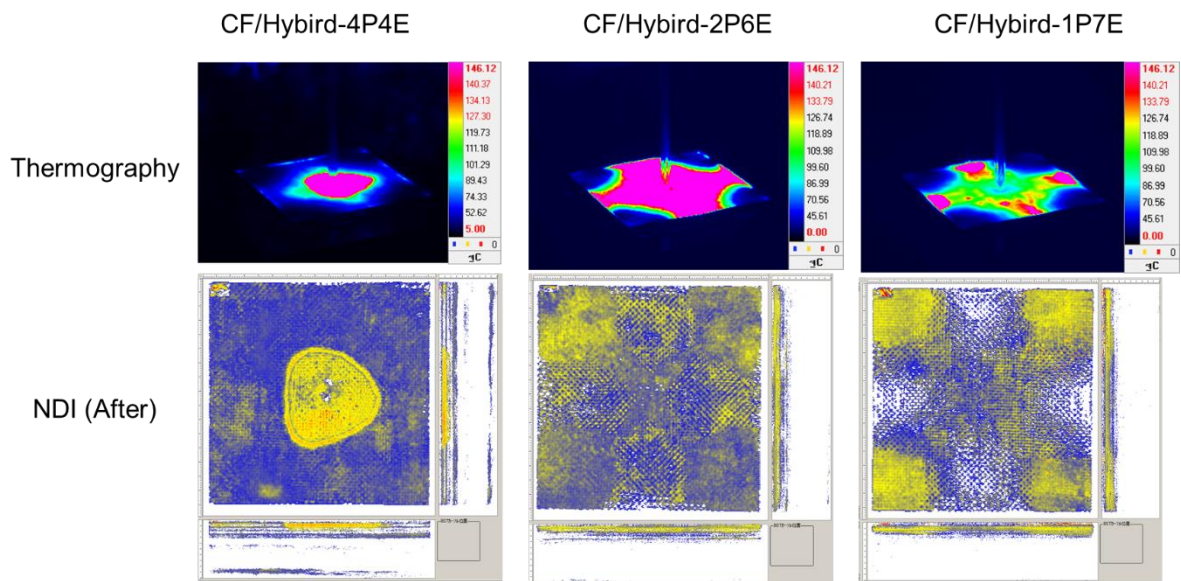
Figure 4-33 Comparison between NDI and thermography of the same specimen

The NDI image of CF/Hybrid-4P4E has a similar shape of area with the thermography image after lightning strike 0.06 second, which showed in the pink area. The area showed the highest temperature detected. After several seconds, the pink area shrunk and faded, but the damage remains as shown in the NDI image. This meant that the specimen suffered from temperature rise in the area due to joule heating. The exact temperature that triggers joule heating should be studied further. From comparing the temperature distribution and the damage area, the trigger temperature is around 140 ℃.

Comparison of NDI image and thermography image of CF/Hybrid-2P6E is vague to see the clear relation between both results. The thermography image after the lightning strike 0.06 second shows a large area of maximum detectable temperature. This area related to the damaged area in NDI images. Although I could not see a clear pattern here, if I closely observe, I can see a cross shape in NDI images which correspond to the shape in thermography images.

For CF/Hybrid-1P7E, its NDI image and thermography images conform clearly. I can clearly see the cross shape in NDI image similar to one in thermography. One distinct point in its thermography is that the 3 edges of the cross shape were pink. This meant that the temperatures in these areas are high. This is because as the layer transfers the lightning through the panel, joule heating effect occurs at the corners and damaged these areas greatly that delamination also occurs. I can confirm this by observing the specimen after the test as well as

78

UT image.

The other way to use UT images is to calculate and compare the area before and after lightning strike test. To perform this, the UT images were converted into black-and-white pictures, so-called binarization. The black area represents intact part of the panel. The white area represents the damaged part. Figure 4-34 shows the example of binarization of the UT images.

Before   After
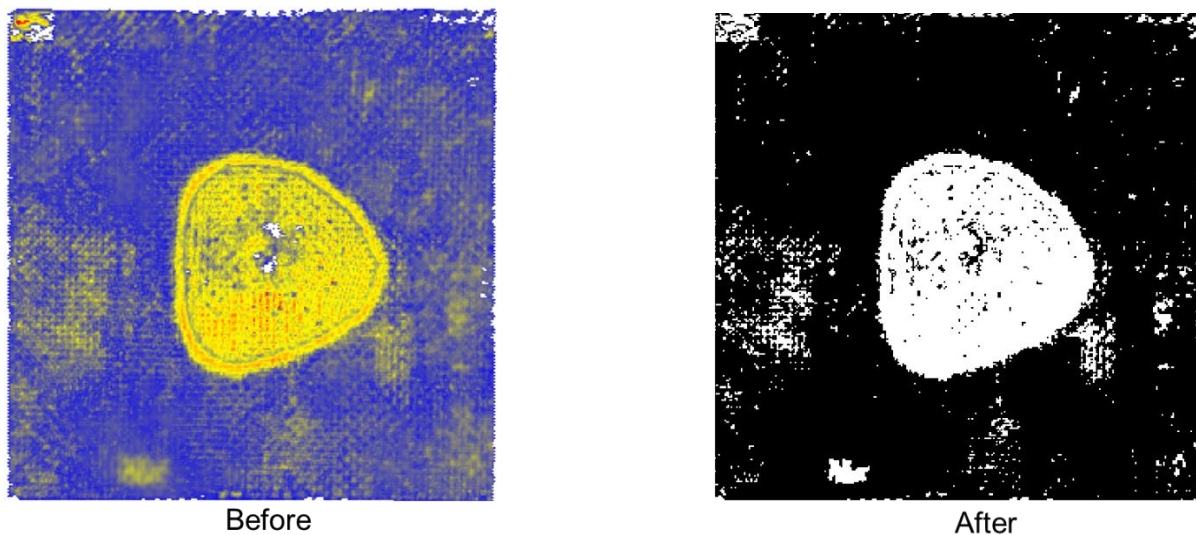
Figure 4-34 Binarization of ultrasonic image

Figure 4-35 compares the binarization of CF/PANI sides and the damaged areas were calculated and shown in Table 4-4. The percentage of damaged area after lightning strike test increase drastically. This confirmed the damage on CF/PANI. Note that the white areas at four corners of the CF/Hybrid-1P7E includes the white area that originally appeared in UT image. Since the cross-section images of the samples and thermography images showed evidence that they were damaged, the white areas at all corners were considered as damaged area.

On the other hand, the binarization of CF/Epoxy was compared in Figure 4-36 and the area calculation is shown in Table 4-5. The damaged areas increase slightly comparing to their CF/PANI counterparts. This aligned with the assumption that the insulating adhesive layer help preventing lightning current passing through. Note that high percentage of damaged area in CF/Hybrid-1P7E is unclear whether the ultrasonic wave detected the damaged from the other side or other causes.
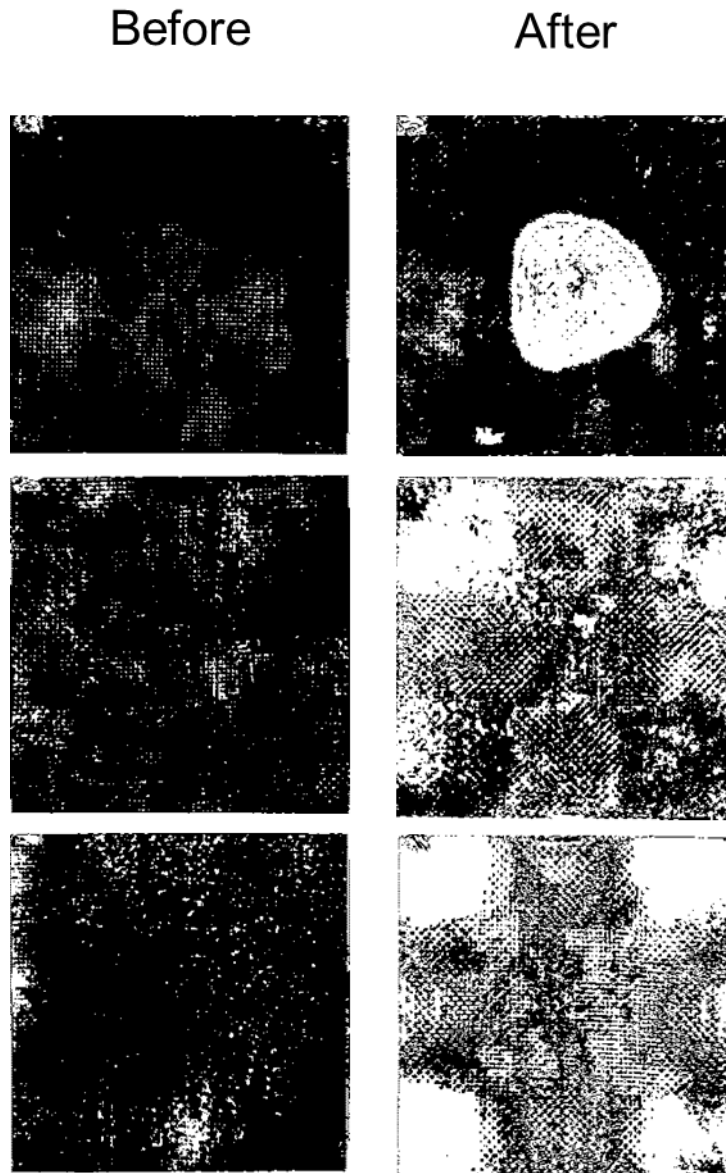
Figure 4-35 Binarization of UT images on CF/PANI side

Table 4-4 Calculation of the damaged area of binatization on CF/PANI side

% Damaged area	Before (%)	After (%)
CF/Hybrid-4P4E	3.84	19.32
CF/Hybrid-2P6E	5.78	48.11
CF/Hybrid-1P7E	6.70	61.60
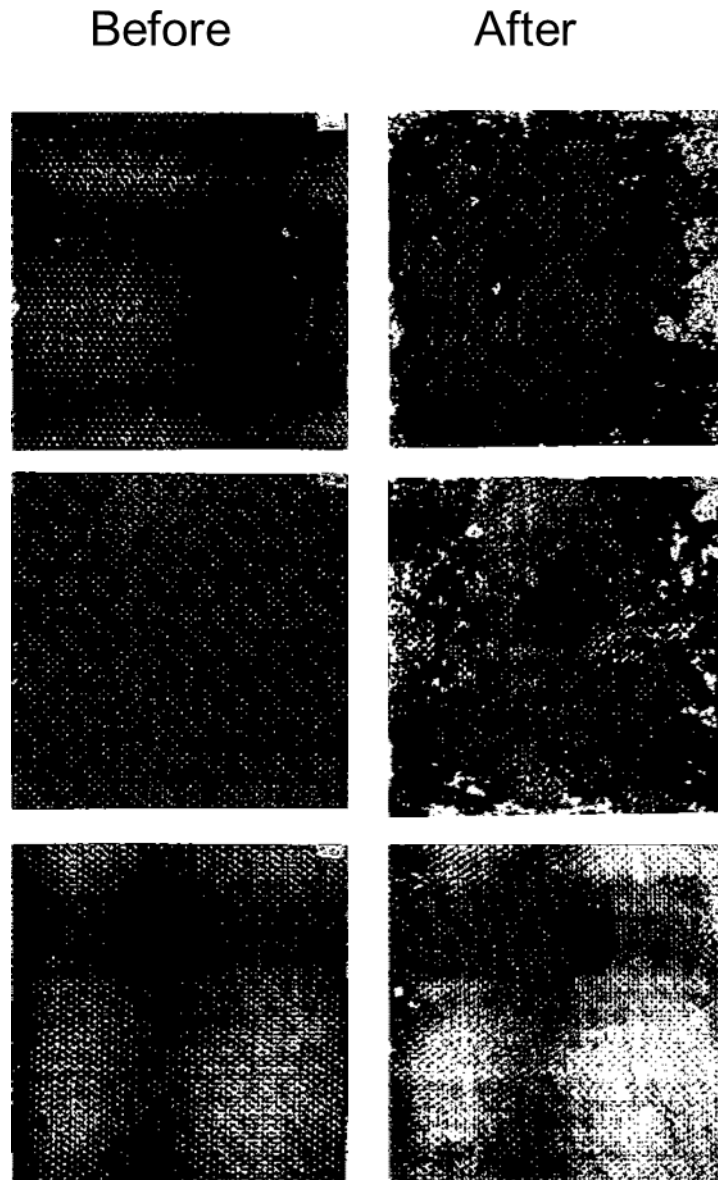
Figure 4-36 Binarization of UT images on CF/Epoxy side

Table 4-5 Calculation of the damaged area of binatization on CF/Epoxy side

% Damaged area	Before	After
CF/Hybrid-4P4E	4.00	6.94
CF/Hybrid-2P6E	3.35	8.85
CF/Hybrid-1P7E	9.91	33.15

To summarize, I can utilize thermography images to provide surface temperature distribution over time. I can combine these images with high-speed camera, NDI images as well as observing the real specimens to clarify the damage mechanism.

4.7   Residual strength

Subsequent to the lightning strike test, the specimens were measured for their residual bending strengths. The specimens were cut at the centre where the lightning strike into 15-mm width while the length remained 150 mm to avoid causing unexpected damages. Due to the limitation of specimens, I conducted the test only on the CF/PANI side and only 2 specimens. As shown in Table 4-6, the tested results were compared with the corresponding CF/Hybrid on CF/PANI side. The residual bending strength in the case of CF/hybrid-4P4E has decreased to 232 MPa (around 70% of the intact specimens). However, in the cases of CF/Hybrid-2P6E and CF/Hybrid-1P7E, the residual bending strengths were much higher than the corresponding intact specimens. This is probably because the CF/PANI sub-laminates of the tested specimens has completely failed and could not withstand any mechanical loading. Instead, the residual bending strength indicated the bending strength of the CF/Epoxy sub-laminates.

The load-displacement curves of residual specimens and the comparison with pristine specimen are shown in Figure 4-38 and Figure 4-39 for CF/Hybrid-4P4E, Figure 4-40 and Figure 4-41 for CF/Hybrid-2P6E, Figure 4-42 and Figure 4-43 for CF/Hybrid-1P7E. These can help identify the differences clearly.

Table 4-6 Residual strengths of specimens

Samples	Intact bending stress (MPa)	Residual stress (MPa)	Residual ratio	Mode of failure
CF/Hybrid-4P4E	328.17 ± 32.5	232.0 ± 33.6	0.71	Delamination
CF/Hybrid-2P6E	194.89 ± 26.7	384.05 ± 1.67	1.97	Tensile failure
CF/Hybrid-1P7E	212.93 ± 25.3	471.9 ± 51.15	2.22	Tensile failure
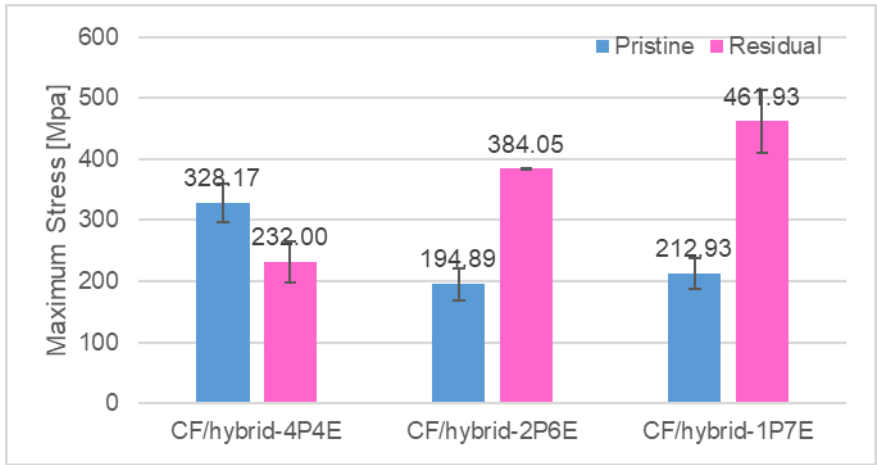
Figure 4-37 Residual strength compared with pristine
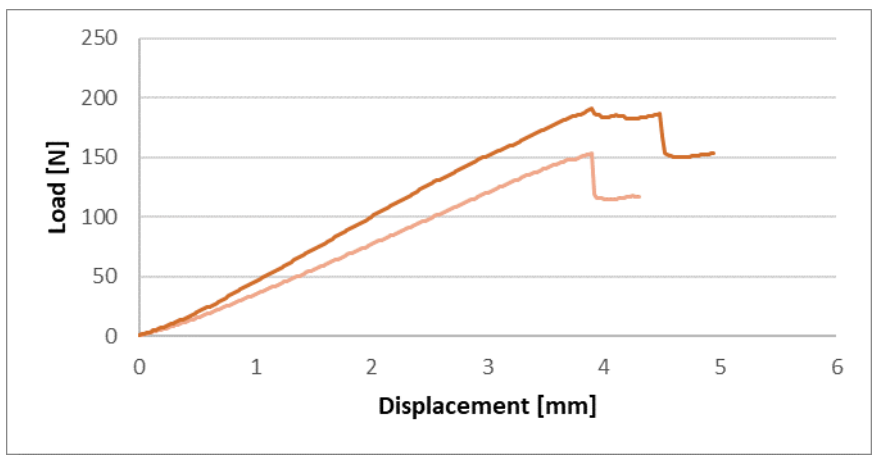
Figure 4-38 Load-displacement curve of CF/Hybrid-4P4E after lightning strike
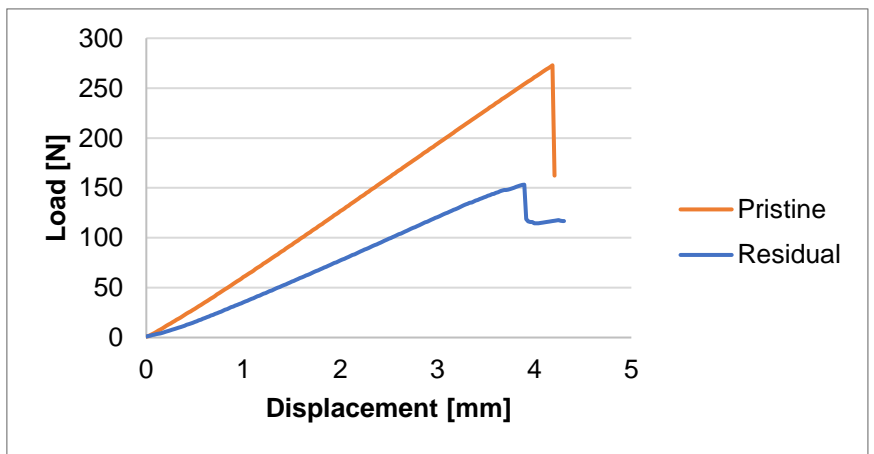
Figure 4-39 Load-displacement of pristine and residual specimens of CF/Hybrid-4P4E
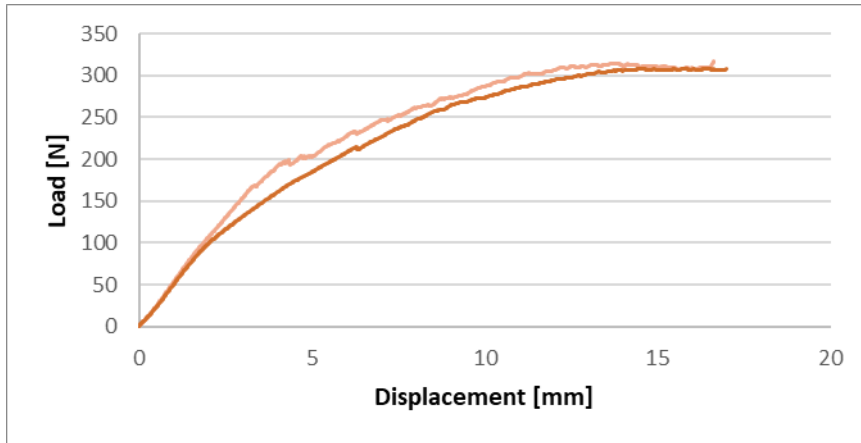
Figure 4-40 Load-displacement curve of CF/Hybrid-2P6E after lightning strike
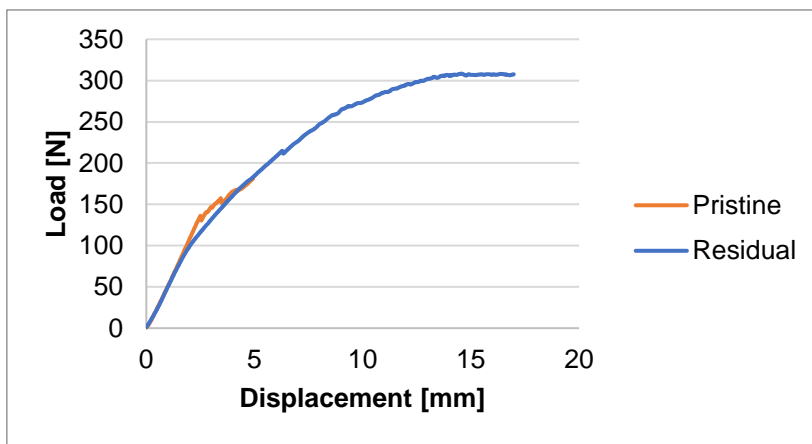
Figure 4-41 Load-displacement of pristine and residual specimens of CF/Hybrid-2P6E
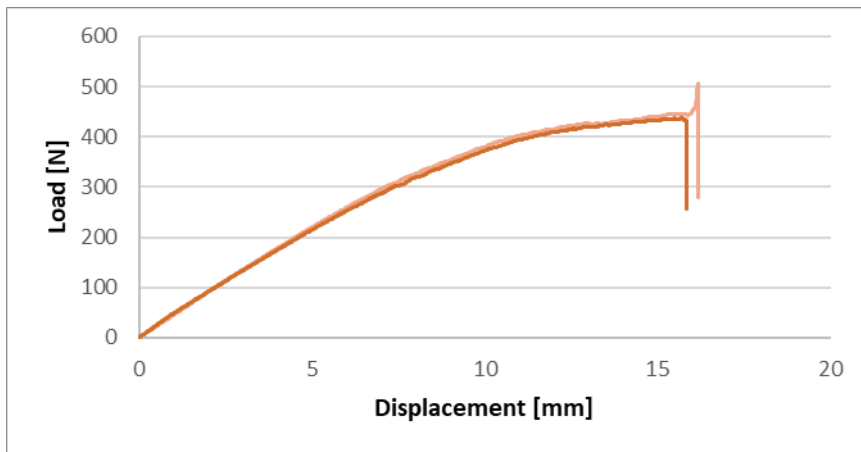
Figure 4-42 Load-displacement curve of CF/Hybrid-1P7E after lightning strike
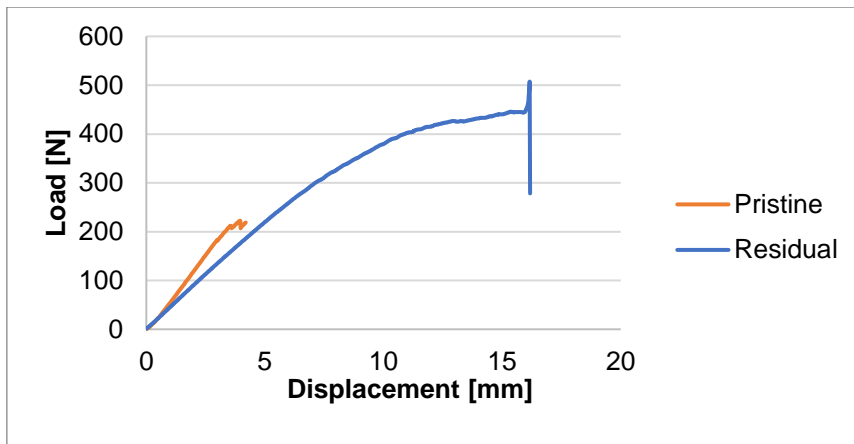
Figure 4-43 Load-displacement of pristine and residual specimens of CF/Hybrid-1P7E

The cross-sectional images of specimens after residual test were captured to observe the mode of failure. Figure 4-44 shows the cross-sectional images from the residual specimens of CF/Hybrid-4P4E. They show large gap between CF/PANI and CF/Epoxy which indicates the delamination between them. The delamination was widened after the residual test compared to Figure 4-10.

Figure 4-45 shows the cross-sectional images from the residual specimens of CF/Hybrid-2P6E. The failure mode is the fibre breakage of CF/Epoxy underneath. This meant that the CF/PANI could not bear the load and the CF/Epoxy has taken the load instead. That is CF/PANI has been damaged heavily during lightning strike. The same goes for CF/Hybrid-1P7E as shown in Figure 4-46.
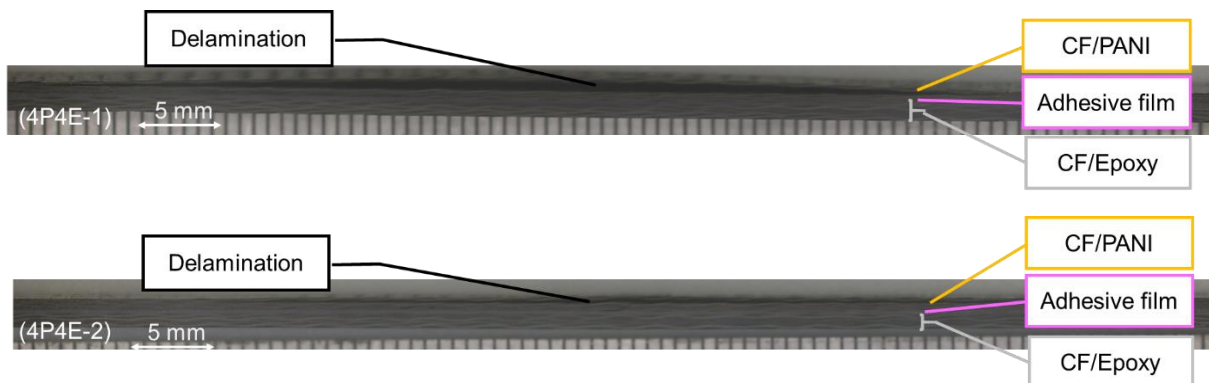
Figure 4-44 Cross-sectional images of CF/Hybrid-4P4E after residual strength at 15 mm and 30 mm from the centre
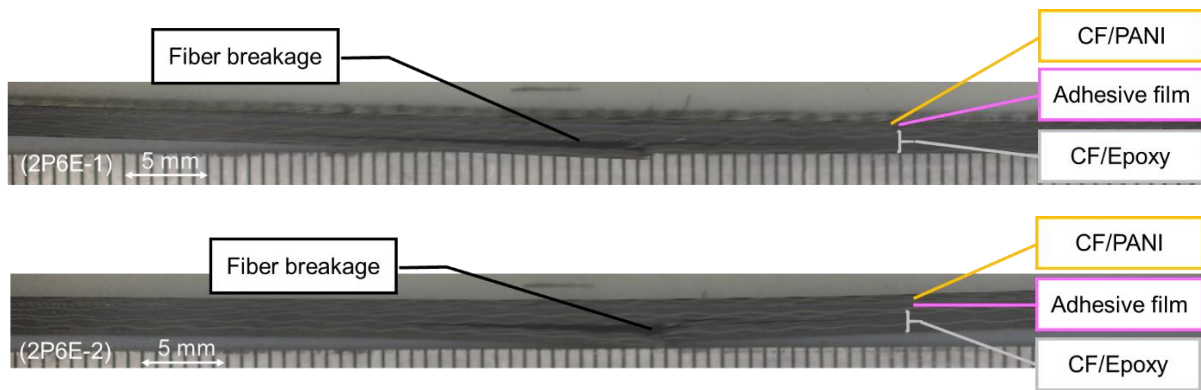
Figure 4-45 Cross-sectional images of CF/Hybrid-2P6E after residual strength at 15 mm and 30 mm from the centre
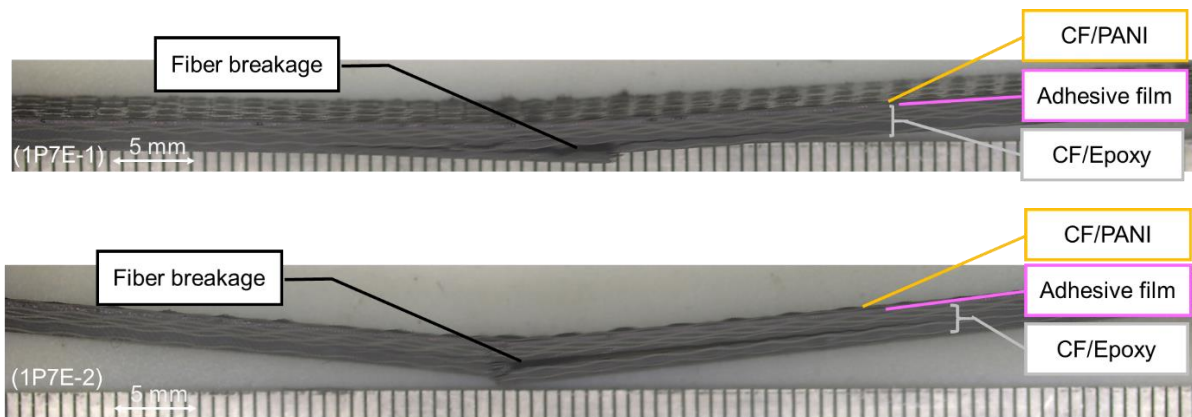
Figure 4-46 Cross-sectional images of CF/Hybrid-1P7E after residual strength at 15 mm and 30 mm from the centre

Therefore, I can conclude that although I did not detect any damage in specimens from the visual inspection and NDI images, I could not ensure that the specimen did not mechanically fail. This finding reiterated the importance of assuring the inspection and maintenance if the structure is put into practice.

4.8 Summary

The effectiveness of lightning strike has been tested and inspected using various equipment and methods combined together. A short moment that lightning strike has many incidents inside and I clarified them. I visually inspected the specimens and could not see obvious damages. However, with assistance of NDI, I can clearly see the changes between before and after the test. Also, using high speed images as well as thermography images, I can see the patterns of lightning strike in the specimens. This helps explaining the damage mechanisms on the panels. With these findings, I came to understand the requirements to

design LSP for CF/Epoxy that they should have at least some certain layers to be lightning current path. The quest to quantification this path is still underway to discover.

Chapter 5   Conclusion and Recommendations

5.1   Conclusion

This study has presented the evaluation of a conceptual structure of hybrid layerwise laminates (CF/Hybrid) which consist of 2 laminae with different resins: conventional epoxy resin and electrically conductive resin. With the aim to prevent lethal accidents due to lightning strike and substitute the current lightning strike protection (LSP) system, the structure has adopted the PANI-based resin system of the successful research experiment to make the conductive CFRP layer (CF/PANI) that will protect the conventional epoxy CFRP (CF/Epoxy) underneath. This hybrid layerwise laminate (CF/Hybrid) is expected to replace the current metal mesh LSP which is more complicated and more weight addition.

This thesis tries to verify the characterisation by using mechanical tests: four-point bending test, interlaminar shear strength test, and fracture toughness test in mode one and two. The tests were conducted on both sides of the specimens due to different properties. For lightning strike preparation, the electrical conductivity was measured. There were altogether 3 cases of CF/Hybrids which were varied by CF/PANI and CF/Epoxy to obtain 8 layers of laminate: CF/Hybrid-4P4E, CF/Hybrid-2P6E, and CF/Hybrid-1P7E where the number before P represents the number of CF/PANI layers and the number before E represents the number of CF/Epoxy layers. The bending strength of hybrid laminates were in range of 194 MPa to 328 MPa on CF/PANI side and in range of 554 MPa to 684 MPa on CF/Epoxy side. In the same trend, the flexural moduli decrease with increasing number of CF/Epoxy in the laminates. This is because the CF/Epoxy in this study has low volume fraction. When I look closer at the damages, the specimen tested on CF/PANI sides are mostly failed by compressive failure and damage did not go through into CF/Epoxy layer. On the other hand, the specimens tested on CF/Epoxy side failed by either delamination of CF/PANI or fibre breakage of CF/Epoxy.

The ILSS tests were conducted in the same manner. The ILSS were in range of 33 MPa to 53 MPa on CF/PANI side and in range of 37 MPa to 53 MPa on CF/Epoxy side. For ILSS, the results on both sides are not distinguished because the maximum shear planes were in CF/Epoxy layers. Also, the mode of failure of 8-layer specimens are not explicitly shear failure. Therefore, the experiment is repeated with thicker specimens of 16 layers. The ILSS of CF/PANI and CF/Epoxy remain unchanged. However, the ILSS of CF/Hybrid-16L varied due to its thickness.

The interlaminar fracture toughness tests were conducted on both CF/PANI and CF/Epoxy sides except fracture toughness test mode I. The results show obvious differences between CF/PANI and CF/Epoxy and CF/Hybrids fall either between or higher than CF/Epoxy. This is because the interfaces were strengthened by the adhesive film and they prevented crack propagation. The values that measured in CF/Hybrid specimens did not represent the true interfaces properties due to the adhesive film insertion.

Conductivity of the hybrid specimens were measure in thickness direction. However, the results are nearly zero. Therefore, the CF/PANI part of the CF/Hybrid were separated and measured. The electrical conductivity of the specimens varies from 0.49 S/cm to 0.78 S/cm.

After confirming that the CF/Hybrids have sufficient strength as well as high electrical conductivity, the CF/Hybrids were inspected using non-destructive inspection (NDI) before testing against lightning strike.

Simulated lightning strike tests were conducted with modification from the standard SAE ARP-5412B. The specimen was fixed to a picture-frame-type copper jig, which was attached to the ground of the impulse current generator. The specimen was held by the base plate and cover frame at all edges by screw-clamping. Lightning current was applied at the centre of the specimen surface, where the gap between the tip of the discharge probe and the surface of specimen is 2 mm. Additionally, several observation methods were employed to help clarify the lightning strike phenomena: high-speed cameras, and a thermography camera. After the test, damages were evaluated and analyzed.

These results have indicated that to achieve the coexistence of structural strength and electrical conductivity, at least 4 layers of CF/PANI should be incorporated on the top of CF/Epoxy. This is because the experimental results of CF/Hybrid-4P4E have proven the highest potential to withstand lightning strikes both mechanically and electrically. In terms of mechanical properties, although other specimens showed higher strength due to higher number of CF/Epoxy layers, higher number of CF/PANI layers indicates higher strength as well as effectiveness to withstand lightning strike damages. By comparing damages visually, CF/Hybrid-4P4E obviously shows less damages compared to other cases. When observing the phenomena during lightning strike, CF/Hybrid-4P4E shows the potential to conduct lightning current quickly. In high-speed cameras, the pyrolysis could, which was generated from resin burnt, expanded steadily as a sphere shape from the centre. This means the lightning moved steadily within the CF/PANI layers unlike the case of CF/Hybrid-7P1E that the cloud generated

in a cross shape due to fast flow of lightning current. The thermography images also confirm this trend. Within the same period of time, the surface temperature of the CF/Hybrid-4P4E panel decreases considerably faster than others (less high temperature area). The other method that confirms this result is residual strength test. The residual strength of CF/Hybrid-4P4E shows residual ratio of 0.71 while others are more than 2.5. This meant that the CF/PANI of other cases delaminated and did not contribute to the strength, so the CF/Epoxy parts bear all the load and resulted in high strength ratios.

This thesis has introduced the concept of layerwise hybrid laminates using both CF/PANI and CF/Epoxy to achieve the coexistence of electrical conductivity as well as structural strength without compromising additional weight. This structure can cover each disadvantage and bring about possible application as LSP for aircraft. This concept has been built on simple methods and has a potential to apply with different materials or structure to accomplish synergistic results.

5.2   Recommendations

5.2.1   Improve the strength and electrical conductivity of resin

Even though the author tried to incorporate high strength layer of CF/Epoxy, the failure in CF/PANI layer is inevitable and requires improvement. Also, according to SAE ARP-5412B, the peak current that the specimens need to be able to withstand is -200 kA. This study conducted the lightning strike test at only -40 kA, which is just a small portion of the peak current. Therefore, the conductive laminates that are suitable to replace the current system must be able to satisfy requirements of both mechanical strength and electrical conductivity.

5.2.2   Fracture toughness test of CF/Hybrid without adhesive film

In this study, the CF/Hybrid was conducted fracture toughness test with adhesive film to represent the properties of the whole specimens. However, adhesive film has prevented the crack propagation and lead to undesirable results. One suggestion is to conduct the test on CF/Hybrid without adhesive so that the results can be obtained.

5.2.3   Consider acoustic shock effect

Acoustic shock which is a unique type of loading during the lightning strike. It is worth studying the effect on the structure, so that the structural design could be improved. More complicated test could be performed to understand the coupling effect, too.

Reference

[1]   "Composites VS. Aluminum - Composites Compared | Composites Lab." [Online]. Available: http://compositeslab.com/composites-compared/composites-vs-aluminum/. [Accessed: 24-Jun-2021].

[2]   "The first composite fuselage section for the first composite commercial jet | CompositesWorld." [Online]. Available: https://www.compositesworld.com/articles/the-first-composite-fuselage-section-for-the-first-composite-commercial-jet. [Accessed: 24-Jun-2021].

[3]   B. Alemour, O. Badran, and M. R. Hassan, "A review of using conductive composite materials in solving lightening strike and ice accumulation problems in aviation," *Journal of Aerospace Technology and Management*, vol. 11. Journal of Aerospace Technology and Management, 28-Mar-2019.

[4]   W. L. Golding, "In-Flight Icing and How Airlines Are Coping In-Flight Icing and How Airlines Are Coping Scholarly Commons Citation Scholarly Commons Citation IN-FLIGHT ICING AND HOW AIRLINES ARE COPING," *J. Aviat. Educ. Res.*, vol. 13, no. 3, 2004.

[5]   "TWA Flight 800 - Wikipedia." [Online]. Available: https://en.wikipedia.org/wiki/TWA_Flight_800. [Accessed: 24-Jun-2021].

[6]   A. Broc *et al.*, "A lightning swept stroke model: A valuable tool to investigate the lightning strike to aircraft," *Aerosp. Sci. Technol.*, vol. 10, no. 8, pp. 700–708, Dec. 2006.

[7]   B. Peyrou, A. Chazottes, P. Q. Elias, L. Chemartin, and P. Lalande, "Direct Effects of Lightning on Aircraft Structure : Analysis of the Thermal , Electrical and Mechanical Constraints," *J. Aerosp. Lab*, no. 5, pp. 1–15, 2012.

[8]   "Lightning Strikes: Protection, Inspection, and Repair." [Online]. Available: https://www.boeing.com/commercial/aeromagazine/articles/2012_q4/4/. [Accessed: 29-May-2021].

[9]   "Protecting Aircraft Composites from Lightning Strike Damage | COMSOL Blog." [Online]. Available: https://www.comsol.com/blogs/protecting-aircraft-composites-from-lightning-strike-damage/. [Accessed: 24-Jun-2021].

[10]   Y. Shi, L. Peng, Y. Ding, Y. Zhao, and G. Yu, "Nanostructured conductive polymers for

advanced energy storage," *Chem. Soc. Rev.*, vol. 44, no. 19, pp. 6684–6696, 2015.

[11]   C. W. Lin, B. J. Hwang, and C. R. Lee, "Methanol sensors based on the conductive polymer composites from polypyrrole and poly (vinyl alcohol)," *Mater. Chem. Phys.*, vol. 55, no. 2, pp. 139–144, Sep. 1998.

[12]   J. Tsukamoto, "Recent advances in highly conductive polyacetylene," *Adv. Phys.*, vol. 41, no. 6, pp. 509–546, Jan. 1992.

[13]   B. Hideki Shirakawa, E. J. Louis, A. G. Macdiarmid, C. H. W A N K Chiang, and A. J. HEEGERt, "Synthesis of Electrically Conducting Organic Polymers : Halogen Derivatives of Polyacetylene, (CH)," 1977.

[14]   K. Kaneto, K. Yoshino, and Y. Inuishi, "Electrical and optical properties of polythiophene prepared by electrochemical polymerization," *Solid State Commun.*, vol. 46, no. 5, pp. 389–391, May 1983.

[15]   R. J. Waltman, J. Bargon, and A. F. Diaz, "Electrochemical Studies of Some Conducting Polythiophene Films," 1983.

[16]   S. Ghosh and O. Inganäs, "Electrochemical Characterization of Poly(3,4-ethylene dioxythiophene) Based Conducting Hydrogel Networks," *J. Electrochem. Soc.*, vol. 147, no. 5, p. 1872, May 2000.

[17]   A. V. Murugan, B. B. Kale, C.-W. Kwon, G. Campet, and K. Vijayamohanan, "Synthesis and characterization of a new organo-inorganic poly(3,4-ethylene dioxythiophene) PEDOT/V 2 O 5 nanocomposite by intercalation."

[18]   D. R. Gagnon, J. D. Capistran, F. E. Karasz, and R. W. Lenz, "Conductivity anisotropy in oriented poly(p-Phenylene vinylene)," *Polym. Bull.*, vol. 12, no. 4, pp. 293–298, Oct. 1984.

[19]   D. R. Gagnon, J. D. Capistran, F. E. Karasz, R. W. Lenz, and S. Antoun, "Synthesis, doping, and electrical conductivity of high molecular weight poly(p-phenylene vinylene)," in *Polymer*, 1987, vol. 28, no. 4, pp. 567–573.

[20]   J. C. Carter *et al.*, "Operating stability of light-emitting polymer diodes based on poly(p-phenylene vinylene)," *Appl. Phys. Lett.*, vol. 71, no. 1, pp. 34–36, Jul. 1997.

[21]   Y. Hirano *et al.*, "Lightning damage suppression in a carbon fiber-reinforced polymer with a polyaniline-based conductive thermoset matrix," *Compos. Sci. Technol.*, vol. 127,

pp. 1–7, 2016.

[22] Y. Hirano *et al.*, "Effectiveness of Lightning Damage Protection of CFRP with Polyaniline-Based Conductive Thermoset Matrix," vol. 64, no. 4, pp. 223–228, 2016.

[23] T. Yokozeki, Y. Iwahori, S. Ishiwata, and K. Enomoto, "Mechanical properties of CFRP laminates manufactured from unidirectional prepregs using CSCNT-dispersed epoxy," *Compos. Part A Appl. Sci. Manuf.*, vol. 38, no. 10, pp. 2121–2130, 2007.

[24] A. Katunin, K. Krukiewicz, R. Turczyn, P. Sul, and K. Dragan, "Lightning strike resistance of an electrically conductive CFRP with a CSA-doped PANI/epoxy matrix," *Compos. Struct.*, vol. 181, pp. 203–213, Dec. 2017.

[25] A. Katunin, K. Krukiewicz, R. Turczyn, P. Sul, A. Łasica, and M. Bilewicz, "Synthesis and characterization of the electrically conductive polymeric composite for lightning strike protection of aircraft structures," *Compos. Struct.*, vol. 159, pp. 773–783, Jan. 2017.

[26] V. Kumar, T. Yokozeki, T. Goto, and T. Takahashi, "Mechanical and electrical properties of PANI-based conductive thermosetting composites," *J. Reinf. Plast. Compos.*, vol. 34, no. 16, pp. 1298–1305, 2015.

[27] V. Kumar, T. Yokozeki, T. Goto, and T. Takahashi, "Synthesis and characterization of PANI-DBSA/DVB composite using roll-milled PANI-DBSA complex," *Polym. (United Kingdom)*, vol. 86, pp. 129–137, 2016.

[28] V. Kumar, Y. Zhou, G. Shambharkar, V. Kunc, and T. Yokozeki, "Reduced de-doping and enhanced electrical conductivity of polyaniline filled phenol-divinylbenzene composite for potential lightning strike protection application," *Synth. Met.*, vol. 249, pp. 81–89, Mar. 2019.

[29] S. Pati, V. Kumar, T. Goto, T. Takahashi, and T. Yokozeki, "Synthesis and characterization of PANI/P-2M conductive composites: Thermal, rheological, mechanical, and electrical properties," 2019.

[30] V. Kumar *et al.*, "Effect of through-thickness electrical conductivity of CFRPs on lightning strike damages," *Compos. Part A Appl. Sci. Manuf.*, vol. 114, pp. 429–438, Nov. 2018.

[31] Y. Zhou *et al.*, "Comparison of semi-doped PANI/DBSA complex achieved by thermal

doping and roll-mill process: A new perspective for application," *Polymer (Guildf).*, vol. 202, p. 122723, Aug. 2020.

[32] G. Marom, S. Fischer, F. R. Tuler, and H. D. Wagner, "Hybrid effects in composites: conditions for positive or negative effects versus rule-of-mixtures behaviour," *J. Mater. Sci.*, vol. 13, no. 7, pp. 1419–1426, 1978.

[33] Z. S. Wu, C. Q. Yang, Y. H. Tobe, L. P. Ye, and T. Harada, "Electrical and Mechanical Characterization of Hybrid CFRP Sheets," *J. Compos. Mater.*, vol. 40, no. 3, pp. 227–244, 2006.

[34] M. M. Davoodi, S. M. Sapuan, D. Ahmad, A. Ali, A. Khalina, and M. Jonoobi, "Mechanical properties of hybrid kenaf/glass reinforced epoxy composite for passenger car bumper beam," *Mater. Des.*, 2010.

[35] K. S. Ahmed and S. Vijayarangan, "Tensile, flexural and interlaminar shear properties of woven jute and jute-glass fabric reinforced polyester composites," *J. Mater. Process. Technol.*, vol. 207, no. 1–3, pp. 330–335, Oct. 2008.

[36] E. J. Garcia, B. L. Wardle, A. John Hart, and N. Yamamoto, "Fabrication and multifunctional properties of a hybrid laminate with aligned carbon nanotubes grown In Situ," *Compos. Sci. Technol.*, vol. 68, no. 9, pp. 2034–2041, Dec. 2008.

[37] M. Miura, Y. Shindo, T. Takeda, and F. Narita, "Effect of damage on the interlaminar shear properties of hybrid composite laminates at cryogenic temperatures," *Compos. Struct.*, vol. 93, no. 1, pp. 124–131, Dec. 2010.

[38] A. I. Selmy, A. R. Elsesi, N. A. Azab, and M. A. Abd El-Baky, "Interlaminar shear behavior of unidirectional glass fiber (U)/random glass fiber (R)/epoxy hybrid and non-hybrid composite laminates," *Compos. Part B Eng.*, vol. 43, no. 4, pp. 1714–1719, Jun. 2012.

[39] S. S. Wicks, W. Wang, M. R. Williams, and B. L. Wardle, "Multi-scale interlaminar fracture mechanisms in woven composite laminates reinforced with aligned carbon nanotubes," *Compos. Sci. Technol.*, vol. 100, pp. 128–135, Aug. 2014.

[40] X. Ma, F. Scarpa, H. X. Peng, G. Allegri, J. Yuan, and R. Ciobanu, "Design of a hybrid carbon fibre/carbon nanotube composite for enhanced lightning strike resistance," *Aerosp. Sci. Technol.*, vol. 47, pp. 367–377, Dec. 2015.

[41] D. W. Y. Wong, H. Zhang, E. Bilotti, and T. Peijs, "Interlaminar toughening of woven fabric carbon/epoxy composite laminates using hybrid aramid/phenoxy interleaves," *Compos. Part A Appl. Sci. Manuf.*, vol. 101, pp. 151–159, Oct. 2017.

[42] M. R. Sanjay, G. R. Arpitha, P. Senthamaraikannan, M. Kathiresan, M. A. Saibalaji, and B. Yogesha, "The Hybrid Effect of Jute/Kenaf/E-Glass Woven Fabric Epoxy Composites for Medium Load Applications: Impact, Inter-Laminar Strength, and Failure Surface Characterization," *J. Nat. Fibers*, vol. 16, no. 4, pp. 600–612, May 2019.

[43] A. S. Zalhaf, M. Abdel-Salam, D.-E. A. Mansour, M. Ahmed, and S. Ookawara, "An Experimental Study of Lightning Overvoltages on a Small-scale Wind Turbine Model," *Energy Procedia*, vol. 156, pp. 442–446, Jan. 2019.

[44] E. C. Botelho, R. A. Silva, L. C. Pardini, and M. C. Rezende, "Evaluation of adhesion of continuous fiber-epoxy composite/aluminum laminates," *J. Adhes. Sci. Technol.*, vol. 18, no. 15–16, pp. 1799–1813, 2004.

[45] A. Fink, P. P. Camanho, J. M. Andrés, E. Pfeiffer, and A. Obst, "Hybrid CFRP/titanium bolted joints: Performance assessment and application to a spacecraft payload adaptor," *Compos. Sci. Technol.*, vol. 70, no. 2, pp. 305–317, 2010.

[46] H. Kim and J. Lee, "The effects of interfacial adhesion strength on the characteristics of an aluminum/CFRP hybrid beam under transverse quasi-static loading," *Compos. Part B Eng.*, vol. 67, pp. 595–606, 2014.

[47] P. Manikandan and G. B. Chai, "A layer-wise behavioral study of metal based interply hybrid composites under low velocity impact load," *Compos. Struct.*, vol. 117, no. 1, pp. 17–31, Nov. 2014.

[48] H. Ning *et al.*, "Experimental and numerical study on the improvement of interlaminar mechanical properties of Al/CFRP laminates," *J. Mater. Process. Technol.*, vol. 216, pp. 79–88, Feb. 2015.

[49] O. Laban and E. Mahdi, "Enhancing mode I inter-laminar fracture toughness of aluminum/fiberglass fiber-metal laminates by combining surface pre-treatments," *Int. J. Adhes. Adhes.*, vol. 78, pp. 234–239, Oct. 2017.

[50] B. Yu, P. He, Z. Jiang, and J. Yang, "Interlaminar fracture properties of surface treated Ti-CFRP hybrid composites under long-term hygrothermal conditions," *Compos. Part A Appl. Sci. Manuf.*, vol. 96, pp. 9–17, May 2017.

[51] Y. Pan *et al.*, "Composite interfaCes," vol. 23, no. 5, pp. 453–465, 2016.

[52] C. Bellini, V. Di Cocco, and L. Sorrentino, "Interlaminar shear strength study on CFRP/Al hybrid laminates with different properties," *Frat. ed Integrita Strutt.*, vol. 14, no. 51, pp. 442–448, Jan. 2020.

[53] M. Akhsin Muflikhun, R. Higuchi, T. Yokozeki, and T. Aoki, "Delamination behavior and energy release rate evaluation of CFRP/SPCC hybrid laminates under ENF test: Corrected with residual thermal stresses," 2020.

[54] V. Kumar *et al.*, "Polyaniline-based all-polymeric adhesive layer: An effective lightning strike protection technology for high residual mechanical strength of CFRPs," *Compos. Sci. Technol.*, Jan. 2019.

[55] V. Kumar, T. Yokozeki, T. Goto, T. Takahashi, S. R. Dhakate, and B. P. Singh, "Irreversible tunability of through-thickness electrical conductivity of polyaniline-based CFRP by de-doping," *Compos. Sci. Technol.*, vol. 152, pp. 20–26, 2017.

[56] V. Kumar *et al.*, "Cationic scavenging by polyaniline: Boon or bane from synthesis point of view of its nanocomposites," *Polymer (Guildf).*, vol. 149, pp. 169–177, Aug. 2018.

[57] J. H. Han *et al.*, "The combination of carbon nanotube buckypaper and insulating adhesive for lightning strike protection of the carbon fiber/epoxy laminates," *Carbon N. Y.*, vol. 94, pp. 101–113, Aug. 2015.

[58] S. DAS and T. YOKOZEKI, "Polyaniline-Based Self-Sensing Structural Strain Sensor Characterization under Flexural Loading," *Mater. Syst.*, vol. 37, pp. 15–20, 2020.